THE UNIVERSITY OF MICHIGAN

INDUSTRY PROGRAM OF THE COLLEGE OF ENGINEERING

USE OF FLOW PATTERNS IN PREDICTING SHELL-SIDE HEAT TRANSFER COEFFICIENTS FOR BAFFLED SHELL-AND-TUBE HEAT EXCHANGERS

Rajeshwar Kumar Gupta

This dissertation was submitted in partial fulfillment of the requirements for the degree of Doctor of Philosophy in the University of Michigan, 1956.

September, 1956

IP-179

ACKNOWLEDGMENT

We wish to express our appreciation to the author for permission to give this thesis limited distribution under the Industry Program of the College of Engineering.

ACKNOWLEDGEMENTS

The author wishes to express his gratitude to all those persons who helped in making the present study a success.

In particular he wishes to acknowledge the encouragement and advice given by Professor D. L. Katz, chairman of the doctoral committee, by Professors L. E. Brownell, R. G. Folsom, J. L. York, and E. H. Young, members of the doctoral committee, and by Professor W. W. Hagerty, a member of the doctoral committee before he left for the University of Delaware. The author also wishes to thank Professors R. L. Hess and H. A. Ohlgren for their continued interest.

The shop and secretarial personnel of the Chemical and Metallurgical Engineering Department were most helpful at all times. Thanks are especially due Mr. Cleatis Bolen, the welder, for assistance in the construction of the experimental equipment.

Mr. R. L. Callard of the Corning Glass Works was extremely helpful at all times. Mr. H. W. Wienert of the University Photographic Services was most generous with his time in assisting the author with the photographic work involved in this study. The interest of Messrs. Zargan and Osterlund of the Fischer Scientific Company is greatly appreciated.

The author is indebted to the Corning Glass Works for contributing replacement tubes for the glass heat exchanger, and to Carbide and Carbon Chemicals Company for contributing some of the propylene glycol used in the present study.

Thanks are due Mr. R. E. Carroll and his Industry Program Staff for assistance in preparing this dissertation.

TABLE OF CONTENTS

TABLE OF CONTENTS (CONT.)

LIST OF TABLES

LIST OF FIGURES

LIST OF FIGURES (CONT.)

LIST OF FIGURES (CONT.)

NOMENCLATURE

Symbols - English Alphabet:

a = intercept of Wilson plot

A = heat transfer area, sq ft

A_o = total effective outside heat transfer area, sq ft

A_p = heat transfer area in the characteristic flow zone "p", sq ft

b = slope of Wilson plot

C = constant

C_N = factor to correct the cross flow heat transfer for number of rows of tubes in cross flow less than ten

C_p = specific heat of liquid, Btu/(lb)(°F)

D_e = equivalent diameter, ft

D_e' = equivalent diameter, inches

D_o = outside diameter of tube, ft

D_s = inside diameter of shell, ft

f = friction factor for cross flow in baffled shell

f_o = friction factor for overall flow in baffled shell (corresponding to total shell-side ΔP)

g_c = gravitational constant, consistent units

g_c' = gravitational constant, 32.17

G = mass flow velocity, W/S, lbs/ (hr)(sq ft)

G_p = shell-side mass flow velocity, lbs/(hr)(sq ft), for the characteristic flow zone "p"

h_o = shell-side heat transfer film coefficient, BTU/(hr)(sq ft)(°F)

h_p = heat transfer film coefficient for the characteristic flow zone "p", Btu/(hr)(sq ft)(°F)

j = coefficient (defined by reference 60) depending on Re

k = thermal conductivity of liquid, Btu/(hr)(sq ft)(°F/ft)

k_g = thermal conductivity of glass

L = total effective length of the tube bundle, ft

L_a = width of true cross flow zone near entrance window, ft

L_b = width of true cross flow zone near exit window, ft

L_c = width of true cross flow zone at shell diameter, ft

m = exponent

n = exponent

N_B = number of baffles in the bundle

N_o = total number of tubes in the bundle

N_w = number of tubes in the baffle window

Nu = Nusselt number, $h\ D/k$

p = tube pitch, center to center, ft

ΔP = shell-side pressure drop, lbs/sq in.(unless otherwise specified)

Pr = Prandtl number, $C_p\mu/k$

Q = heat transferred, Btu/hr

R = resistance to flow of heat

Re = Reynolds number, $D\ G/\mu$

s^2 = sum of the squares of the deviations in obtaining the least square fit for a Wilson plot

S = cross-sectional area for flow, sq ft

T = temperature, °F

u = velocity, ft/sec

U_o = overall heat transfer coefficient based on outside area, Btu/(hr)(sq ft)(°F)

W = flow rate, lbs/hr

W' = flow rate, gallons/hr

x_g = thickness of glass tube wall, ft

X = baffle spacing, face to face, ft

Symbols - Greek Alphabet

ϵ = void fraction, dimensionless, (defined by reference 60)

μ = viscosity of liquid, lbs/(hr)(ft)

ρ = density of liquid, lbs/cu ft

Σ = summation

Φ = arrangement factor, dimensionless, (defined by reference 60)

Subscripts:

b = bulk property

c = pertaining to the "True Cross Flow Zones"

(c + e) = pertaining to the "Apparent Cross Flow Zones"

e = pertaining to the "Eddy Zones"

f = film property

g = pertaining to glass tube wall

i = pertaining to the inside of tubes

ℓ = pertaining to the "Longitudinal Flow Zones"

o = pertaining to the outside of tubes

p = any particular characteristic flow zone: c, (c + e), e, or ℓ

s = shell-side

s.b. = shell-side, bulk

s.s. = shell-side, surface

t = tube-side

t.b. = tube-side, bulk

w = evaluated at the baffle window

STATEMENT OF THE PROBLEM

The purpose of this investigation is to gain an insight into the mechanism of heat transfer on the shell side of baffled shell-and-tube heat exchangers. It is aimed at establishing the significance of the shell-side flow patterns in determining the shell-side heat transfer film coefficients through a simultaneous study of the fluid flow patterns and the heat transfer characteristics on the shell side of segmentally baffled shell-and-tube heat exchangers.

The current practice in predicting shell-side heat transfer coefficients involves the use of empirical correlations. These empirical correlations assume the shell-side flow to be partly longitudinal to and partly across the tubes and use some kind of an average velocity for these two types of flow in the shell. It was felt that the mechanism of flow on the shell side should be followed more closely, and instead of using a single correlation (involving an average velocity) to predict the heat transfer coefficient, separate correlations for the different characteristic flow zones should be tried, the total shell-side coefficient being given by a weighted summation of the heat transfer coefficients for the various zones.

ABSTRACT

The purpose of this investigation is to gain an insight into the mechanism of heat transfer on the shell side of baffled shell-and-tube heat exchangers and to establish the significance of the shell-side fluid flow patterns in determining the shell-side heat transfer coefficients. A simultaneous study of the flow patterns, heat transfer characteristics, and pressure drops on the shell side of a segmentally baffled shell-and-tube heat exchanger, with the shell and the tubes made of Pyrex brand glass, was conducted.

Data are reported on shell-side flow patterns, heat transfer characteristics, and pressure drops for six tube bundles with the same tube size and arrangement but with different combinations of baffle cuts and baffle spacings. Though the study is restricted to baffles of the segmental type, it is felt that the ideas presented here can be extended to other baffle types. The baffles for the test bundles were specially designed to eliminate the tube-to-baffle and the baffle-to-shell leakage. The tube arrangement was such that very little empty space was left around the peripheral tubes, thus appreciably reducing the bundle by-pass.

The flow pattern studies reveal that the flow on the shell-side may be divided into zones of three different flow characteristics, namely:

1) The "longitudinal flow" zones,
2) The "true cross flow" zones,
3) The "eddy" or "dead" zones.

In the conventional concept of the shell-side flow, only longitudinal and cross flow regimes are recognized. According to current practice, the shell-side heat transfer film coefficients are calculated by a single empirical correlation using some kind of an average velocity for the longitudinal and the cross flow zones. The correlations available for this purpose do not take the eddy zones into account, and the sum of the regions found in the present study to be in cross flow and those in the eddy zones are considered as cross flow regions. This is equivalent of assuming the mechanism of heat transfer in the eddy zones to be the same as that in cross flow. The present study shows that this inherent assumption in the correlations available in the literature is not valid. The mechanisms of fluid flow and heat transfer in the eddy zones are shown to be considerably different from those in cross flow, thus necessitating the treatment of the eddy zones separately from the other characteristic zones in calculating the shell-side film coefficients.

Using the correlations available in the literature for predicting the film coefficients for flow of fluids outside and parallel to tube bundles and those for flow of fluids across tube bundles, a correlation for the eddy zone heat transfer film coefficients is obtained from a knowledge of experimental total shell-side film coefficients and of the shell-side flow patterns. By using this correlation for predicting the eddy zone coefficients and the correlations from the literature for the other two types of zones, the film coefficients for the three types of zones can be calculated. The total shell-side film coefficients can then be obtained by a weighted (on heat transfer area) summation of

the three component film coefficients. Within the range of the present study the film coefficients predicted by the proposed method lie within $\pm$ 10 % of the experimental values.

The pressure drop data obtained in the present study are also correlated. The pressure drop correlation is between the overall shell-side friction factor (defined as

$$f_o = \frac{\Delta P \, g_c \, \rho \, X}{2 \, L \, G_w^2}$$

and the baffle-window Reynolds number). All the pressure drop data for the six bundles tested fit the proposed correlation with deviations less than $\pm$ 10 percent.

CHAPTER I

INTRODUCTION

One of the most widely used types of heat transfer equipment consists of a number of parallel tubes enclosed in a relatively close-fitting cylindrical shell, and is commonly referred to as a "shell-and-tube" heat exchanger. One fluid flows inside the tubes and is called the "tube-side" fluid; the other flows outside the tubes and is called the "shell-side" fluid. On the shell-side, cross baffles of various types are often inserted at right angles to the tubes to increase the velocity and to give more cross flow in long heat exchangers. In such a design, the flow of the shell-side fluid is partly parallel to and partly across the tubes. Figure 1 shows a typical shell-and-tube heat exchanger of the rigid tube sheet type.

Procedures for the prediction of the tube-side (inside tubes) heat transfer film coefficient are well known. Since the geometry is quite simple, namely, that of flow in a pipe, standard correlations can be used for the heat transfer calculations. These correlations are available in all the textbooks and reference books dealing with heat transfer. Therefore, no attention will be paid to the methods of calculation of tube-side film coefficients in the present work.

On the shell side (outside the tubes), a more complicated geometry exists and the procedures for predicting the heat transfer coefficients on the outside of the tubes in baffled shell-and-tube heat exchangers are still in a state of development. The prediction of shell-side heat transfer coefficients has, up to the present, been

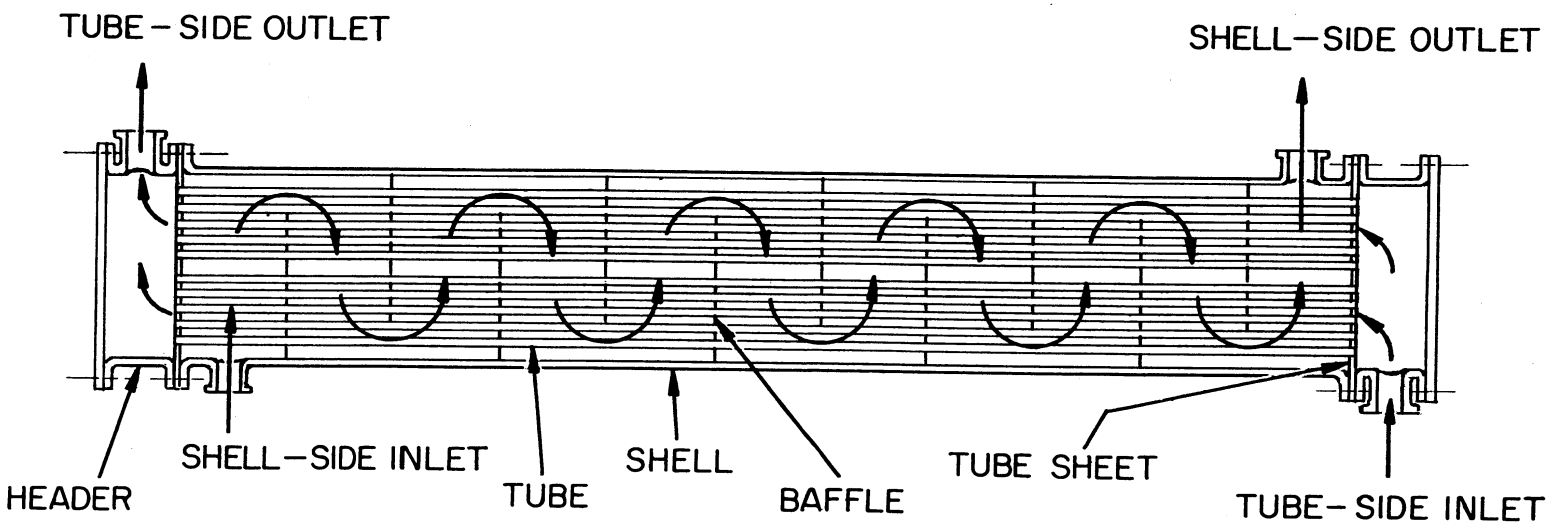

Fig. 1 Typical shell-and-tube heat exchanger, (Rigid - tube sheet type)

uncertain to about ± 50 percent. The current practice in regard to the prediction of the shell-side coefficients involves the use of empirical correlations obtained by fitting experimental data to equations based on dimensional analysis and patterned after the correlations for predicting the coefficients for flow of fluids inside tubes. Many variations and refinements of such empirical correlations are available in the literature.

It has long been felt that the shell side heat transfer film coefficients for baffled shell-and-tube heat exchangers should in some way be related to the flow pattern of the shell-side fluid. Very little work has been done to prove this view and to establish it on some quantitative basis. Some two-dimensional flow pattern studies on baffled channels have been reported in the literature. However, the geometry in a real exchanger is considerably different from that for a two-dimensional model.

It was proposed to carry out a simultaneous study of the flow patterns and the heat transfer on the shell side of a segmentally baffled shell-and-tube heat exchanger. It was felt that if the flow on the shell side could be divided into regions of different flow characteristics, the heat transfer coefficient for each such zone could be computed individually and the coefficients for the various zones combined in the ratios of the heat transfer area in each zone because heat transfer takes place simultaneously in all these zones.

CHAPTER II

LITERATURE REVIEW

The subject of shell-and-tube heat exchangers is treated quite extensively by most of the standard chemical engineering texts and reference books. Badger and Banchero,[1] Brown, et al.,[8] Kern,[32] McAdams,[37,38] Nelson,[41] Ohlgren, et al.,[42] Stoever,[54] etc. cover the subject of the general description of various types of shell-and-tube heat exchangers quite extensively. Many of the available design methods are also reviewed in these references. TEMA Standards[58] gives a very good treatment of the detailed design of shell-and-tube heat exchangers. The various procedures available for the prediction of tube-side heat transfer film coefficients are well treated by McAdams[37,38] and some of the other references cited above. Since the present study is primarily concerned with the shell-side heat transfer coefficients, the literature review will be restricted to that phase only.

It is widely recognized that the flow on the shell-side of a baffled shell-and-tube exchanger is partly longitudinal and partly transverse to the tubes. It can therefore be expected that the heat transfer relations for the baffled shell would be of the same general form and probably be a function of the heat transfer for flow of fluids outside unbaffled tube bundles for the two types of flow, namely that of flow parallel to the tubes and for flow across the tubes. These two cases are reviewed in the following discussion.

Longitudinal Flow Correlations

Very little published data are available for the case of heat transfer to a fluid flowing outside tubes in a bundle, with flow parallel to the tube axes. Of the standard texts, McAdams[37,38] and Jacob[30] do not mention this case. Eckert[16] recommends using the equation for turbulent flow inside tubes, with an equivalent diameter

$$D_e = \frac{4 \times \text{flow area}}{\text{wetted perimeter}} .$$

His recommendation is evidently made on theoretical grounds, since no data are cited. It is, however, supported by McAdams' statement in the heat transfer section of The Chemical Engineers' Handbook[46] where he mentions that test data for gases flowing outside and parallel to axes of tubes are in rough agreement with the equations for gases inside pipes when the equivalent diameter is taken as four times the ratio of free cross-section to total "wetted" perimeter. Studies of Griffiths and Awbery[23] on a single iron pipe placed longitudinally along the direction of an air stream and the comparison of their results with data for fluids flowing inside a tube, further seem to indicate that the heat transfer per unit area between a fluid flowing longitudinally along a pipe and the surface of the pipe is the same whether the fluid is inside or outside the pipe; in other words, the transfer is independent of the sign of the curvature of the pipe. One of the correlations most widely used for predicting heat transfer to fluids in turbulent flow inside tubes and pipes is that given by Colburn.[10] This is a modification of the original correlation by Dittus and Boelter.[13] Using the equivalent diameter defined above, Colburn's correlation becomes:

$$\frac{h D_e}{k} = 0.023 \left(\frac{D_e G}{\mu_f}\right)^{0.8} \left(\frac{C_p \mu_f}{k}\right)^{1/3} \qquad (1)$$

Some data for heat transfer in unbaffled shell-and-tube heat exchangers have been reported by Heinrich and Stuckle[28] and by Short.[52] Donohue[14] has correlated these data by the equation:

$$\frac{h D_e}{k} = 0.128 \, (D_e')^{0.6} \left(\frac{D_o G}{\mu}\right)^{0.6} \left(\frac{C_p \mu_f}{k}\right)^{0.33} \qquad (2)$$

where D_e' is the equivalent diameter in inches. The exponent of 0.6 on the Reynolds number in this correlation is in disagreement with the rest of the work on heat transfer to fluids flowing outside and parallel to the axes of tubes. This discrepancy can probably be attributed to errors in obtaining the shell side coefficient by the Wilson plot technique by these workers. The 0.8 exponent for the Reynolds number has been verified by the recently published work of Miller, et al.[39] on heat transfer to water flowing parallel to a rod bundle. These workers obtained heat transfer data for parallel flow of water in a triangular lattice of cylindrical rods, at high temperature, high flow rate, and high heat flux. The experimental values were 40 percent higher than would be predicted by using Colburn's equation for flow inside tubes, with the equivalent diameter, D_e, replacing the tube diameter, as shown in equation (1). Their heat transfer data fit the equation:

$$\frac{h D_e}{k} = 0.032 \left(\frac{D_e G}{\mu_f}\right)^{0.8} \left(\frac{C_p \mu_f}{k}\right)^{1/3} \qquad (3)$$

Cross Flow Correlations

Considerable data have been reported in the literature for heat transfer to fluids flowing across tube banks. In 1933 Colburn[10] proposed the following dimensionless correlation for data on flow of gases across staggered tube banks for $\frac{D_o G_{max}}{\mu_f}$ from 2,000 to 32,000:

$$\frac{h D_o}{k_f} = 0.33 \left(\frac{D_o G_{max}}{\mu_f}\right)^{0.6} \left(\frac{C_p \mu}{k}\right)_f^{1/3} \qquad (4)$$

For banks of tubes in line (not staggered) Colburn suggested that the constant be reduced from 0.33 to 0.26. MmAdams[37,38] suggests the use of Colburn's equation for Reynolds numbers above 2000 for both liquids and gases. For Reynolds numbers from 2000 to 150 he recommends the use of a curve drawn in continuation of the line for equation (4) but parallel to the curve for single cylinders. He contends that this procedure is supported by unpublished data for liquids. For number of rows of tubes in cross flow less than 10, he recommends multiplying the value of h obtained by the above procedure by factors given by Grimison.[24] Work of Pierson,[47] Huge[29] and Grimison[24] on the flow of air streams in cross flow to tube banks supports the Colburn equation. Schmidt,[51] in 1951, described the variation of heat transfer with the number of rows of tubes transverse to the fluid flow. According to him the second row usually has a lower heat transfer than the others, particularly the first one. He further states that for staggered tubes the film coefficient from the third row onwards remains constant, and for in-line tubes it does not usually become constant until the fifth row. The variation

of heat transfer for different rows can be attributed to the different degrees of turbulence introduced by the different rows.

In the recent years an extensive study has been conducted at the University of Delaware on heat transfer and pressure drop for liquids flowing across banks of tubes. Most of this work is in the viscous flow range (below Reynolds numbers of 1000). Various papers by Bergelin and associates[2,3,43] describe this work. One of the reported studies in this series included the transition zone between viscous and turbulent flow.[4] The data reported agree fairly well with the previously available correlations.

Heat transfer and flow friction design data were recently reported by Kays, London, and Lo[31] for air in turbulent flow across banks of tubes for the Reynolds number range 500 to 20,000. These data supplement the high Reynolds number data of Pierson, Huge, and Grimison, and the low Reynolds number viscous-flow-range data of Bergelin, et al. The data can be correlated by Colburn's equation (equation 4). In a recent paper Weisman[60] presented a correlation relating the heat transfer characteristics of cross-flow heat exchangers to the void-volume-and-tube-pitch ratio. The correlation is essentially in agreement with the previously available correlations except for the introduction of an additional term $\epsilon^{\Phi j}$, where:

ϵ = void fraction, dimensionless

Φ = arrangement factor, dimensionless

j = coefficient depending on the Reynolds number (fixed at 1 for $DG/\mu\epsilon = 4{,}000$)

In a recently declassified U. S. Atomic Energy Commission report, Dwyer, et al.[15] report on heat transfer rates for cross flow of water through a tube bank at high Reynolds numbers. A small portion

of their data for Reynolds numbers below 75,000 confirms the Colburn equation (equation 4). However, as the Reynolds number is increased above 75,000 the coefficients begin to deviate markedly from the extrapolated curve of the Colburn equation. The best line for their data (neglecting the effect of Prandtl number) is represented by the equation:

$$h = 0.185\ (Re)^{0.8} \qquad (5)$$

All the studies for heat transfer to fluids flowing across tube banks reported in the literature and reviewed here are on square banks only. The author did not find any reported studies on bundles with varying number of tubes in successive rows. It would appear that such a study would be more pertinent for direct application to the cross flow zone in shell-and-tube heat exchangers than the studies on square banks of tubes.

Correlations for Baffled Exchangers

Perrone,[45] back in 1935, recognized the fact that in a segmentally baffled shell-and-tube heat exchanger the average cross-section of flow is quite complicated and that it is to be expected that any relation giving anywhere near an average velocity will be somewhat complicated. He described the idealized average path of a fluid flowing on the shell-side of such an exchanger as consisting of two components: one in cross-flow normal to the tubes extending from the center of gravity of one baffle window to that of the next, the other parallel to the tubes having a length equal to the baffle spacing. On this basis he calculated an average velocity from the velocity u_2, perpendicular to the tubes, velocity u_1, parallel to the tubes, and the total distance traveled by the fluid; each velocity being multiplied

by the fraction of the total distance the shell fluid traveled at this velocity. This concept has been accepted generally as a rational method of analysis, and this approach forms the basis of most of the empirical correlations available in the literature. Nelson,[40] using a similar reasoning, proposed the following equation for estimating the effective shell-side velocity of a single shell-pass exchanger with segmental baffles:

$$u = \frac{W'}{13{,}000\ D_s^2}\ (C + D_s/X) \qquad (6)$$

where

u = velocity, ft per sec

W' = rate of flow, gal per hr at exchanger temperature

D_s = inside shell diameter, ft (or more exactly, the length of cross travel across the shell due to baffles)

X = baffle spacing, ft

C = a constant which normally has a value of 1.5 to 2.0 but ranges from 0.5 to 3.0 depending on velocity

A more common procedure used in developing empirical correlations reported in the literature is to calculate some kind of an average cross-sectional area for flow and to use this average area for the calculation of the velocity in the Reynolds number term, or to directly average the velocities for flow in various regions. The two commonly used methods of averaging the areas are the arithmetic mean and the geometric mean. Short[52] recommends the use of an arithmetic mean of the velocities through baffle windows, through maximum area perpendicular to tubes, and through minimum area perpendicular to tubes, whereas Donohue[14] recommends the use of a geometric mean of the flow areas or velocities in the window and for cross-flow at the shell diameter.

Bergelin, et al.[2,3,4,43] use the Donohue method of averaging except for the modification that the cross-flow area is taken as an average of all the rows rather than that at the shell diameter.

Considerable amount of data is available in the literature for heat transfer on the shell side of segmentally baffled heat exchangers. Donohue[14] has correlated the experimental data reported by Bowman,[6] Gardner and Siller,[21] Short,[52,53] Tinker,[56,57] and Williams and Katz.[62,63] He reported the following correlation:

$$\frac{h\,D_o}{k} = C\left(\frac{D_o\,G_m}{\mu}\right)^{0.6}\left(\frac{C_p\,\mu}{k}\right)^{0.33}\left(\frac{\mu}{\mu_{wall}}\right)^{0.14} \qquad (7)$$

where G_m is the geometric mean of the mass velocities through the window and for cross flow at the shell diameter. The constant C varied with various sets of data and sometimes for the various bundles within a particular set of data. The deviation of the experimental data from the correlation, using the right constant C for the particular set of data, is about ± 25 percent. Short[52] proposed the following correlation on the basis of his own data:

$$\frac{h\,D_o}{k} = 1.28\left(\frac{p - D_o}{p}\,D_o\right)^{0.4}\left(\frac{C_p\,\mu}{k}\right)^{1/3}\left(\frac{D_o\,G_{av}}{\mu}\right)^{0.8} \qquad (8)$$

where p is the tube pitch, center to center of tubes, in feet, and G_{av} is the arithmetic mean mass velocity as defined by Short and mentioned earlier in this section. Bergelin, et al.[5] and Sullivan and Bergelin[55] recently reported some data on baffled exchangers from the heat exchanger project at the University of Delaware. The former is a study of a cylindrical baffled exchanger without internal leakage while the latter is a study on a rectangular shell-and-tube heat exchanger with a single baffle. In the paper by Bergelin, et al.[5] an attempt is made to

separate the heat transfer in the window and that in the cross-flow zone. The work of Williams and Katz[62,63] on segmentally baffled plain tube shell-and-tube heat exchangers essentially confirms Donohue's correlation, except for the fact that they found that an exponent of 0.65 instead of 0.6 (as used by Donohue) gives a better fit of the data.

The best discussions available for the mechanisms of the fluid flow and heat transfer on the shell side of baffled exchangers are by Fritzsche[20] and Tinker.[56,57] Tinker took the various leakage and by-pass streams on the shell side into consideration and proposed an effective area to be used in place of the usual average flow area. But Tinker's correlation is very complicated and for this reason is rather impractical for design purposes. It contains a number a constants represented by C with suffixes 1-13 and another represented by x, some of which are clearly defined while others such as C_{10} and x are obscure. Probably the biggest service done by Tinker's work was to point out as to how complicated was the mechanism of flow on the shell-side of a baffled exchanger. Whistler[61] has analyzed the problem of shell-side leakage mathematically. Fabregas[18] recently proposed a method for correcting shell-side coefficients for leakage.

No attempt to relate the heat transfer characteristics directly to the flow patterns has been reported in the literature.

Flow Patterns in Baffled Exchangers

No flow pattern studies for the shell-side of baffled shell-and-tube heat exchangers have been reported in the literature, to the author's knowledge. C. F. Braun and Company[7] have done some work on flow patterns but the data are not available for general use. A motion picture made by them shows some isothermal flow patterns. A study by Gunter, Sennstrom, and Kopp[25] on flow patterns in a two dimensional

model, consisting of a baffled channel without any tubes, is the nearest thing available in the literature. These are reproduced in the Bulletin on Fluid Dynamics and Heat Transfer by Knudsen and Katz.[33] But the flow patterns in real shell-and-tube heat exchangers, which are usually circular in cross-section, would not be expected to be the same as in a two-dimensional model. This is proved by the fact that the flow patterns obtained in the present study for baffle designs comparable to some of the designs studied by Gunter, et al., differ considerably from the patterns reported by them.

Liquid Flow Pattern Study Techniques

The problem of studying flow patterns can be divided into two parts: that of making the flow visible and that of recording the pattern. Most flow visualization techniques require the introduction of foreign matter into the fluid stream under consideration. Relf,[49] in 1913, used small drops of a mixture of olive oil and nitrobenzene of unit density to show the lines of flow of water around an aerofoil. Different combinations of liquids can be used to make the tracer drops. Goldstein[22] suggests that best results are obtained when the refractive index of the drops is such that the angle between the incident and emergent rays is 90°, for then all the illuminated drops can be brought into focus on the photographic plate at the same time, if the plane of illumination is sufficiently thin. Prandtl and Tietjens[48] mention about the use of solid spheres made of a mixture of wax and rosin by Marey in 1893. With the advent of a wide variety of polymers the problem of getting tracers of a particular density has been eased somewhat because plastic beads are available in a wide range of densities. Sachs and Rushton[50] used plastic beads in the latter part of their

study of the discharge flow from turbine-type mixing impellers. The use of these various types of particular tracers for flow visualization is very useful in determining local velocities and lines of flow. The methods of recording the patterns in this case are almost invariably photographic. Specially, in a closed system of the type used in the present study, the particles can be introduced only momentarily and should not be recycled, thus necessitating the use of photographic techniques for recording the patterns. Loudenslager, et al.[35] and Sachs and Rushton[50] have proposed methods for quantitative interpretation of the photographs to obtain local velocities in three dimensional systems. Due to heat transfer considerations, a large concentration of the tracer particles cannot be tolerated in the fluid under study.

Use of birefringent dilute solutions or suspensions has been used quite extensively for flow visualization. Peebles, et al.[44] used an organic dye (Allied Chemical and Dye Company, Milling Yellow, MYNGS) for the purpose. Hauser and Dewey[27] used a dilute colloidal bentonite suspension for studying two-dimensional flow patterns, whereas Ullyott[59] utilized aqueous solutions of vanadium pentoxide for flow visualization. Gunter, et al.[25] in their flow pattern studies in two-dimensional models of baffled exchangers successfully used a suspension of powdered aluminum in distilled water containing a wetting agent. These methods using suspensions are quite good for giving overall flow patterns but do not give accurate information on local velocities. However, a very accurate study of local velocities is not necessary at present for baffled heat exchangers because it would not be possible to utilize it for any quantitative design purposes, considering the complicated geometry

involved. But, if the heat transfer is to be studied simultaneously with the flow patterns, the introduction of the various suspended materials would not be desirable because they can appreciably affect the heat transfer and the fluid properties, especially when present in appreciable concentrations. Hagerty[26] recently reported that it is a property of certain concentrations of glycerine-water solutions, when in a state of steady flow, that the planes of equal shear in the liquid become visible in ordinary light if viewed along a path tangent to the shear plane. This method seems to offer some promise though it is apparent that its applicability would be restricted to the fluids which exhibit this property.

It is very difficult to photograph flow patterns in cylindrical shells which are normally encountered in shell-and-tube heat exchangers. The use of glass as the material of construction for the shell, though necessary for being able to see the flow, becomes a further hindrance in photographing the patterns due to the reflections from the glass surface.

CHAPTER III

EXPERIMENTAL EQUIPMENT AND MATERIALS

Experimental equipment was designed and constructed for a simultaneous study of the heat transfer performance and fluid flow patterns on the shell side of a segmentally baffled shell-and-tube heat exchanger with a removable tube bundle in order to allow changes in the baffle design. Figure 1a shows a general view of the experimental equipment. A schematic flow diagram of the equipment is shown in Figure 2. The heat flows from the shell-side fluid to the tube-side fluid.

The main features of the equipment are:

1) The test exchanger with both the shell and the tubes made of Pyrex brand glass and the six test bundles with the same tube size and arrangement but with different baffle cut and baffle spacing combinations.

2) The shell-side fluid circulation system with a fairly wide range of pumping capacities and with an ability to control the temperature of the inlet stream to the shell side of the test exchanger.

3) The cooling water system with a fairly wide range of flow rates available and with an ability to control the temperature of the inlet cooling water to the tube side of the test exchanger. The cooling water flows counter-current to the shell-side fluid.

4) Instrumentation to measure temperatures of the inlet and outlet streams of both the shell and the tube sides, to measure flow rates of the shell and the tube side streams, and to measure

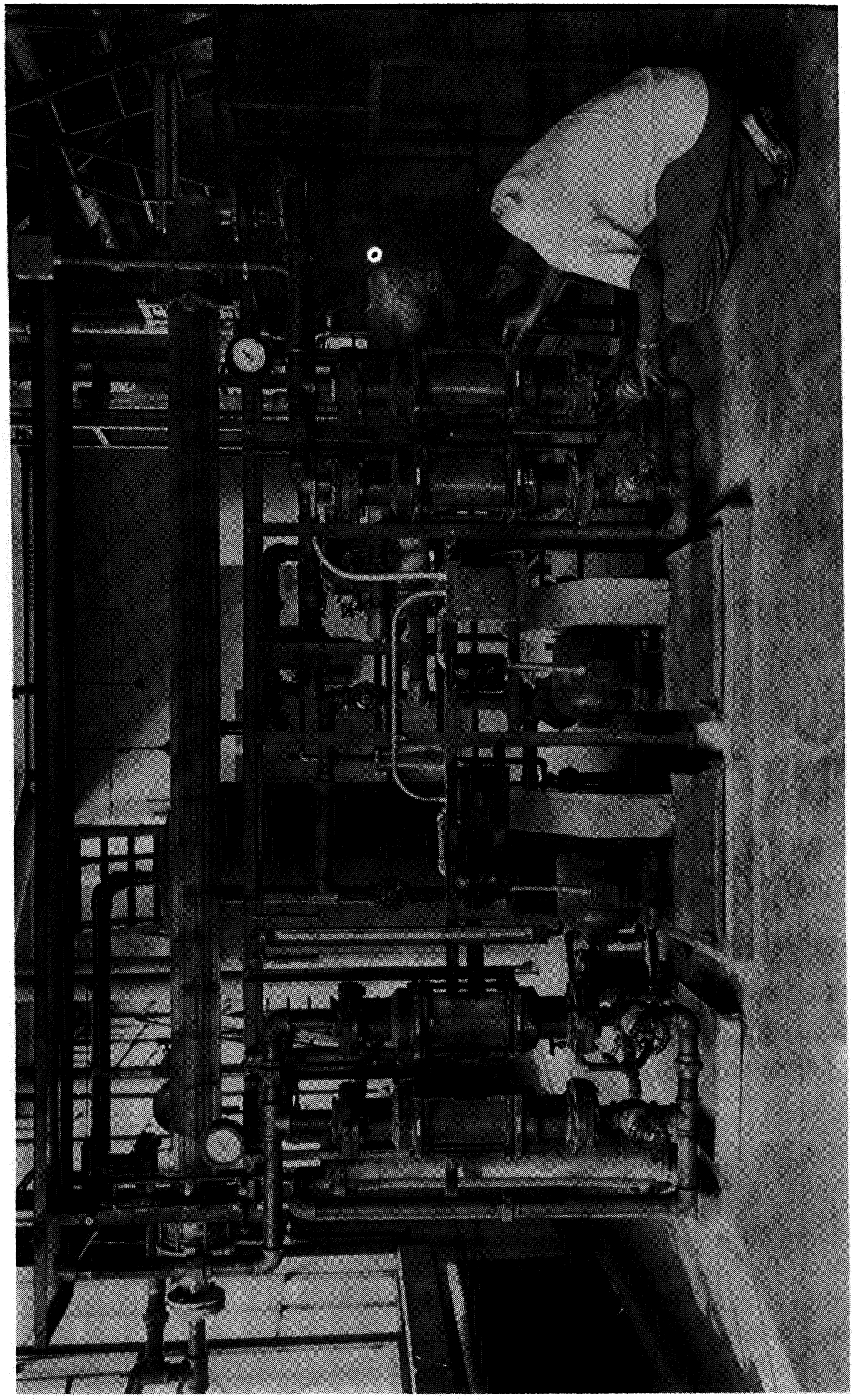

Fig. Ia. General view of experimental equipment

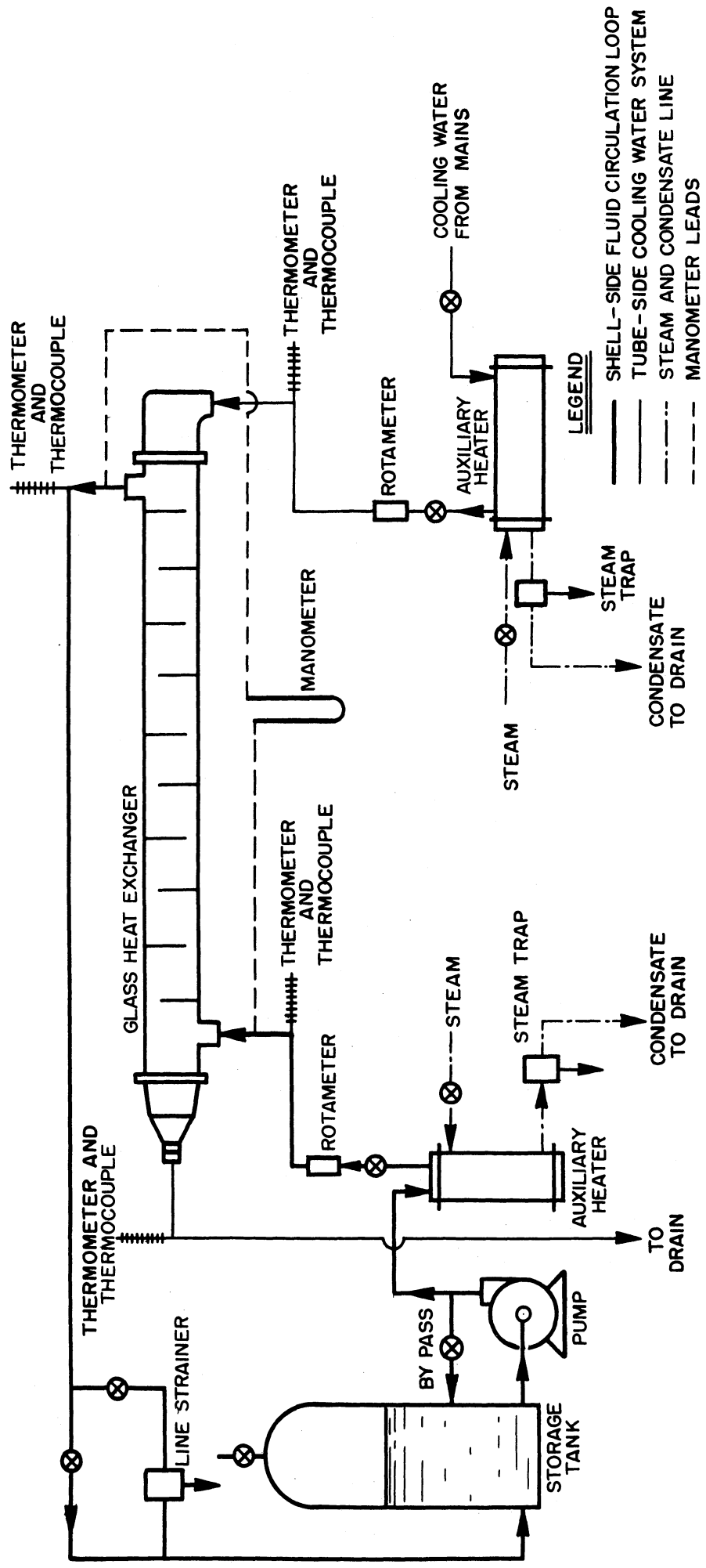

Fig 2 Schematic flow diagram of experimental equipment

the pressure drop between the inlet and outlet of the shell side of the test exchanger.

5) Equipment and materials for the flow pattern studies.

Test Exchanger and Bundles

A 50 sq ft unit of the Pyrex shell-and-tube heat exchanger, recently developed by the Corning Glass Works, was acquired. This unit consists of a thick Pyrex glass shell, 6 in. inside diameter, with 26 Pyrex glass tubes, 3/4 in. outside diameter and 0.03 in. wall, having a total external effective heat transfer area of 50.8 sq ft. It has a single pass both on the shell and the tube sides. Figure 3 shows a drawing of the exchanger taken from the Corning bulletin describing this exchanger.[11] The unit has a rather ingenius design for the header assembly, shown in the drawing in Figure 4 reproduced from the Corning bulletin.[11] The seal between the shell side and the tube side of this unit is affected by a Silastic sealer sheet. This acts as a fluid and is put under fluid pressure by the force created in tightening the flange bolts. The fluid is completely retained in the cavity formed by the tubes and the Retainer Ring around the outside of the tube sheets. The Silastic sealer sheet is compressed against the Teflon Sealer Sheet Protector which presses against the precision finished tube ends, thus creating an effective seal. With this arrangement each tube is free to float as it expands thermally. The company bulletin recommends that the shell-side Sealer Sheet Protector can be eliminated when using non-corrosive liquids on the shell-side. However, the author's experience indicated that elimination of this Protector caused leakage of the shell-side fluid through the seal. The Flange Take-Up Springs in the header assembly serve to (a) compensate for cold flow

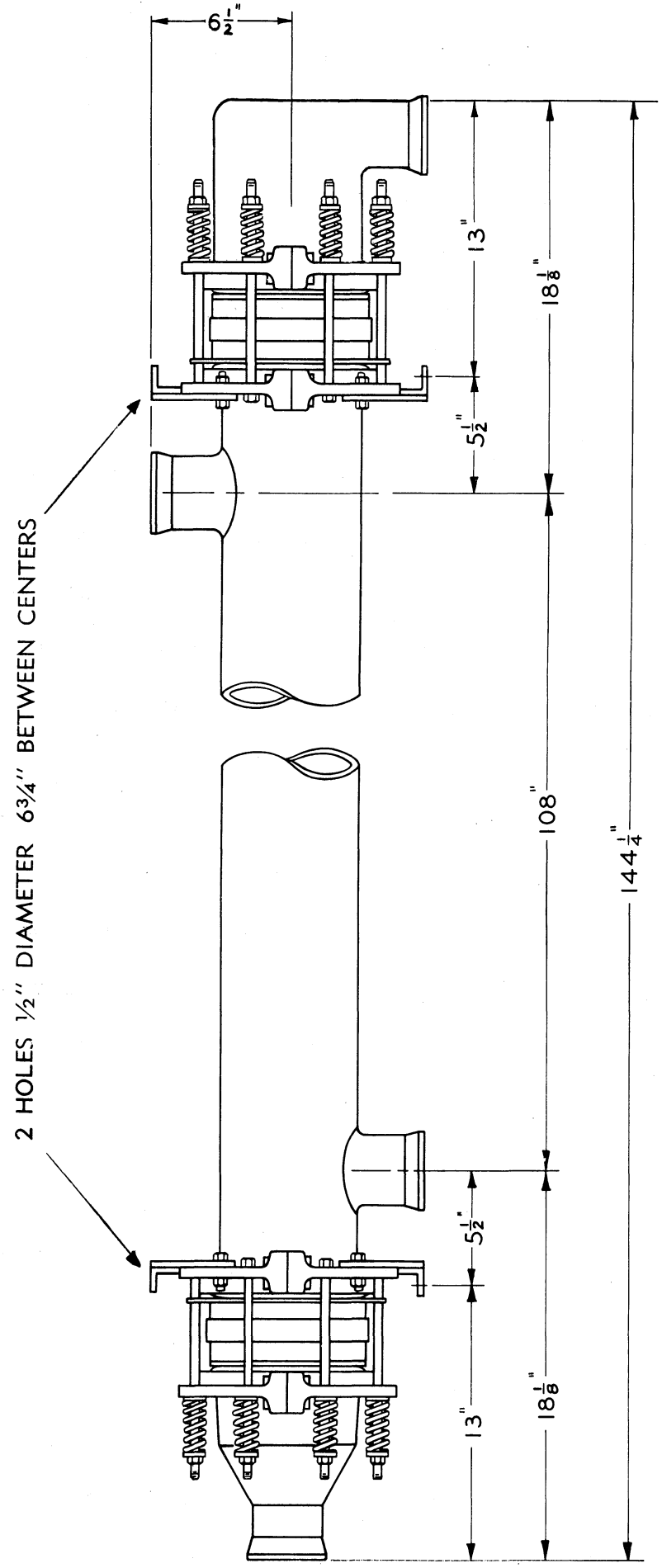

Fig. 3. The glass heat exchanger (courtesy Corning Glass Works)

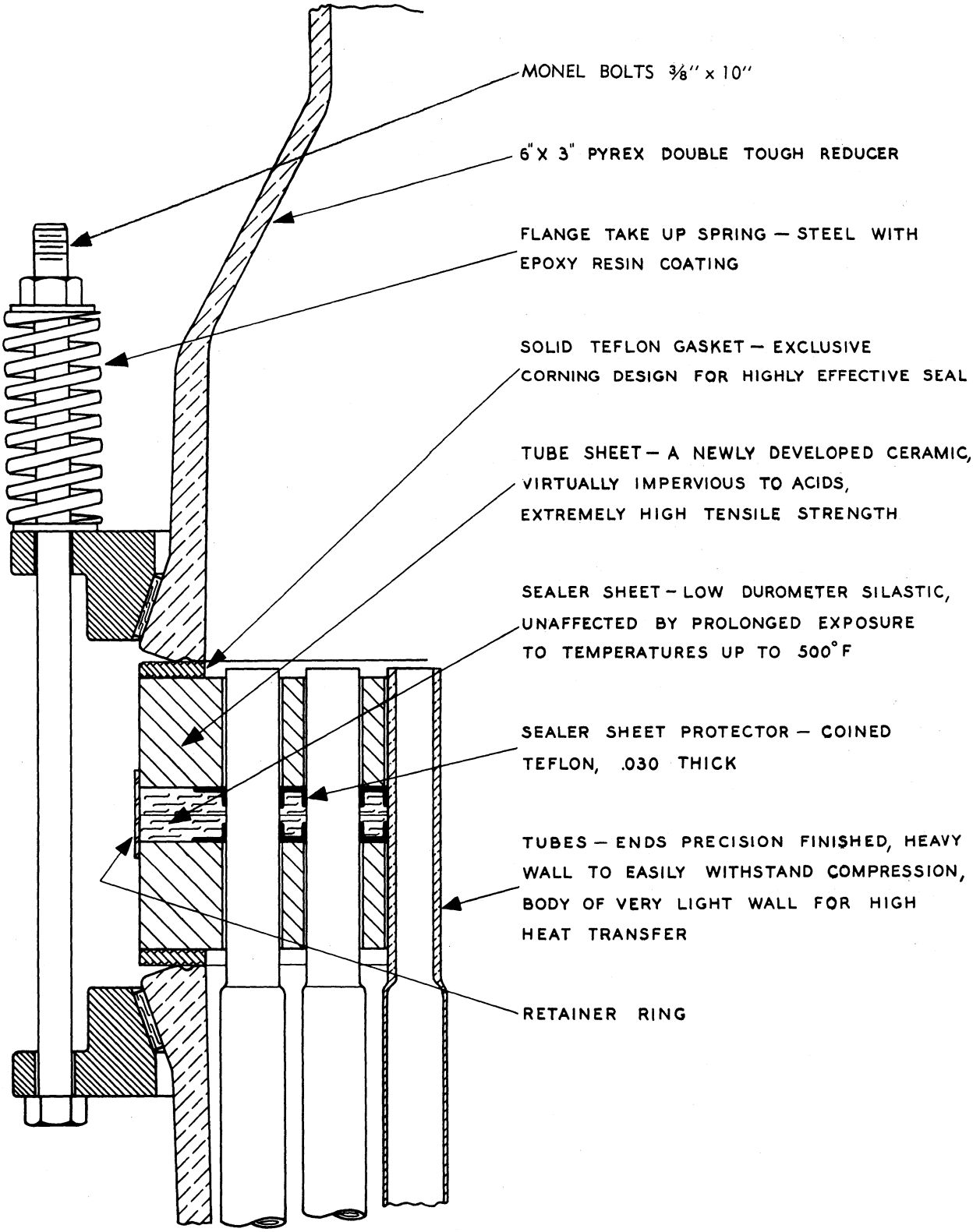

Fig. 4. Glass exchanger header assembly (courtesy Corning Glass Works)

of the solid Teflon gaskets and asbestos inserts in the flanges, (b) compensate for the thermal expansion of all sealing members, and (c) act as a pressure relief valve to protect the unit against damage in event of accidental pressure overloading. The maximum recommended pressure for the unit is 20 psi for both the tube side and the shell side.

The original bundle design contained 18 baffles, made of asbestos sheet, with a baffle window area 25 percent of the shell cross-sectional area, placed at 6 in. center-to-center spacing. The tube holes in the baffles were 13/16 in. diameter (as compared to the tube outside diameter of 3/4 in.) and the baffle diameter was 5-7/8 in. (as compared to the shell inside diameter of 6 in.), thus giving a tremendous amount of tube-baffle and baffle-shell leakage. The baffle tie rods, made of glass, extended only a few baffle spaces each. This, added with the fact that the asbestos baffles become quite pliable when wet, caused a tremendous distortion of the baffles when the shell-side flow was turned on. In view of these facts the original baffles were considered inadequate for the present study, and an improvement was sought.

The distortion of the baffles could be easily taken care of by using baffles made out of a rigid material and by extending the tie rods from end to end of the bundle. However, the elimination of the tube-baffle and the baffle-shell leakage was not so easy. The problem could not be solved simply by reducing the clearances. In fact large clearances are desirable from a mechanical viewpoint. The dimension tolerances of the glass shell and the tubes are fairly large as compared to metal shell and tubes. Therefore, reducing the clearances could

cause damage to the shell or at least to the rather delicate tubes. The problem was solved, after some research, by developing new baffles. The baffles, which eliminated the above problems and were used in this study, are of a sandwich design, consisting of two 1/16 in. brass plates with a layer of a 1/16 in. rubber sheet as sandwiching material (Figure 5). The brass plates, with the rubber in between, were riveted together to give the desired baffle. The diameter of the brass plates and that of the holes in them were essentially of the same size as those in the original asbestos baffles. This was done to ensure that the new baffles will not damage the shell or the tubes. The diameter of the rubber sheet was made larger than the inside shell diameter and the diameter of the holes smaller than the outside tube diameter. Such a design eliminated the tube-baffle and the baffle-shell leakage almost completely. Since these baffles are rigid and since the brass tie rods used extended from end to end of the tube bundle, the problem of the distortion of the baffles was also eliminated. Eight tie rods were used in each bundle. Figure 5 gives the drawing (to scale) of a baffle in place in the exchanger. It also shows the location of the tie rods and lines indicating the three baffle cuts used in this study.

Six tube bundles with the same tube size and arrangement but with different combinations of baffle cuts and baffle spacings were studied. Table I gives the baffle cuts and baffle spacings studied. Figure 6 gives the relationship between the baffle cut as a fraction of cross-sectional area and that as a fraction of diameter of the shell. Table II in Appendix A gives the detailed characteristics for the six bundles. In addition to the regular number of baffles in a bundle one uncut baffle on each end (next to the tube sheets) was used to lessen

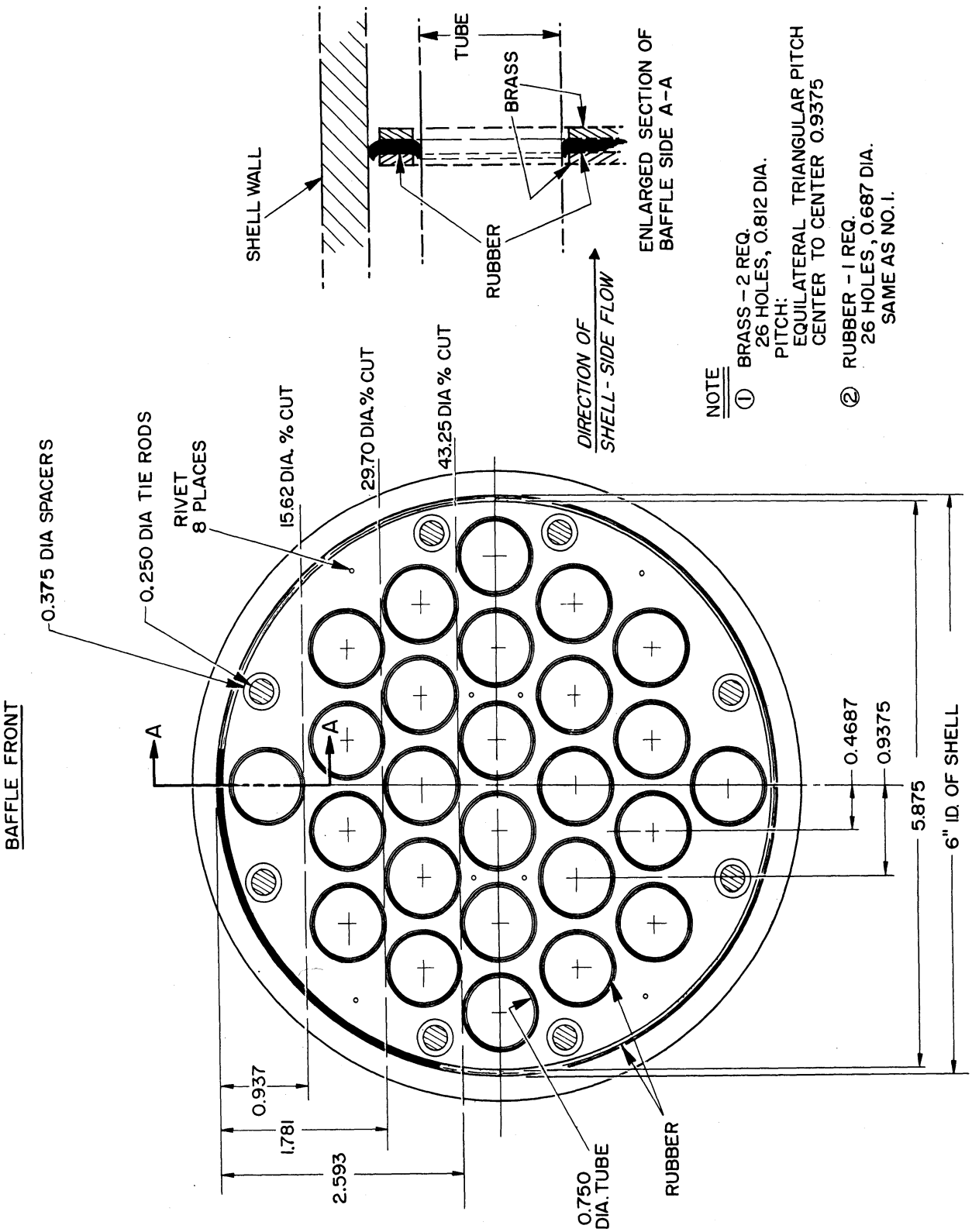

Fig. 5 Sandwich baffle, in place in the exchanger
(to scale)

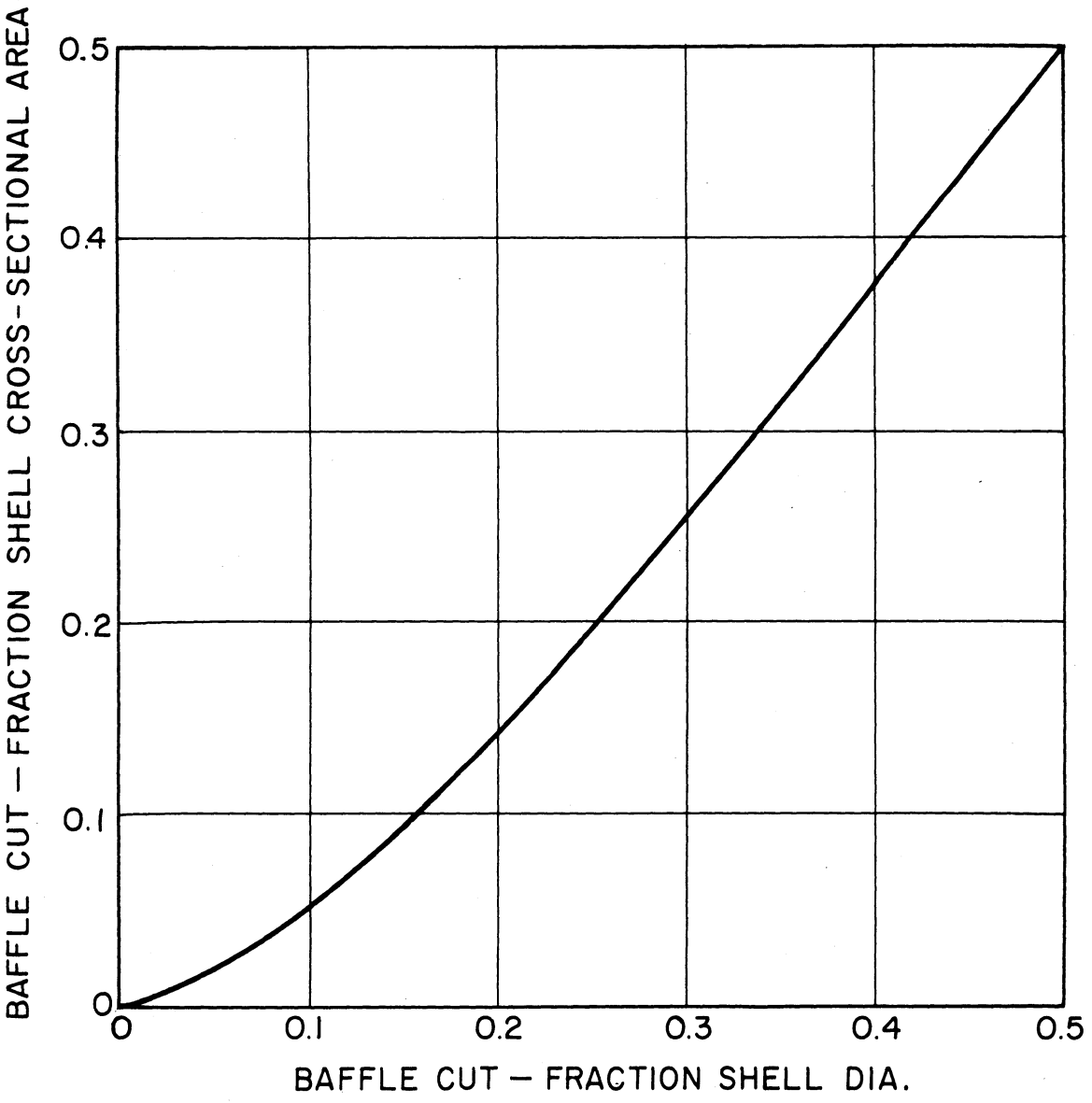

Fig. 6. Relationship between fraction diameter and fraction area baffle cuts

TABLE I. BAFFLE CUTS AND SPACINGS FOR THE SIX BUNDLES STUDIED

Bundle No.	Baffle Cut Dia. Percent	Baffle Cut Area Percent	Baffle Spacing Inches	Baffle Spacing/Shell Dia.
1	15.62	9.97	5.85	0.975
2	15.62	9.97	3.92	0.653
3	15.62	9.97	9.15	1.525
4	29.70	24.90	5.85	0.975
5	29.70	24.90	3.92	0.653
6	43.25	41.45	5.85	0.975

the load on the sealing system. Sections of appropriate length of 3/8 inch copper tubing slipped onto the 1/4 inch brass tie rods were used as baffle spacers. The test bundles were prepared outside the shell by first assembling the baffles, tie rods and spacers and tightening them in position with brass nuts (bearing on the end uncut baffles) on the threaded ends of the eight tie rods, and then slipping the tubes into the baffle tube holes after lubrication of the tubes and the rubber around the tube holes. After a bundle was ready it was slipped into the shell and the headers assembled in order to get the exchanger ready for operation.

All the four outlets from the glass exchanger were connected to the piping system through one-foot lengths of 2 inch diameter flexible brass hose. The glass exchanger was installed on an angle iron frame using rubber cushioning to absorb vibrations created by the pump. A galvanized sheet steel roof was provided above the glass exchanger in order to insure protection from falling objects.

Shell-Side Fluid Circulation System

Since the tubes in the test exchanger are made of glass and have a fairly high resistance to heat transfer [k/x_g = 260 Btu/(hr)(sq ft)(°F)], it was considered necessary to use such a fluid on the shell side which would give low values of film heat transfer coefficient in order to avoid the glass tube walls controlling the overall heat transfer. A water solution of propylene glycol (60-80 wt. percent) was chosen for this purpose and was used as the hot fluid on the shell side.

The circulation loop is illustrated in the flow diagram in Figure 2. The glycol solution was pumped from a storage tank through an auxiliary heater, a control valve, and a calibrated rotameter to the shell inlet of the glass test-exchanger. From the shell outlet the fluid went back to the storage tank. The piping used for the fluid circulation loop was 2 inch standard brass pipe. Threaded joints using common pipe dope were used for pipe connections. A double valve system for the introduction of plastic beads into the main fluid line before shell entrance was provided. Also a pipe strainer was provided in a by-pass streamline down-stream of the shell outlet to remove the plastic beads if and when introduced at the shell inlet. The major pieces of equipment in the circulation loop are described below.

Storage Tank

One hundred and twenty gallon capacity closed tank provided with an air vent. Material of construction of the tank was copper.

Circulation Pump

A Viking, special 2-1/2 inch iron fitted, rotary pump with special bronze bushings was used (type ZLQ). It was run by a 3 H.P. motor by means of V-belt pulleys. The pump was rated for a capacity of

90 gallons per minute at 390 revolutions per minute. A 2 inch by-pass stream from the outlet of the pump back to the storage tank was provided in order to regulate the pumping capacity.

Auxiliary Heater

A Ross "BCF" oil cooler (cat. no. 842) manufactured by the Ross Heater and Manufacturing Company, Buffalo, New York, was used for the purpose. This unit has an 8 inch copper shell and 214 brass tubes, 3/8 inch diameter and 4 feet long. The heat exchanger is of a fixed-head type and has four passes on the tube side and one pass on the shell-side. The shell side is equipped with segmental baffles. The fluid was passed on the tube side and 60 psig steam on the shell side. This was done because only the inside of the tubes in the exchanger could be cleaned, it being of the fixed-head type. A steam trap was installed at the shell outlet.

Rotameters

See under instrumentation.

Line Strainer

A Schutte and Koerting pipe line strainer (bronze) 2 inch size, angle type (Figure 956 of Schutte and Koerting Bulletin No. 9-S) with a 30 mesh screen was used. Ordinarily the flow by-passed the strainer. The flow passed through the strainer only when plastic beads were being introduced at the inlet of the test-exchanger shell.

Particle Introduction System

This consisted of a 1/2 inch pipe attached vertically to the 2 inch main line just before the entrance to the shell side of the test-exchanger. Two gate valves were provided in this pipe so that the particles could be introduced without the fluid from the main line

leaking out. In the actual study, for reasons described in a later section, the particle introduction method was not used for the flow pattern studies, and therefore the particle introduction system and the line strainer were not used.

Cooling Water System

Since it was necessary that the shell-side heat transfer resistance be a major part of the overall heat transfer resistance in the glass test-exchanger, and since the resistance of the glass tubes was fixed, it was considered necessary that the tube-side resistance be low. Due to this consideration and the fact that it is the most easily available cooling agent, water was used as the cooling agent on the tube-side of the glass test-exchanger. A flow diagram for the cooling water circuit is included in Figure 2. Cooling water from the mains is passed through the shell-side of an auxiliary heater to regulate the temperature of the inlet stream to the tube side of the glass test-exchanger. From the auxiliary heater, which was exactly of the same construction as that in the shell-side fluid circulation loop, the cooling water was piped to the tube-side entrance of the glass test exchanger after having passed through a set of two globe valves and two calibrated rotameters arranged in parallel in the water line. Two rotameters were used because of capacity considerations. From the outlet of the glass test-exchanger tube-side the water was piped to the drain. The piping used was 2 inch standard brass pipe before entrance into the test-exchanger and 2 inch standard wrought-iron pipe from the outlet of the exchanger to the drain.

Instrumentation

Proper instrumentation was provided to measure the flow rates of the shell and the tube side streams, to measure the temperatures of the inlet and outlet streams of both the shell and the tube sides, and to measure the pressure drop between the inlet and outlet of the shell side of the test-exchanger.

Flow Rate Measurement

Two Fischer and Porter Figure No. 26P-E Rotameters in parallel were used in each line to measure the shell-side and the tube-side flow rates. The use of two rotameters in each line was necessitated because one was inadequate to handle the maximum flow rates expected to be encountered. These rotameters have a brass body, a Fischer and Porter Company Precision Bore Rotameter Tube No. 12LL-25 graduated from 0 to 200 standard cubic feet per minute (in 2 CFM divisions) for a gas with a specific gravity of 0.877 at 14.7 psi absolute pressure and 60°F, and are equipped with stainless steel floats. Each of the four rotameters was calibrated with water from the mains by weighing the amount flowing into a weighed tank in a given time. The calibrations were corrected for densities of the liquids whose flow rates were actually measured during the heat transfer tests, according to charts provided by the manufacturer.[19] The viscosity correction for the range of use in the present study was found to be negligible.

Temperature Measurement

Both thermometers and thermocouples were provided at the inlets of the shell- and the tube-sides as well as at suitable points downstream of the outlet from the two sides of the test exchanger. The thermometer bulb and the thermocouple junction in a line were so placed

as to give the mixed mean temperature of the stream. This was accomplished by locating them in elbows or tees in the piping in order to give thorough mixing of the stream at the point of temperature measurement. The thermometers used had a range of 0 to 100°C and were graduated in 0.1°C intervals. All the four thermometers were calibrated against a National Bureau of Standards calibrated thermometer. The thermometers were used as a check on the thermocouples and for quick readings necessary when controlling the mean of the inlet and outlet temperatures of a particular stream at a constant value. For the temperatures to be used in the heat transfer calculations copper-constantan thermocouples were used. The thermocouples were prepared in the laboratory and checked against a National Bureau of Standards calibrated Thermometer. The leads from all the four thermocouple hot junctions were connected to a Multiple-Point Rotary Selector Switch from which one couple at a time could be routed on a single pair of insulated leads to a potentiometer (Leeds and Northrup Portable Precision Model 8662) and a cold junction in a melting ice bath. The galvanometer sensitivity of the potentiometer permitted readings within 2 microvolts. The reproducibility of thermocouple readings during runs varied from 2 to 10 microvolts (approximately 0.1 to 0.5°F). The millivolts read from the potentiometer were converted directly to the temperature in degrees F using Leeds and Northrup Standard Conversion Tables.[34]

Pressure Drop Measurement

The pressure drop between the inlet and the outlet of the shell side of the glass test-exchanger was measured with a Meriam manometer with a scale range of 0 to 31 inches using mercury as the manometer fluid.

The manometer was connected to the shell inlet and outlet by 1/4 inch copper tubing.

Equipment and Materials for Flow Pattern Studies

In the initial phases of the study the flow was made visible by the introduction of polystyrene beads (Dow) about 20 mesh size. The beads were introduced in the shell-side fluid at the shell inlet through a double valve system and were removed from the stream by a pipe strainer downstream from the shell outlet. However, in the major portion of the actual study the particles were not considered necessary for the flow visualization.

Westinghouse Reflector Photoflood RFL-2 lamps were used for lighting of the exchanger both for photographing and for visual observations. A 4 inch by 5 inch Crown-Graphic camera on a tripod (or on a proper clamp for pictures from the bottom) was used for photography. Different negative sheet film materials and printing papers were tried. As indicated in a later section, for the actual flow pattern studies the photographic recording of the flow patterns was discarded in favor of sketches drawn from visual observations, since the latter method of recording was considered more practical for the present studies.

CHAPTER IV

EXPERIMENTAL PROCEDURE

Each tube bundle tested was assembled outside the shell, and then slipped into position in the shell. The headers were then assembled and the exchanger connected to the system piping. The exchanger was then ready for testing. The experimental procedure is discussed here in two sections, namely, measurement of heat transfer and pressure drop, and flow pattern studies.

Heat Transfer and Pressure Drop

To study the shell-side heat transfer characteristics of a shell-and-tube heat exchanger data are usually obtained on the overall heat transfer coefficient, which can be calculated from a knowledge of the flow rates and the inlet and outlet temperatures of the shell-side and the tube-side streams. From a consideration of the basic equation:

$$Q = [W C_p (T_{out}-T_{in})]_t = [W C_p (T_{in}-T_{out})]_s = U_o A_o (T_s - T_t)_{lm} \qquad (9)$$

it is evident that the overall heat transfer coefficient (based on outside area) can be calculated for a particular run if the flow rate of either of the two streams and the inlet and outlet temperatures of the two streams, in addition to the fluid properties at the temperatures concerned, are available. Usually, due to heat losses to the atmosphere there is some discrepancy between the shell side and the tube side heat duties. Normally, when the hot liquid is on the shell-side (as in the present case) the shell side heat duty will be found to be somewhat larger than the tube-side heat duty. For good results this discrepancy

should be fairly small. To check against this possible error, it was considered advisable to measure both the flow rates in place of only one. The difference between the shell-side and the tube-side heat duties was almost always less than 6 percent of the tube-side heat duty. For most heat balances this difference was considerably less than this maximum value. Since the shell-side heat duty includes the heat dissipated to the atmosphere, the tube-side heat duty was used for the calculation of the overall heat transfer coefficient.

The shell-side heat transfer coefficients are usually calculated from the overall heat transfer coefficients by application of the principle of additive resistances, first proposed for this purpose by Wilson[64] in 1915, and commonly known as a Wilson plot. In a shell-and-tube heat exchanger, the heat has to traverse through a shell-side-fluid-film, the tube wall, and a tube-side-fluid-film, in addition to any other films (dirt, etc.) which may be present. Since these films lie in the path of the heat in series the resistances offered by each film must add up to give the total resistance to heat transfer. This can be expressed as:

$$R_{total} = R_{shell} + R_{wall} + R_{tube} + R_{fouling} \qquad (10)$$

or in terms of heat transfer coefficients:

$$\frac{1}{U_o} = \frac{1}{h_o} + \frac{x_g A_o}{k_g A_g} + \frac{A_o}{h_i A_i} + R_{fouling} \qquad (11)$$

The term representing the tube wall resistance can be safely assumed to be constant. The fouling factor during a particular run also remains fairly constant. Equation (11) then reduces to:

$$\frac{1}{U_o} = \frac{1}{h_o} + \frac{A_o}{h_i A_i} + \text{Constant} \qquad (12)$$

A consideration of equation (12) shows that if either h_o or h_i is kept constant during a test, the other will be proportional to U_o, the overall heat transfer coefficient. This offers two alternatives for the test procedure, namely, either to keep h_o constant or to keep h_i constant.

If h_o is kept constant during a particular test, equation (12) reduces to:

$$\frac{1}{U_o} = \frac{A_o}{h_i A_i} + \text{Constant} \qquad (13)$$

If the average tube-side temperature is fairly constant (effect of physical properties can be neglected):

$$h_i = C_t W_t^{0.8} \qquad (14)$$

Substituting equation (14) in equation (13) gives:

$$\frac{1}{U_o} = \frac{A_o}{A_i C_t W_t^{0.8}} + \text{Constant} \qquad (15)$$

Equation (15) indicates that a plot of $1/U_o$ vs. $1/W_t^{0.8}$ will be a straight line with a slope $A_o/A_i C_t$ and an intercept equal to the constant of equation (15) which equals

$$\frac{1}{h_o} + \frac{x_g A_o}{k_g A_g} + R_{fouling}$$

This is the method usually used for the calculation of shell-side coefficients in tests on shell-and-tube heat exchangers. Usually the

value of $x_g A_o / k_g A_g$, the tube wall resistance, is very small and also the fouling resistance is small as compared to the shell side film resistance. So, the shell-side resistance, and thus the coefficient, can be calculated with a fair degree of accuracy. However, in the present case, the tube wall is made of glass and has a high resistance (comparable to or even more than the shell side film resistance) and any errors in the determination of this resistance will greatly affect the shell-side resistance calculated by this method.

Let us consider the other alternative in equation (12). If h_i is kept constant during a particular test, equation (12) reduces to:

$$\frac{1}{U_o} = \frac{1}{h_o} + \text{Constant} \tag{16}$$

From the correlations usually used for shell-side heat transfer coefficient:

$$h_o = C_s W_s^{\,n} \tag{17}$$

if the average shell-side temperature is constant. The value of n usually used is 0.6. Substituting equation (17) in equation (16) gives:

$$\frac{1}{U_o} = \frac{1}{C_s W_s^{\,n}} + \text{Constant} \tag{18}$$

Equation (17) indicates that a plot of $1/U_o$ vs. $1/W_s^{\,n}$ will be a straight line with a slope $1/C_s$ and an intercept equal to the constant of equation (18) Substituting the value of C_s obtained from the slope in equation (17), the shell-side heat transfer coefficient can easily be evaluated for any values of shell-side flow rate for which equation (17) is applicable. This procedure gives the value of the shell-side

heat transfer coefficient independent of the other resistances, and thus the errors involved in subtracting numbers of equal magnitude, as in the first procedure, are eliminated. This procedure has the further advantage that each Wilson plot gives the shell-side coefficient for a number of shell-side flow rates, whereas in the previous procedure, each Wilson plot gives the shell-side coefficient for only one shell-side flow rate.

In view of these facts it was decided to use the second Wilson plot procedure involving a constant tube-side coefficient and variable shell-side flow rate for each run. To keep the tube-side coefficient constant the tube-side flow rate and the average of the inlet and outlet tube-side temperatures were kept constant during each run. The average tube-side temperature was kept constant by adjusting the temperature of the inlet cooling water which was accomplished by regulating the supply of steam to the auxiliary heater in the cooling water system. An average of the inlet and outlet shell-side temperatures was also kept constant in a similar manner. This was done to minimize the effect of the changes in physical properties on the shell-side heat transfer coefficients during a particular run. For purposes of comparison, an average shell-side temperature of about 45°C was used in all the runs. A run consisted of equilibrium flow rate and temperature measurements for a series of shell-side flow rates at a constant tube-side flow rate and constant average shell-side and tube-side temperatures. The shell-side flow rates were varied between 7,000 and 40,000 lbs per hr of the glycol solution used on the shell side. A minimum of seven sets of readings with different shell-side flow rates were recorded for each run. For

some of the runs the number of sets of readings was as high as 11. Two or more runs were made for each of the first four tube bundles tested. Due to the good agreement of the results for different runs in each of these bundles, it was decided to make only one run each for the last two bundles. Each set of readings for a particular shell-side flow rate in a run consisted of recording the positions of the floats in the four rotameters, the pressure differential indicated by the manometer, and the millivolt readings from the potentiometer corresponding to the temperatures of the inlet and outlet of the shell- and the tube-sides. Due to fluctuations in the temperatures, 10 values of the potentiometer reading were recorded for each temperature measurement and a mean of these 10 values used for determining the temperature from the conversion charts. The potentiometer readings for a particular flow rate were recorded in a cyclic order so that readings for all the four thermocouples were recorded one after the other and the cycle repeated 10 times. The order followed in this regard was: tube-side outlet, tube-side inlet, shell-side inlet, shell-side outlet. Each set of the readings for a shell-side flow rate was taken after the system had reached steady state after changing the flow rate and adjusting the tube-side and shell-side inlet temperatures. The variation of the shell-side flow rate in each run was from the highest to the lowest value. The refractive index of the shell-side propylene glycol solution was accurately measured for each run. This was used as a means of finding the propylene glycol concentration of the solution (from tables given by Curme and Johnston[12]), a knowledge of which is essential for determining the fluid physical properties to be used in processing and analysis of the data. Occasionally the viscosity and the density of the glycol solution were also

determined in order to check the glycol concentration obtained from the refractive index measurement. Table III in Appendix A gives a sample data sheet for Run 36 of Bundle No. 6. The data are reported in Table IV in Appendix A.

Flow Patterns

The study of the flow patterns of the fluid on the shell-side posed quite a problem. Several methods which could possibly be used had to be discarded because they would interfere with the heat transfer study. Since it was the objective to carry out the flow pattern study simultaneously with the heat transfer study it was very important that the means used for the flow pattern study should not interfere with the heat transfer study.

As a first attampt, introduction of polystyrene beads into the shell-side stream was used for the visualization of the flow patterns. The beads, about 20 mesh in size (supplied by the courtesy of the Dow Chemical Company) were introduced into the shell-side stream through a double valve system provided for this purpose near the shell-inlet, and were strained out of the system by a Line Strainer provided downstream of the shell-outlet. The beads were, thus, not allowed to circulate through the pump. The particles were illuminated from the back by photo-flood lamps and their motion was recorded photographically by a short exposure. Various negative materials, lens openings, exposure times, and developing procedures were tried. Figure 7 shows an enlarged print on No. 4 (hard) enlargement paper made from a negative on Kodak Royal Pan Sheet Film exposed with a lens opening of f 32 and an exposure time of 1/50 of a second. Normal recommended developing procedure was used. The path of the plastic beads is indicated in this

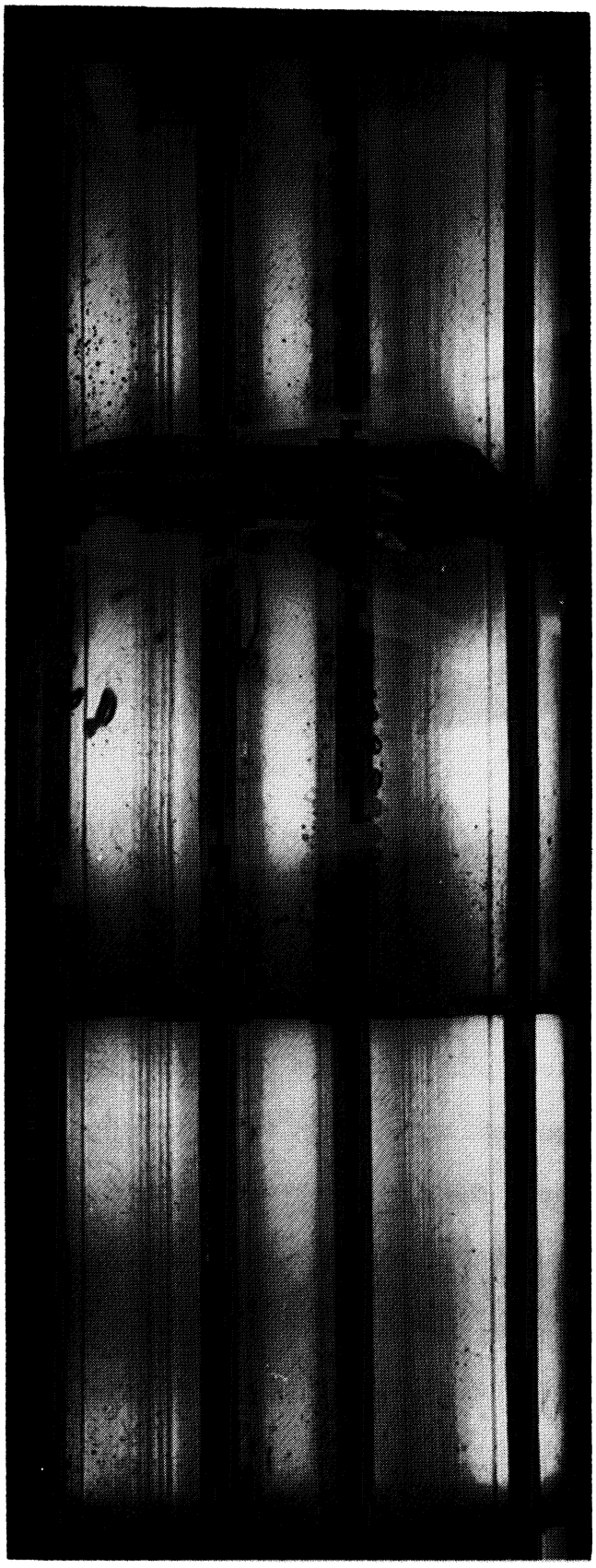

Fig. 7. Photograph of flow pattern with plastic bead tracers

photograph by short streaks. The length of these streaks along with the knowledge of the exposure time and the ratio of the dimensions in the photograph to those in the exchanger can be very useful in a study of the local velocities. But this procedure does not give much useful information about the overall flow patterns in the baffled shell. For dividing the flow in the shell into regions of different characteristic flows a knowledge of the general flow pattern is very essential. A knowledge of the local velocities, though usually of great importance, does not serve the purpose in the present application because at present there is no way of analyzing this information and using it quantitatively for the heat transfer calculations. Further, the effect of the introduction of the plastic beads into the shell-side stream on the heat transfer is uncertain. Due to these facts and the difficulty in manipulating the photographic technique because of the extremely short duration for which the plastic beads stay in the system, this method was abandoned in favor of a more promising technique.

During the flow pattern studies with the introduction of plastic beads with the lighting from the back, it was discovered that the flow patterns became very clearly visible without the introduction of the beads when viewed from the direction of the lighting. This could probably be due to two reasons. Firstly, the solutions of propylene glycol used for the present study may exhibit the property of the planes of equal shear in the liquid becoming visible which was attributed by Hagerty[26] to certain concentrations of glycerine-water solutions. Propylene glycol being similar in physical properties to glycerine could very possibly exhibit this characteristic. Another factor which could be responsible, either by itself or in conjunction with the previously

mentioned factor, for this flow visualization without any tracer particles, is the presence of some dirt and suspended impurities in the glycol solution. A check of the physical properties showed that these impurities were not present in concentrations sufficient to alter the physical properties to any appreciable extent. Whatever this visualization of the flow patterns may be due to, it was found to be a very convenient means of studying the flow patterns in the present study.

Therefore, for the actual study, the lighting was provided from the front and was arranged tangent to the shell. The arrangement of the lights was quite important because due to the front lighting, the reflections from the glass surface become quite significant and must be minimized by proper arrangement of the lights. Usually dim lights gave better results. Attempts at photographing these flow patterns were not very successful. A few good exposures were obtained after considerable research, and a sample of these is included with the data in the next chapter. Even the best photographs obtained did not show the details of the patterns as well as these could be observed visually. Therefore, it was decided to record the flow patterns by sketches (to scale) made from visual observations. The significant dimensions in the patterns could be easily measured by a scale.

CHAPTER V

EXPERIMENTAL AND PROCESSED DATA

A summary of the experimental and processed data is given in Table IV of Appendix A. The experimental data and their processing are described here in three sections, namely, heat transfer, pressure drop, and flow patterns.

Heat Transfer

The original heat transfer data for each run consisted of rotameter and potentiometer readings for a series of shell-side flow rates. (Table III in Appendix A shows a Sample Data sheet.) The ten potentiometer readings for each temperature were averaged and the temperature read off a conversion chart. The rotameter readings were converted to pounds per hour of the fluid flowing on each side by use of the calibration chart, and corrected for density obtained from Figure 32 in Appendix C. Data for the densities of propylene glycol solutions at the temperatures encountered in the present tests are not available in the literature. Carbide's[9] data is reproduced in Figure 33. Figure 32 in Appendix C is an extrapolation of the data published by Curme and Johnston[12] and by MacBeth and Thompson.[36] Knowing the shell-side and the tube-side flow rates and the inlet and outlet temperatures of the shell- and tube-side streams, in addition to the concentration of propylene glycol in the shell-side fluid, the heat duties for both the shell and the tube sides were calculated. The check between the tube-side and the shell-side heat duties was found to be usually better than 6 percent.

The overall heat transfer coefficient for each flow rate was then calculated using the tube-side heat duty, the outside effective heat transfer area of the tubes, and the logarithmic mean temperature difference. When the ratio of the temperature differences on the two ends of the exchanger was 1.1 or less, an arithmetic mean temperature difference was used in the overall heat transfer coefficient calculations. Table IV in Appendix A gives the original data as the shell-side and tube-side flow rates in pounds per hour and the temperatures of the inlet and outlet of the shell-side and tube-side streams in °F, along with the propylene glycol concentration of the shell-side solution. It also gives the calculated overall heat transfer coefficients along with the major intermediate steps in their calculation.

The next step in the processing of the heat transfer data was the calculation of the shell-side heat transfer film coefficients using the Wilson plot technique. Though the average of the inlet and outlet shell-side temperatures was kept constant during the experimentation, it was felt that since the propylene glycol concentration changed from run to run and since for the present case it is the film temperature and not the average temperature at which the physical properties of the shell-side fluid should be evaluated, the effect of the variations in the physical properties on the shell-side heat transfer film coefficient could not be neglected. So in developing the equation representing the Wilson plot, the following equation should be used instead of equation (17):

$$h_o = C\, k_f \left(\frac{W_s}{\mu_f}\right)^n \left(\frac{C_p\, \mu}{k}\right)_f^{0.33} \qquad (19)$$

A least square deviation analysis of the present data showed that the use of a value of 0.65 for n gave a better fit of the data than

the use of the usual value of 0.6. Therefore, n was taken as 0.65 so that equation (19) becomes:

$$h_o = \frac{C W_s^{0.65} C_{p_f}^{0.33} k_f^{0.67}}{\mu_f^{0.32}} \qquad (20)$$

The film temperature of the shell-side fluid was defined as:

$$T_f = 1/2 \, (T_{bulk} + T_{surface}) \qquad (21)$$

The surface temperature required for the calculation of the film temperature was calculated by proportioning the mean temperature difference in the ratio of the film resistances on the tube side and on the shell side:

$$\frac{T_{s.s.\ avg.} - T_{t.b.\ avg.}}{T_{s.b.\ avg.} - T_{t.b.\ avg.}} = \frac{\text{overall resistance - shell-side resistance}}{\text{overall resistance}}$$

$$= \frac{U_o}{U_o - h_o} \qquad (22)$$

As is apparent from equation (22), the calculation of the average surface temperature on the shell side requires a knowledge of the ratio of the heat transfer resistances. However, the values of the resistances or coefficients for this purpose do not have to be very exact since slight errors in the calculated film temperature can be tolerated. The heat transfer film coefficients for this purpose were obtained by making preliminary Wilson plot analysis neglecting the effect of the physical property changes (i.e., plotting $1/U_o$ vs. $1/W_s^{0.65}$). A least square fit of the data was obtained.

Using the film temperature obtained by the procedure outlined above the physical properties (C_p, μ, k) of the shell-side fluid at the film temperature were evaluated from property charts published by the Carbide and Carbon Chemicals Company,[9] and reproduced in Figures 34, 35, and 36 in Appendix C. The shell-side heat transfer film coefficients were then obtained by the Wilson plot technique plotting:

$$\frac{1}{U_o} \quad \text{versus} \quad \frac{\mu_f^{0.32}}{W_s^{0.65} \; C_{p_f}^{0.33} \; k_f^{0.67}}$$

Figure 8 gives a sample Wilson plot for Run 36 on Bundle No. 6. A least square fit of the data was made for the Wilson plots for all the runs. Table IV in Appendix A lists the slope, the intercept, and the sum of the squares of deviations of the data from the straight line (s^2) for all the runs reported. As pointed out earlier, the slope of the Wilson plot is a measure of the shell-side heat transfer film coefficient. Specifically, the slope, b, equals the reciprocal of the constant, C, in equation (20), i.e.,

$$b = \frac{1}{C} = \frac{1}{h_o \left(\dfrac{\mu_f^{0.32}}{W_s^{0.65} \; C_{p_f}^{0.33} \; k_f^{0.67}} \right)} \tag{23}$$

or

$$h_o = \frac{1}{b \left(\dfrac{\mu_f^{0.32}}{W_s^{0.65} \; C_{p_f}^{0.33} \; k_f^{0.67}} \right)} \tag{24}$$

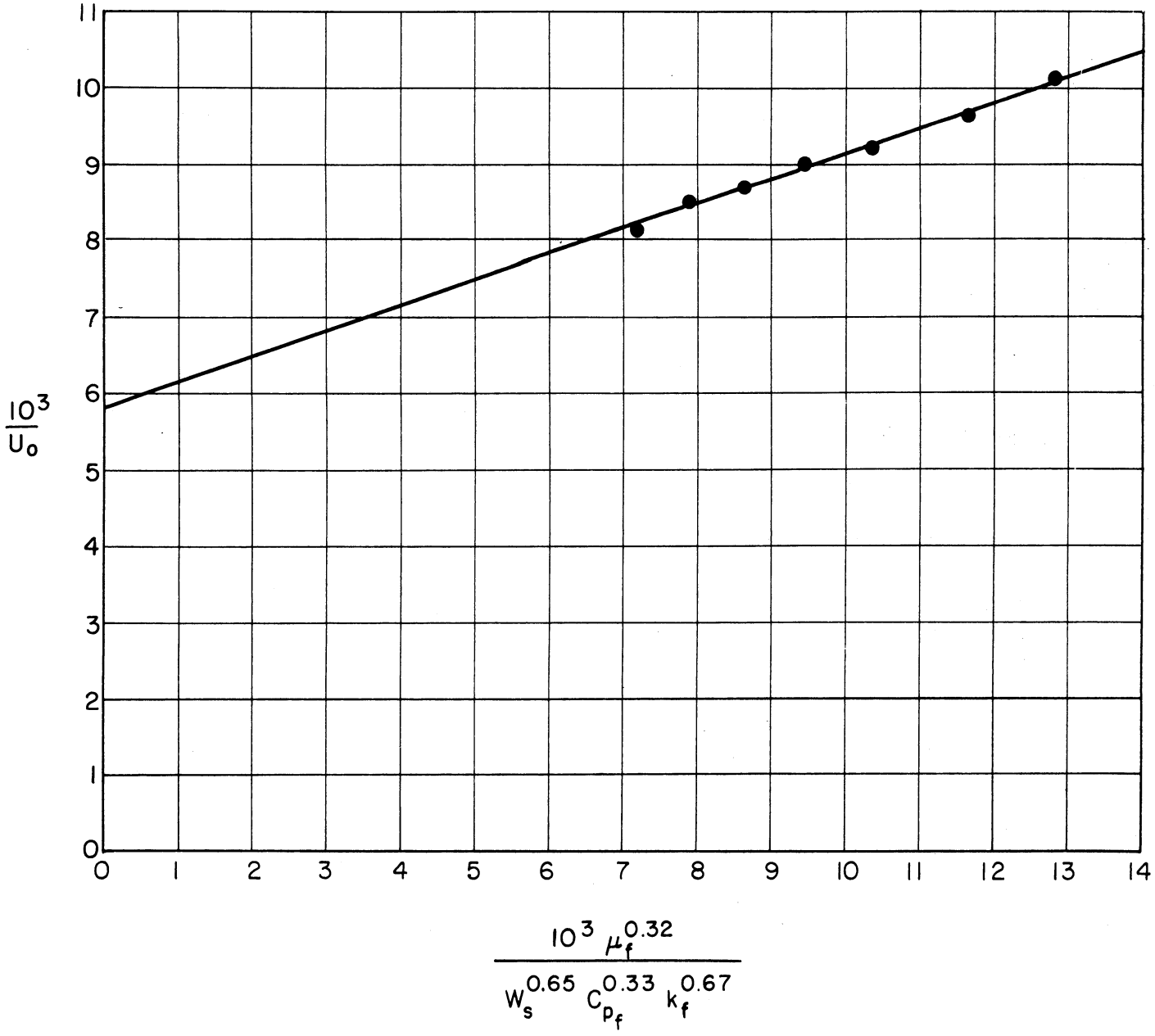

Fig. 8. Sample Wilson plot (run 36, bundle no. 6)

The value of the shell-side heat transfer film coefficient, h_o, for each shell-side flow rate in a run was, therefore, calculated by equation (24) using the slope of the Wilson plot, b, for that particular run. The values of h_o thus calculated for all the runs reported are listed in Table IV of Appendix A. The slope of the Wilson plot, b, being a measure of h_o, is a good measure for the comparison of the shell-side heat transfer performance of the various bundles tested.

The reliability of the results is indicated by the reproducability of the Wilson plot slopes for different runs on the same bundle. A comparison of these slope values given in Table IV (Appendix A) shows that the maximum deviations are of the order of 3 percent.

Pressure Drop

For each shell-side flow rate in all the runs the pressure drop of the shell-side fluid between the inlet and outlet of the shell was read off the mercury manometer (in inches of Hg) when steady state had been attained by the system. The pressure drop data for all the six bundles tested are listed in Table IV of Appendix A. The pressure drop data were obtained mainly to facilitate a comparison of the shell-side performance of the bundles tested, if the present heat transfer data were desired to be used by somebody for that purpose.

Since the pressure drops measured were usually quite large, measurement errors were quite small. The manometer could be read with an accuracy of $\pm$ 0.05 inch. Considering that the lowest pressure drop reading reported is 1.25 inches, the reliability of the pressure drop data is considered better than $\pm$ 4 percent.

Flow Patterns

As pointed out earlier, photographic recording of the flow patterns was not very successful. Only a few successful exposures were made. Figure 9 shows photographs illustrating the front view (plane perpendicular to baffle cut) and the bottom view (plane parallel to baffle cut) of the flow patterns at the shell-side flow rate of 13,700 pounds per hour during Run 19 for Bundle No. 1. The exposures were made on a Kodak Contrast Process Panchromatic 4 in. x 5 in. sheet film with a lens opening of 4.7 and a shutter speed of 1/25 second. The films were developed in Kodak D-11 for 8 minutes and fixed in Kodak F-5. The prints are enlargements on No. 4 (hard) enlarging paper developed in Kodak D-72 for 1 minute.

The photographs of Figure 9 represent the best results that could be obtained photographically. Even in these pictures the details of the flow pattern are not so pronounced as they could be observed visually. Therefore, the flow patterns for all the runs were recorded by sketches (to scale) made from visual observations. For each run the flow pattern was observed throughout the run and was sketched for every shell-side flow rate. For a particular bundle the flow pattern was the same during all the runs. The volumes of the regions of different flow characteristics in the flow pattern remained essentially constant with variations in shell-side flow rate for the range of flow rates studied even though the degree of activity within the various regions varied with the flow rate variations. Within the range of the present study the flow patterns seemed to be affected only by the bundle design. It may be recalled that the six bundles studied differed only in baffle cuts and baffle spacings.

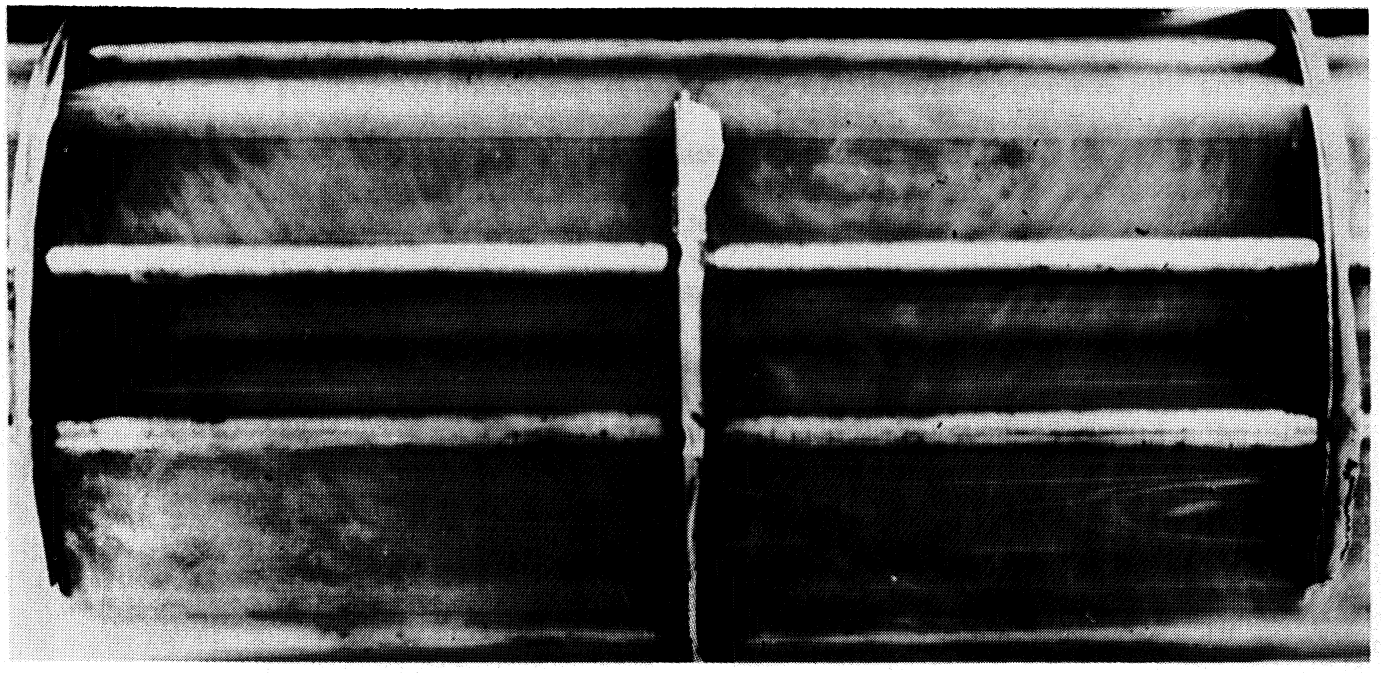

Front view

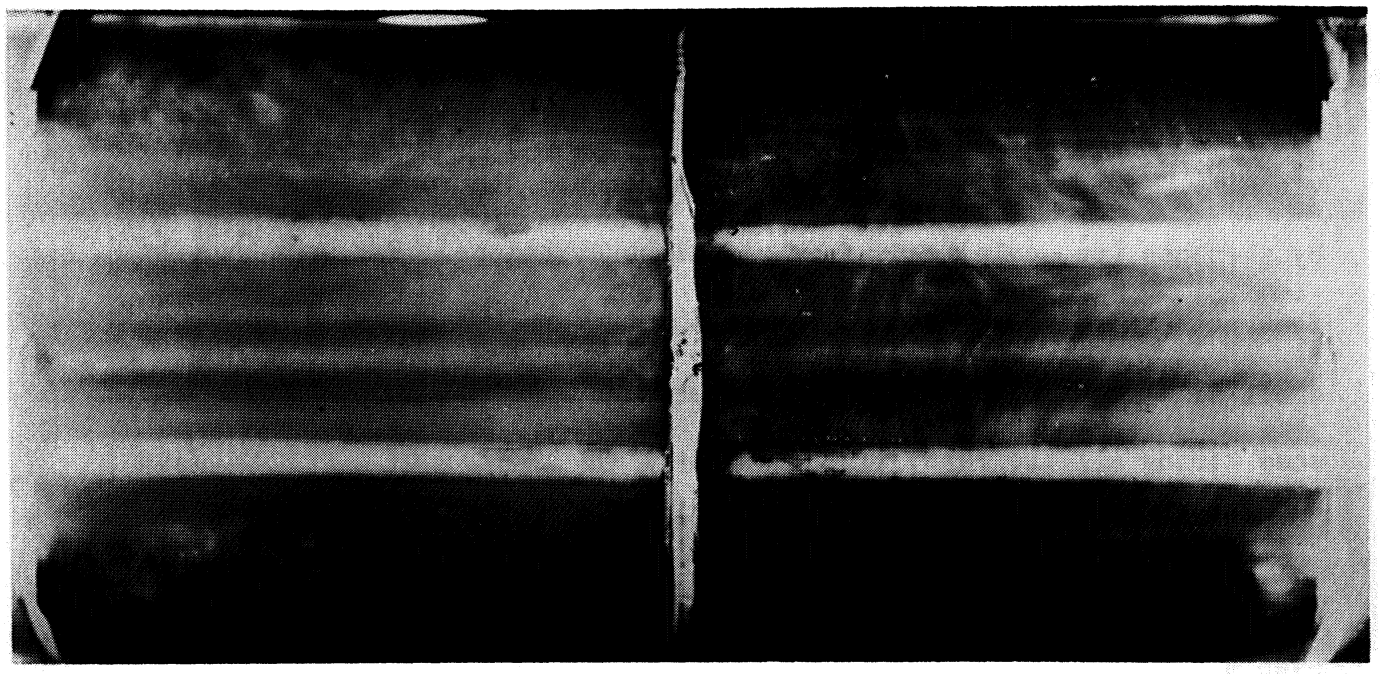

Bottom view

Fig. 9. Photographs of flow pattern at W_s = 13,700 for run 19, bundle no. 1

Figures 10 to 15 give the sketches for the shell-side flow patterns in the exchanger with the six bundles studied. Each figure gives the front (perpendicular to baffle cut) and the bottom (parallel to baffle cut) view of the flow pattern in the exchanger with a particular bundle. The sketches are drawn to scale and the significant dimensions are indicated on them. The measurement of these dimensions could be off by ± 1/4 inch. A study of the flow patterns in Figures 10 to 15 shows that the flow patterns change significantly with changes in baffle cut and baffle spacing.

As reported by Eckert and Irvine[17] for flow in corners of passages with non-circular cross-sections, laminar and turbulent flows exist simultaneously and side by side in the exchanger shell. However, it is not possible to divide the flow into regions of these two categories. Due to the complex geometry on the shell side the flow patterns are quite complicated. Before entering a baffle window the fluid flowing vertically between that baffle and the previous one makes a sharp turn and flows through the window almost parallel to the tubes and countercurrent to the direction of flow of the fluid inside the tubes. This horizontal flow of the fluid through the window is referred to as "Longitudinal Flow" in the ensuing discussion. The flow is very similar to the flow of a fluid outside a tube bundle and parallel to the tubes. After passing through the baffle window and flowing for some distance the fluid makes another turn and then flows vertical to the tubes. The distance for which the fluid travels after passing the baffle window and before turning, as well as the sharpness of the turn are determined by the size of the baffle cut and the distance between successive baffles. The flow of the fluid after it turns from the longitudinal flow region

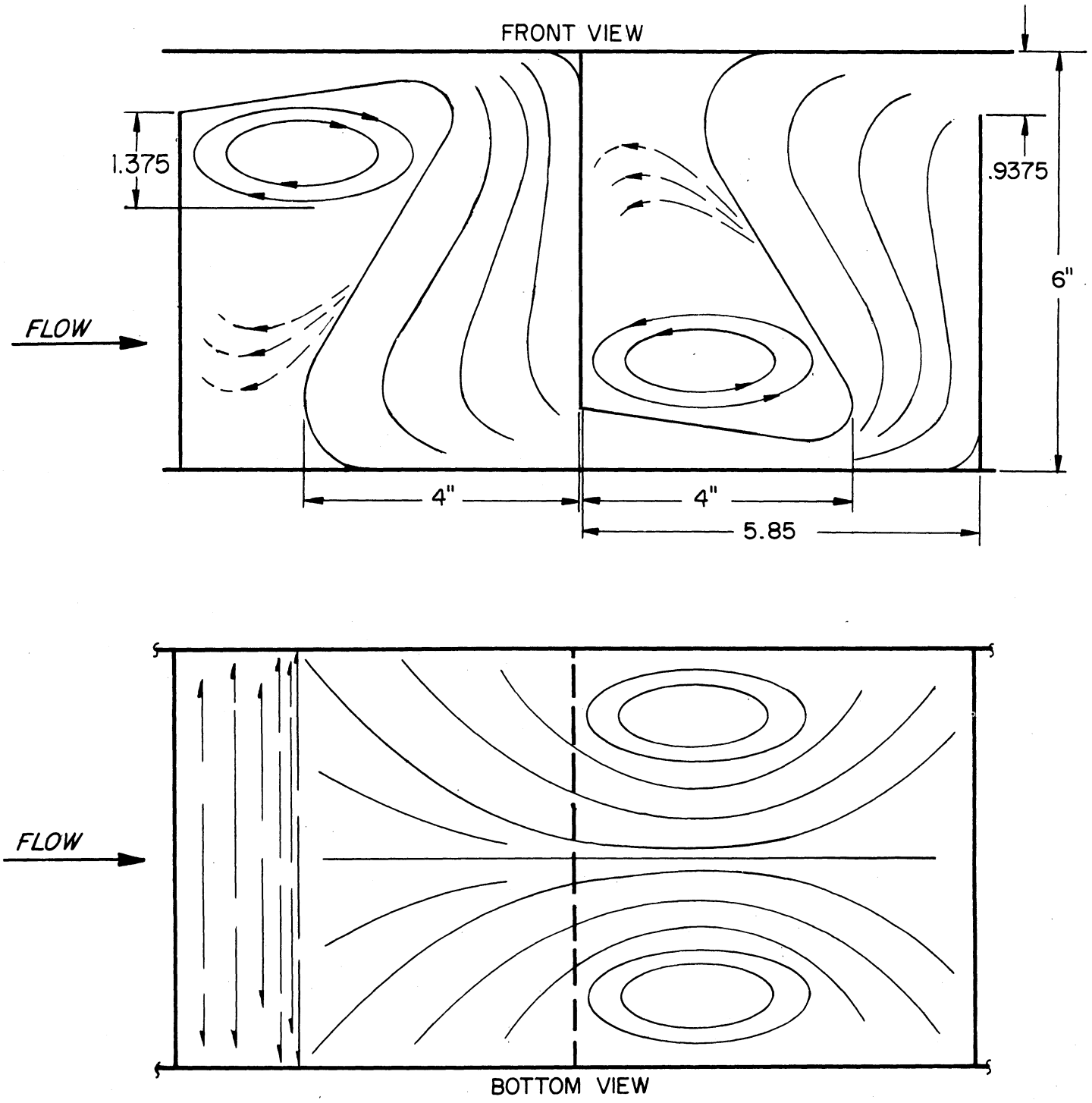

Fig 10 Flow pattern for bundle no 1

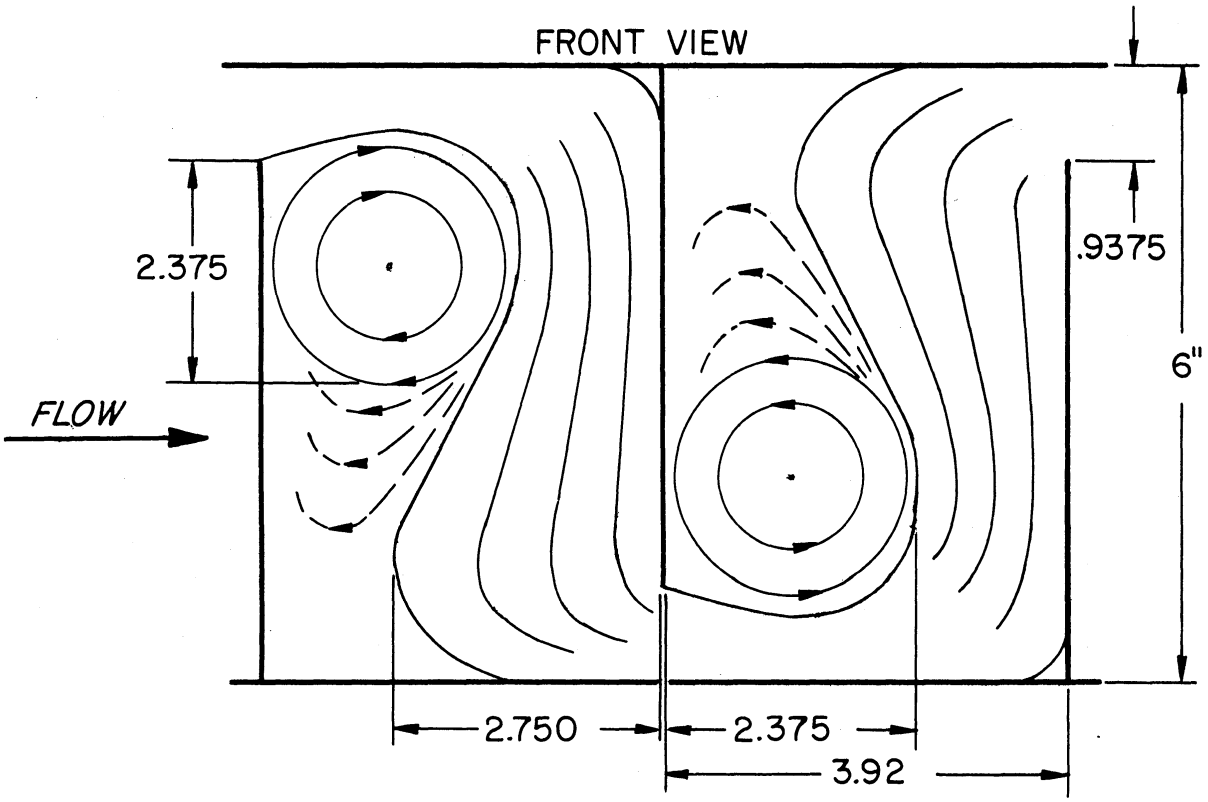

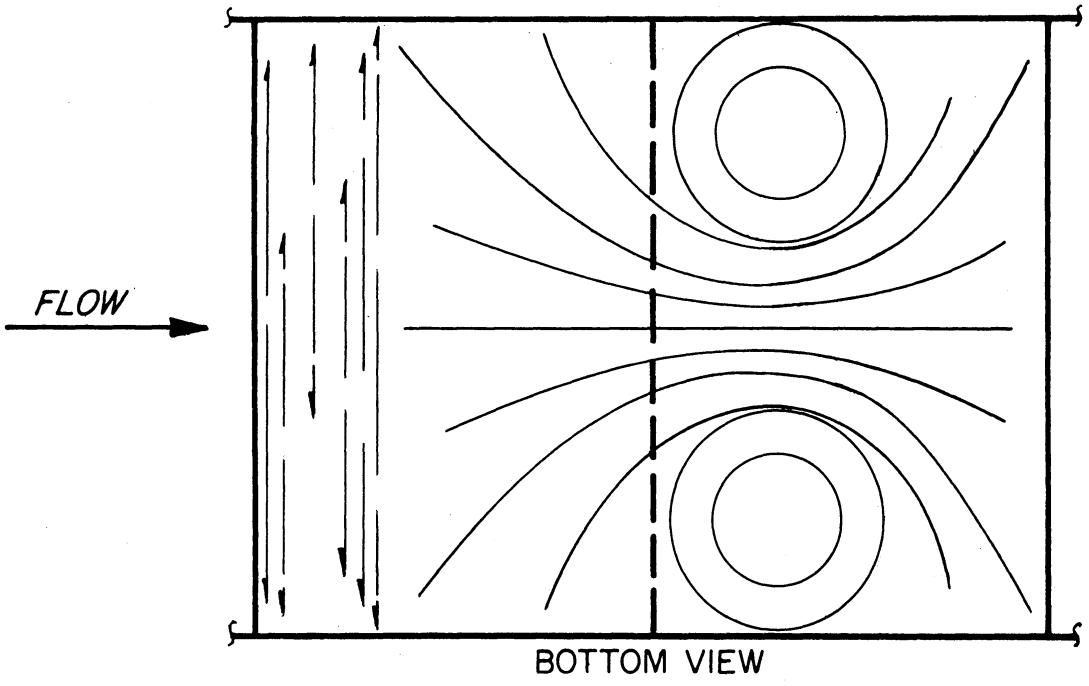

Fig 11 Flow pattern for bundle no.2

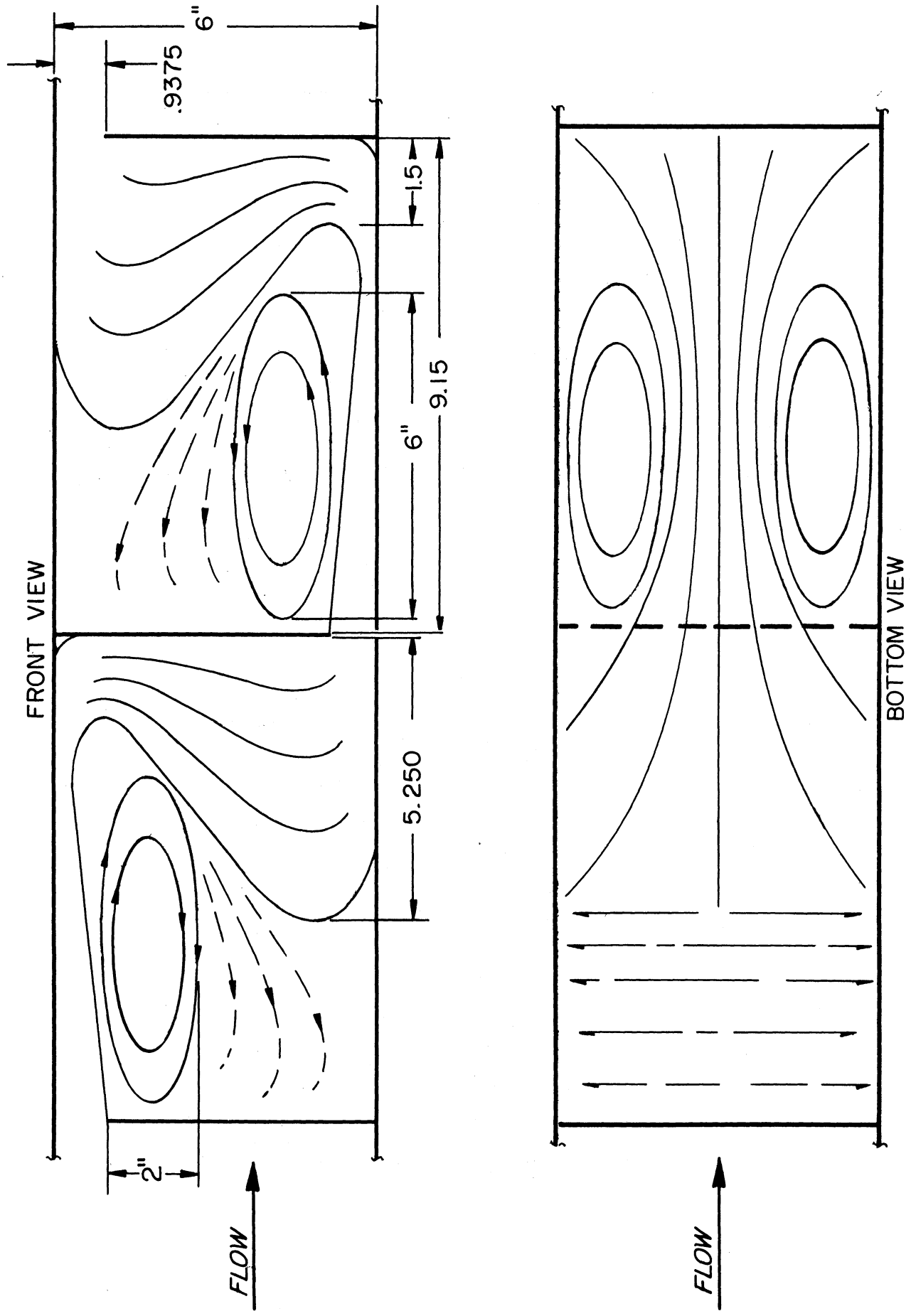

Fig 12 Flow pattern for bundle no.3

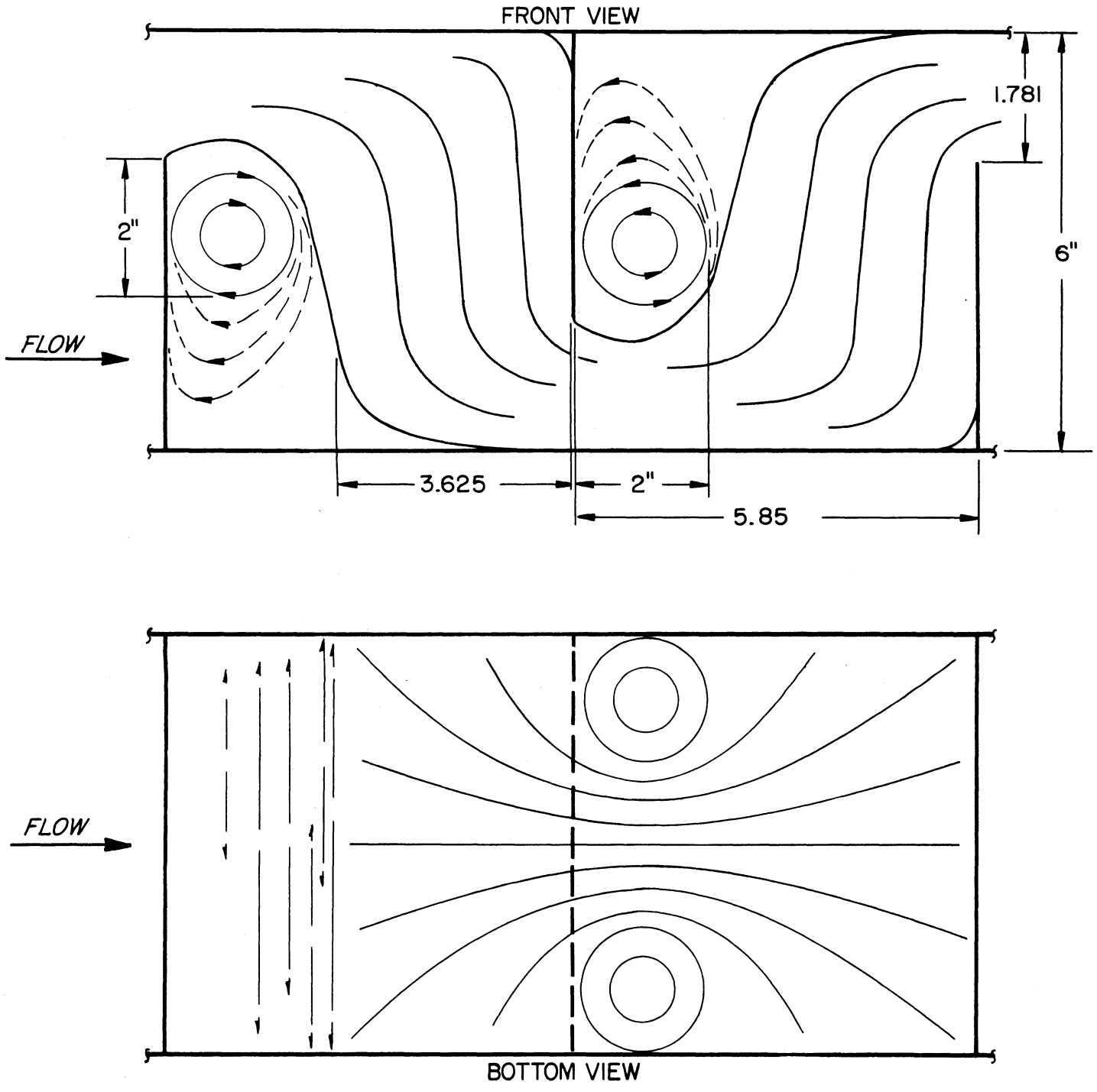

Fig 13 Flow pattern for bundle no.4

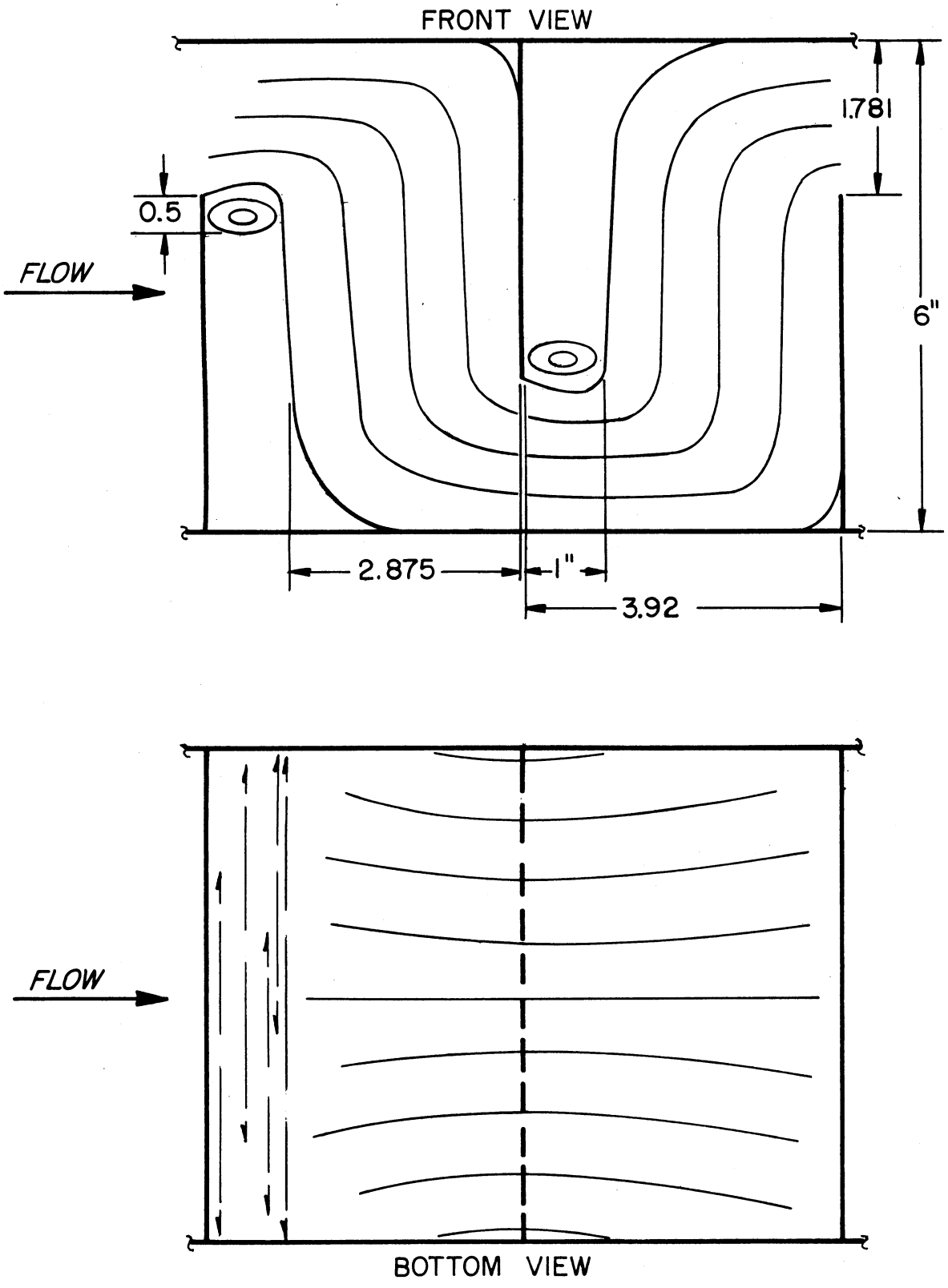

Fig 14 Flow pattern for bundle no.5

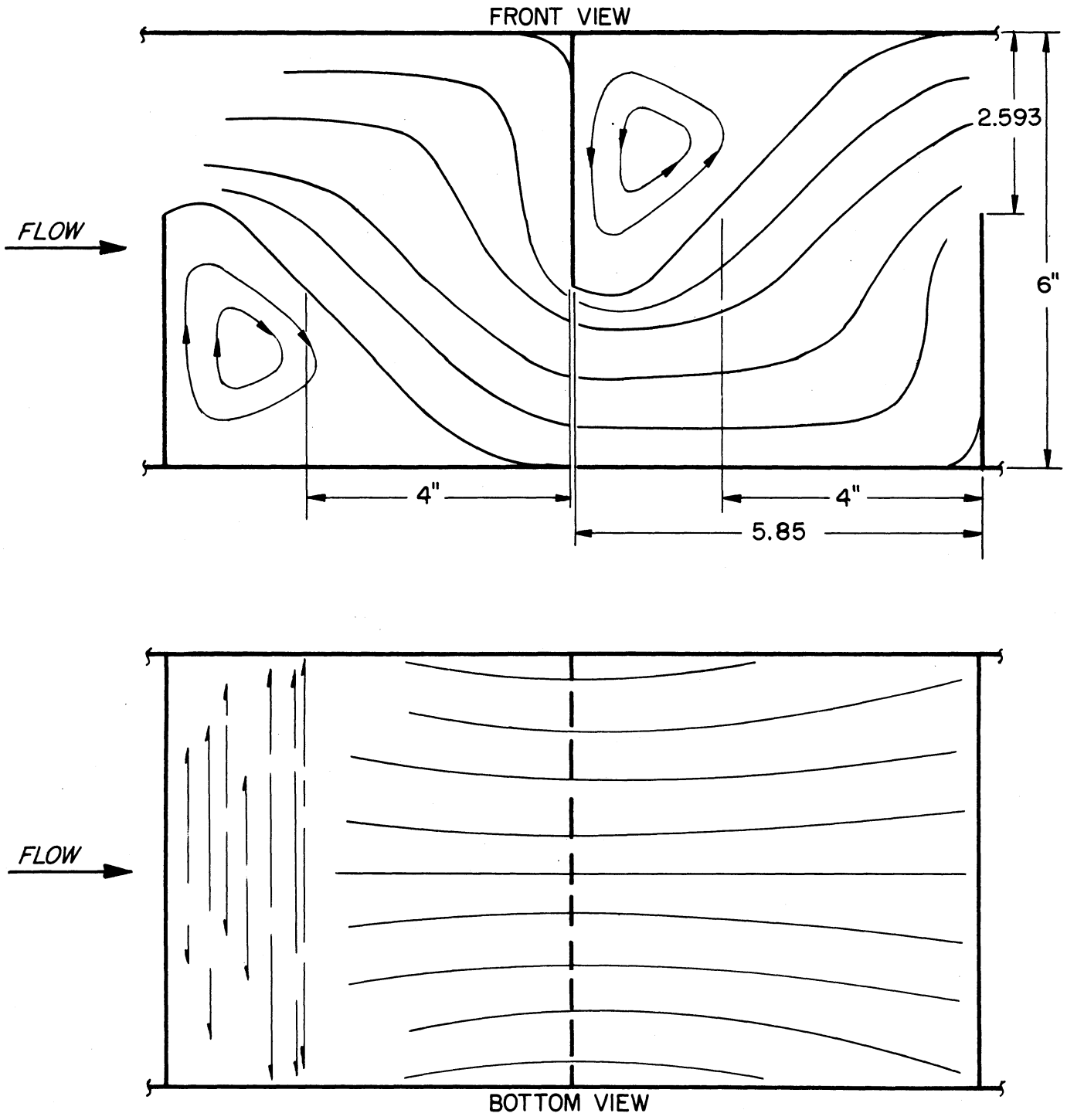

Fig 15 Flow pattern for bundle no. 6

is transverse to the tubes and can be termed as "Cross Flow". This cross flow is confined only to a part of the space between the two baffles. A certain amount of the space between the baffles does not seem to be affected by the cross flow. This region, whose shape and size is governed both by the size of the baffle cut and by the spacing between successive baffles, does not appear to have any net flow of the fluid into or out of it. However, heat transfer calculations indicate that this is not a region of complete recirculation and it does contribute to the heat transfer in the shell though at a rate different from that in the other regions. In most of the baffle designs studied this region consists of a large eddy adjacent to the baffle window and a fairly large space below it in which there is some movement at high flow rates and practically no movement at low flow rates. At very high flow rates a second eddy, very small in size, exists below the large eddy in this zone. For lack of a better name this zone can be called an "Eddy Zone". Due to the relatively slow motion of the fluid in this zone it may also be called a "Dead Zone". However, the name "Eddy Zone" will be used in the ensuing discussion. The length of the large eddy in the eddy zone is usually only slightly smaller than the total width of the eddy zone near the baffle cut edge and is fairly constant with variations in the shell-side flow rate. In Bundle No. 3 (9.97 area % baffle cut and 9.15 in. baffle spacing), however, the length of this eddy increases from 5 inches to 7 inches as the shell-side flow rate is decreased from the maximum value to the minimum value studied. In Bundle No. 6 (41.45 area % baffle cut and 5.85 in. baffle spacing) this large eddy did not exist and the fluid in the entire eddy zone moved in a direction opposite to the cross flow stream and appeared

as a slow eddy. The movement in the large eddy observed in most of the bundles was usually quite fast and was comparable with the movement of the fluid in the other zones. However the rest of the eddy zone had a lesser degree of activity than that in the main eddy and this movement died down as the shell-side flow rate was decreased. For a particular bundle the shell-side flow rate variations affected only the degree of activity in the eddy zone. The overall volume of the eddy zone did not seem to be affected by the shell-side flow rate variations except at very low flow rates. At very low shell-side flow rates the eddy zone started to extend to part of the region under cross flow. The part of the space between baffles which is not occupied by the eddy zone is under cross flow. This region is termed as the "True Cross Flow Zone" to distinguish it from the total volume between the baffles which is often assumed to be in cross flow. In reality, the flow termed as True Cross Flow is not a case of pure cross flow. The area of cross-section of this flow varies as the fluid traverses from one side of the bundle to the other. This variation is not only due to different number of tubes in the successive rows but it also is due to the fact that the fraction of the distance between the baffles which is in this type of flow varies for the successive rows of tubes. Due to this latter factor the so-called true cross flow has in some regions (for most of the bundles) a velocity component parallel to the tubes, either co-current or countercurrent to the flow of the fluid inside the tubes. However, since there is no easy way of separating this effect from the cross component of this zone, the whole "True Cross Flow Zone" is treated as a case of true cross-flow. It must be pointed out that the true cross flow zone is always smaller than what is conventionally considered

as the cross flow region. Conventionally the entire space between the baffles is considered cross flow. This is referred to in this discussion as the "Apparent Cross Flow Zone" and consists of the sum of the true cross flow zone and the eddy zone.

Figures 16 to 21 show the flow patterns for the six bundles divided into the three proposed zones of different flow characteristics, namely:

1) The Longitudinal Flow Zones,

2) The True Cross Flow Zones,

3) The Eddy Zones (including the eddy).

In these figures the longitudinal flow zones are shown as the horizontal cross-hatched areas, the true cross flow zones as the vertical cross-hatched areas, and the eddy zones as the diagonal cross-hatched areas. The longitudinal flow zones are wedge-shaped volumes in the vicinity of the baffle window, with the baffle cut edge forming the sharp edge of the wedge and the base of the wedge being the section of the cylindrical shell above the baffle cut. In the front view of the flow patterns this can be drawn easily by joining the tip of the baffle cut with the wall-ends of the two adjacent baffles. In this two-dimensional view these zones appear as triangular areas. The remaining spaces between the baffles, which appear as parallelograms in the two-dimensional view of Figure 16, are the apparent cross flow zones and each of these apparent cross flow zones consists of a true cross flow zone and an eddy zone. The proportions and shapes of these two components of an apparent cross flow zone vary with the size of the baffle cut and the spacing between successive baffles and are shown in the flow patterns in Figures 10 to 15.

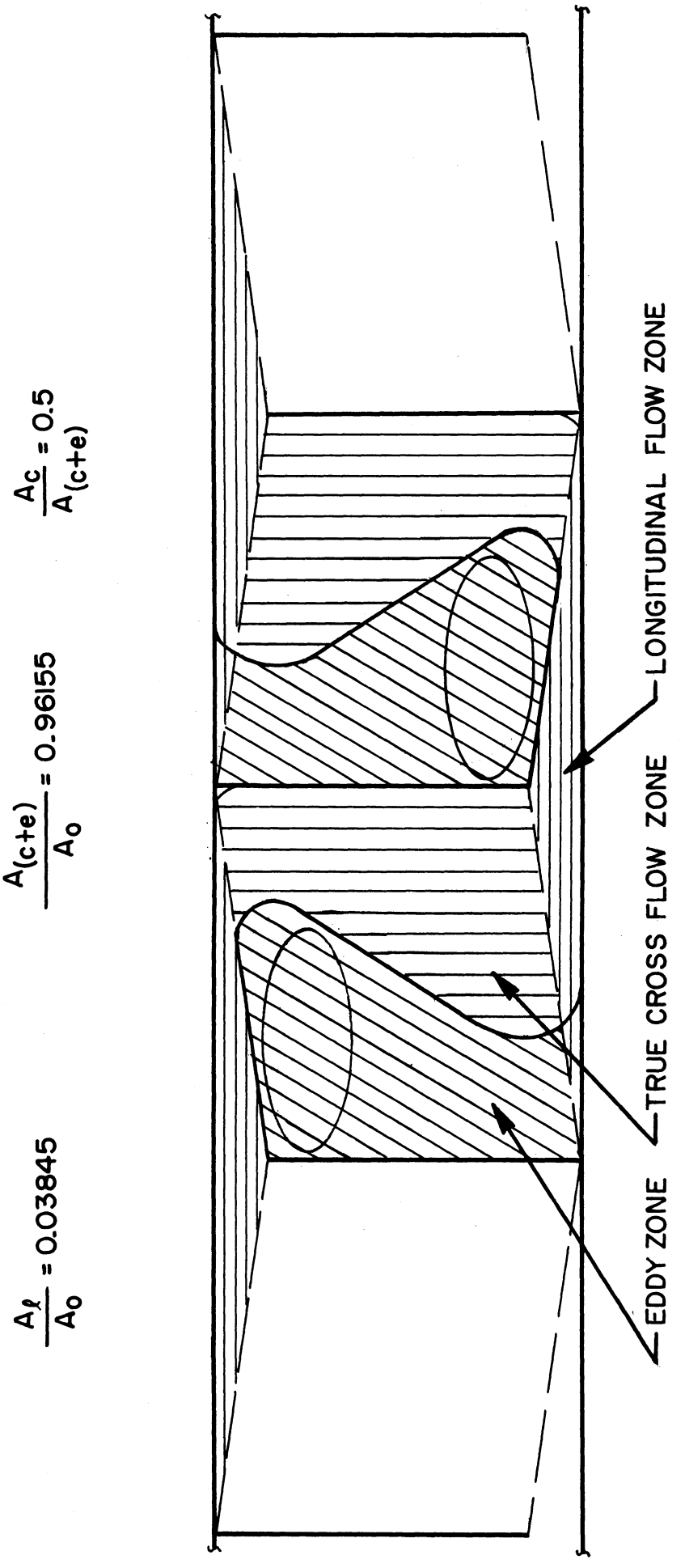

Fig 16 Division of flow pattern into characteristic flow zones for bundle no 1

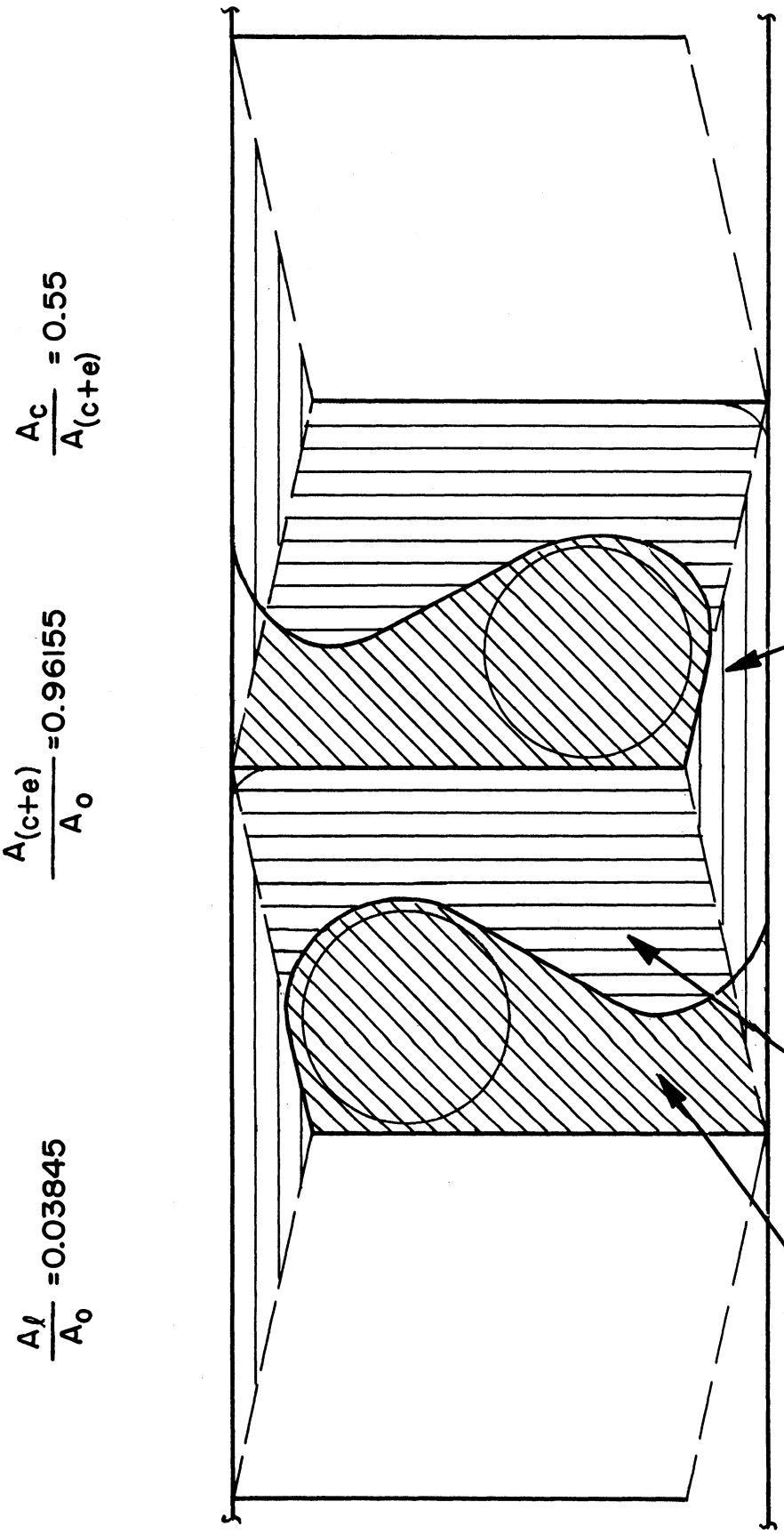

Fig 17 Division of flow pattern into characteristic flow zones for bundle no 2

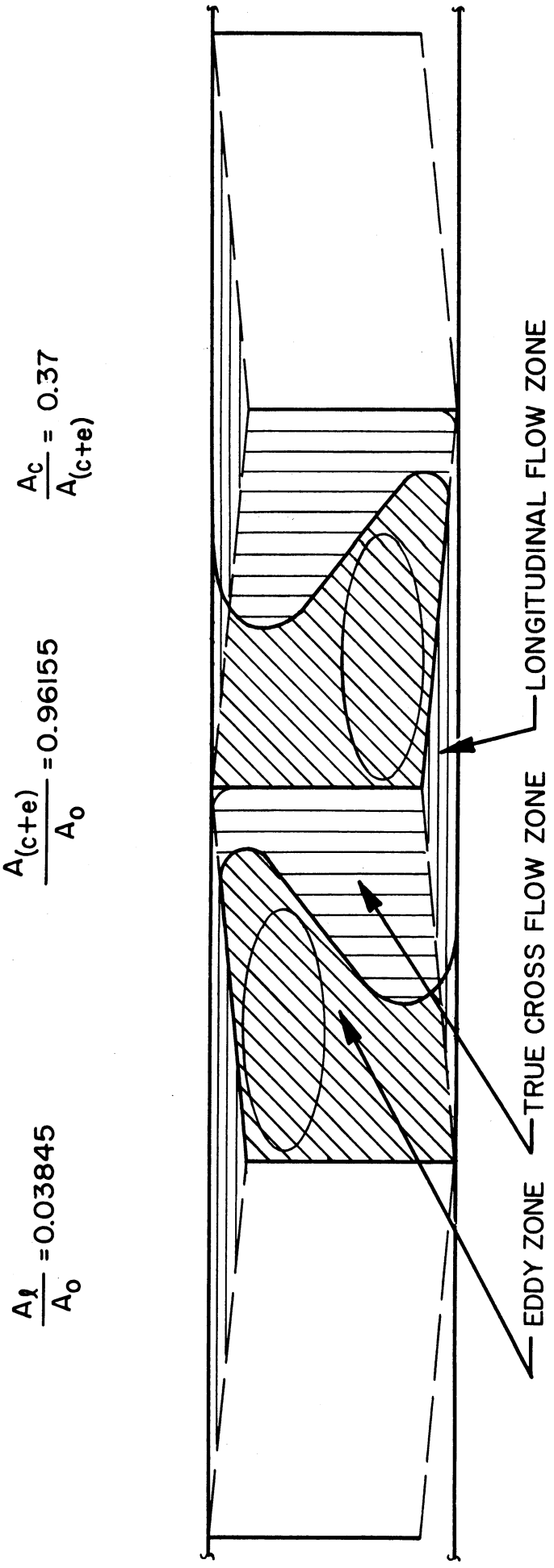

Fig 18 Division of flow pattern into characteristic flow zones for bundle no 3

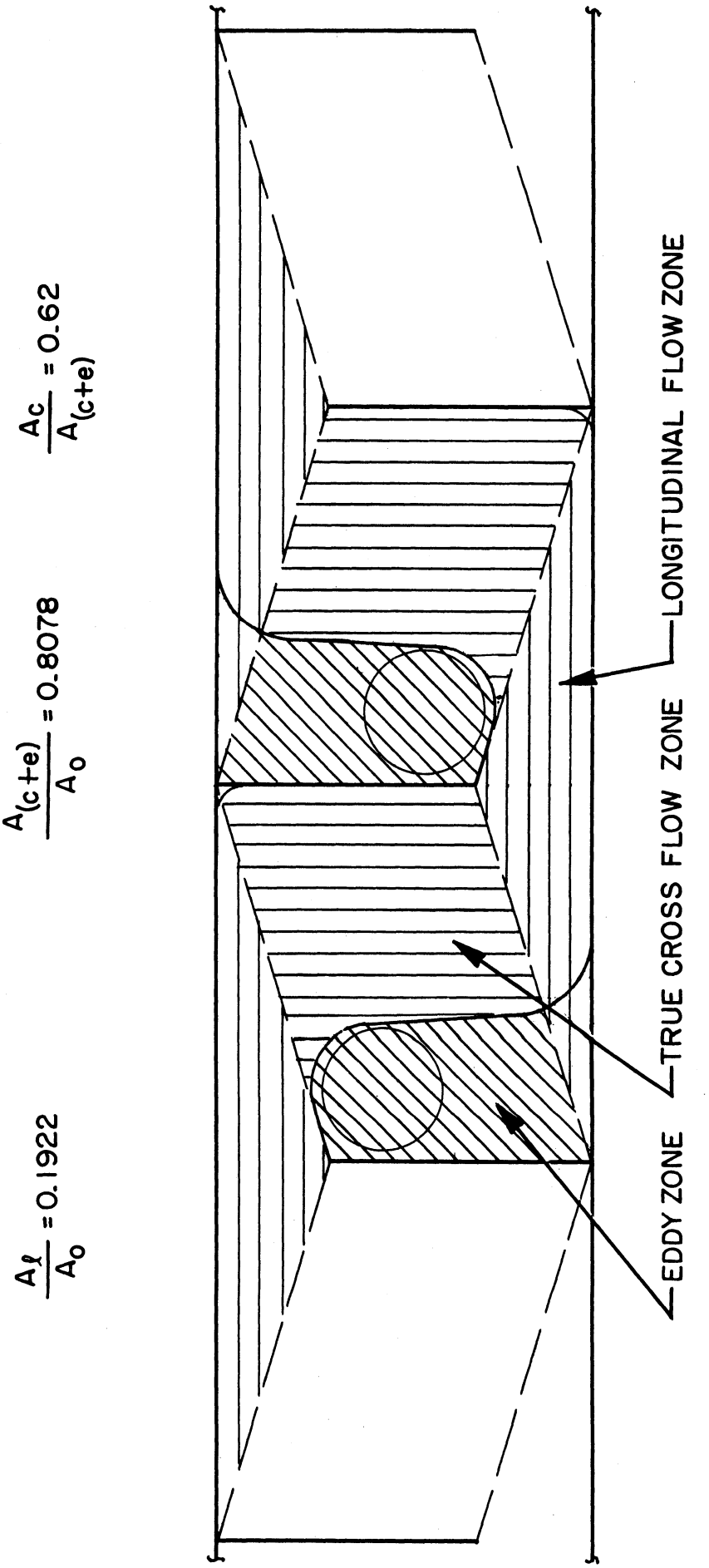

Fig 19 Division of flow pattern into characteristic flow zones for bundle no 4

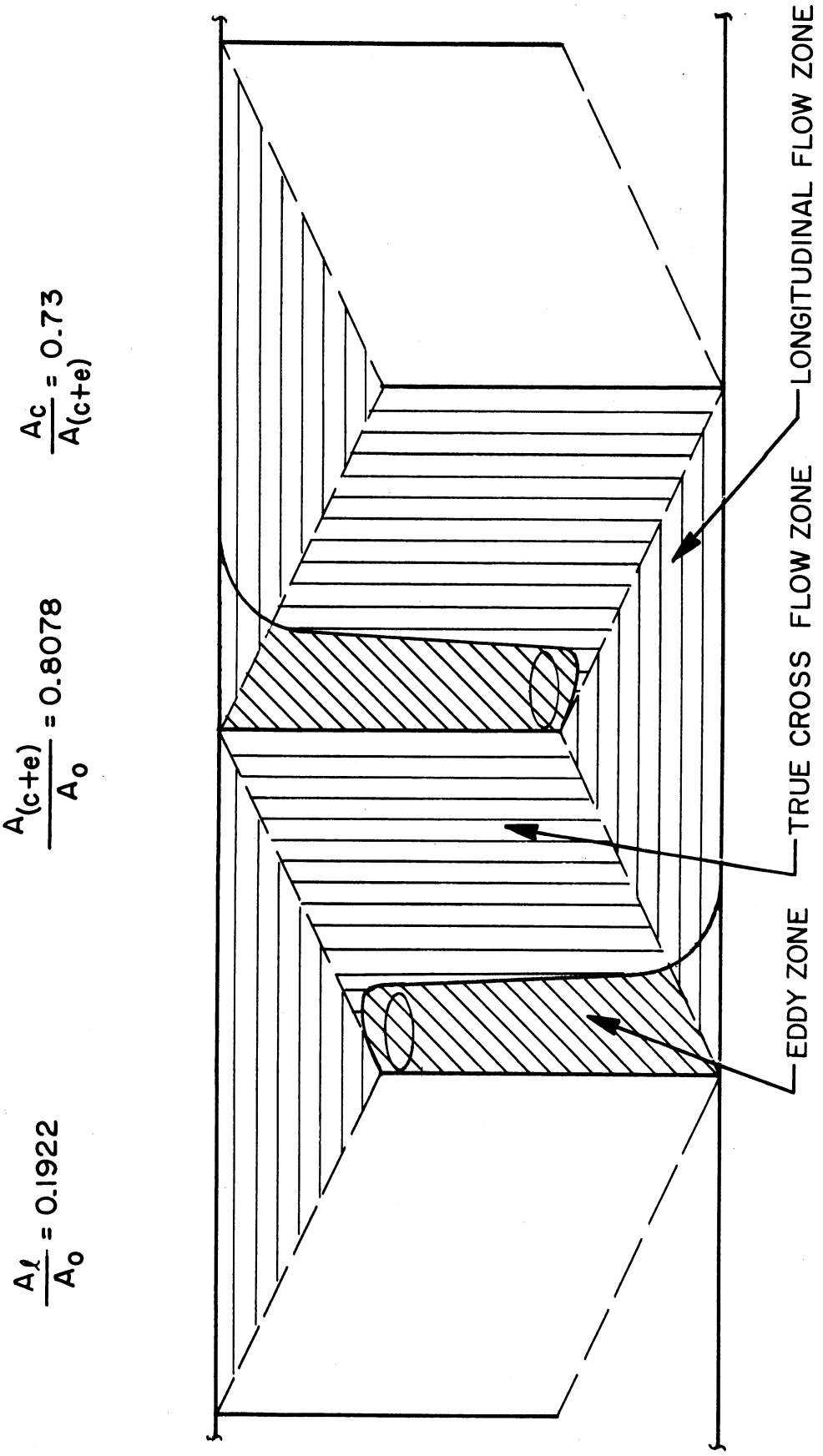

Fig 20 Division of flow pattern into characteristic flow zones for bundle no 5

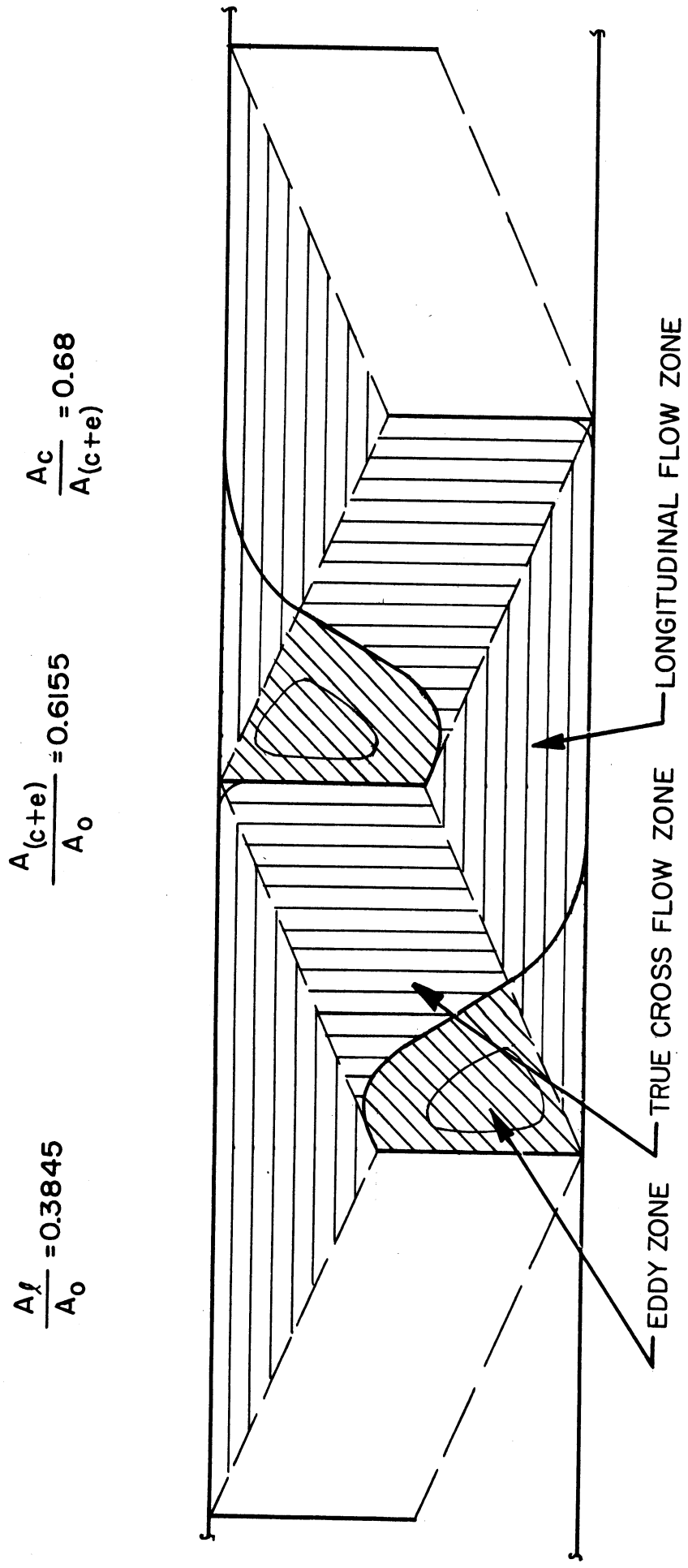

Fig 21 Division of flow pattern into characteristic flow zones for bundle no 6

CHAPTER VI

ANALYSIS AND CORRELATION OF DATA

The values of the calculated shell-side heat transfer film coefficients (from experimental data) for different flow rates and the shell-side pressure drops for these flow rates have already been given for the six tube bundles tested. The shell-side fluid flow patterns for these six bundles have also been given. From these data it is desired to establish a quantitative relationship between the shell-side flow patterns and the film heat transfer coefficients, and to correlate the pressure drop data. The following analysis of the data is divided into two sections, namely, relationship between flow patterns and heat transfer, and correlation of pressure drop data.

Relationship Between Flow Patterns and Heat Transfer

It has already been pointed out during the description of the flow pattern data that the flow pattern in each of the six bundles studied can be divided into zones of three different flow characteristics, namely:

1) Longitudinal Flow Zones,

2) True Cross Flow Zones,

3) Eddy Zones.

These three types of zones coexist in the exchanger shell and heat transfer takes place simultaneously in the three zones.

The basic heat transfer equation defining the shell-side heat transfer film coefficient, h_o, can be written as:

$$Q = h_o A_o (T_{s.b.} - T_{s.s.})_{mean} \tag{25}$$

If various fractions of A_o, the total effective outside heat transfer area in the exchanger, lie in regions of different flow characteristics (with the resulting different mechanisms of heat transfer), and if heat transfer takes place simultaneously in these various regions, the total heat transfer must be given by a summation of the heat transfer in the various regions. Thus:

$$Q = \Sigma (Q)_p = \Sigma [\, h A_o (T_{s.b.} - T_{s.s.})]_p \tag{26}$$

In terms of the three types of zones in which the flow in the shell can be divided, representing lognitudinal flow zones by "ℓ", true cross flow zones by "c", and the eddy zones by "e", equation (26) becomes:

$$Q = Q_\ell + Q_c + Q_e = h_\ell A_\ell (T_{s.b.} - T_{s.s.})_\ell$$

$$+ h_c A_c (T_{s.b.} - T_{s.s.})_c + h_e A_e (T_{s.b.} - T_{s.s.})_e \tag{27}$$

Comparing equations (25) and (27) we get:

$$h_o (T_{s.b.} - T_{s.s.})_{mean} = h_\ell \frac{A_\ell}{A_o} (T_{s.b.} - T_{s.s.})_\ell$$

$$+ h_c \frac{A_c}{A_o} (T_{s.b.} - T_{s.s.})_c + h_e \frac{A_e}{A_o} (T_{s.b.} - T_{s.s.})_e \tag{28}$$

In defining equation (25) a logarithmic mean temperature difference is used. The three temperature differences in the right hand side of equation (28) are average values for the different zones of each of the three types. If these temperature differences are assumed to be equal to each other and in turn equal to the overall logarithmic mean temperature difference, equation (28) reduces to:

$$h_o = h_\ell \frac{A_\ell}{A_o} + h_c \frac{A_c}{A_o} + h_e \frac{A_e}{A_o} \qquad (29)$$

Equation (29) indicates that if the heat transfer film coefficients for the three types of zones can be calculated separately, the total shell-side heat transfer film coefficient, h_o, will be given by a summation of the three component film coefficients in the ratios of the fractions of heat transfer area in the three types of zones. The problem, thus, resolves into the calculation of the film coefficients for the three types of zones and the separation of the heat transfer area into each of the three types of zones. Whereas the fractional areas can be obtained with a fair degree of accuracy from the data on flow patterns, calculation of the three component film coefficients is more complex. Empirical correlations are available for the calculation of heat transfer film coefficients for fluids flowing longitudinal to tube bundles and for flow across tube bundles. Though the geometries originally used for obtaining these correlations are somewhat different from the geometries involved in the longitudinal flow zones and the true cross flow zones encountered in the exchanger shell, these correlations could be used for the calculation of the film coefficients for the two zones. However, no such correlations are available for the calculation of the film coefficient for the type of flow encountered in the eddy zones. There are two ways in which this problem can be solved. One way would be to treat the eddy zones along with the true cross flow zones, thus essentially reducing the characteristic flow zones to two, namely the longitudinal flow zones and the apparent cross flow zones, the latter consisting of the true cross flow zones and the eddy zones. This would

be analogous to the conventional concept of the flow in the exchanger shell. This approach is useful because such a calculation would indicate the importance of the eddy zones. An alternative approach to solving this problem will be to calculate the film coefficients for the longitudinal and the true cross flow zones from correlations available in the literature and using the experimental values of the total shell-side heat transfer film coefficients obtained in the present study to obtain a reasonable correlation for the heat transfer film coefficients in the eddy zones from the differences. This latter approach would be very useful for design purposes, because it would allow the calculation of the total shell-side film coefficients based on the shell-side fluid flow patterns.

Treating the True Cross Flow and the Eddy Zones Jointly

If the true cross flow zones and the eddy zones are treated jointly, equation (29) can be written as:

$$h_o = h_\ell \frac{A_\ell}{A_o} + h_{(c+e)} \frac{A_{(c+e)}}{A_o} \tag{30}$$

when:

$$h_{(c+e)} \frac{A_{(c+e)}}{A_o} = h_c \frac{A_c}{A_o} + h_e \frac{A_e}{A_o} \tag{31}$$

and by definition:

$$A_{(c+e)} = A_c + A_e \tag{32}$$

The zones represented by the subscript (c + e) are the true cross flow zones and the eddy zones taken together and treated as cross flow zones. As pointed out earlier these composite zones, referred to as the apparent cross flow zones in the present discussion, are the same

as the cross flow zones according to the current concept of the flow. It should be pointed out that the current concept of the flow is not consistent with flow pattern studies. The only flow pattern studies reported in the literature by Gunter, Sennstrom, and Kopp[25] are on two-dimensional models of heat exchangers rather than on actual baffled exchangers. Even these studies indicate that true cross flow occurs only in a part of the previously assumed cross flow regions and that the remainder of these regions are under the influence of a different type of flow. Naturally, these studies on two-dimensional models do not agree quantitatively with the present study on an actual baffled exchanger due to the difference of geometries involved in the two studies.

To calculate the value of the total shell-side heat transfer film coefficient, h_o, from equation (30), the fractions of the heat transfer area in the zones of longitudinal and of apparent flow, and the film coefficients for these two types of zones must be evaluated.

Fractions of Heat Transfer Area in the Zones of Longitudinal and of Apparent Cross Flow. Figures 16 to 21 show the division of the flow in the exchanger for the six bundles into three types of zones. Since the zones of apparent cross flow have been defined as the summation of zones of true cross flow and the eddy zones, the division of the flow into zones of longitudinal and of apparent cross flow is also indicated by these figures. Figure 22 shows the division of the flow for Bundle No. 1 into zones of longitudinal and of apparent cross flow only. It is obtained by removing the lines of demarcation between the true cross flow zones and the eddy zones in Figure 16 and showing the resulting apparent cross flow zones without any cross-hatching. It is apparent from Figure 22 that the various longitudinal flow zones in the

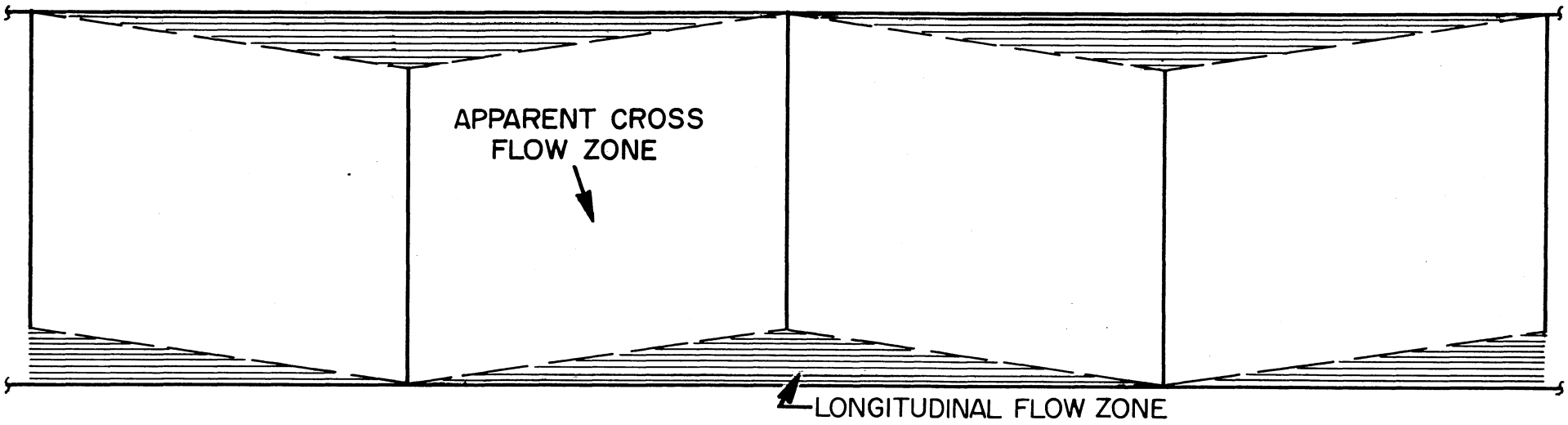

Fig 22 Division of flow pattern into longitudinal and apparent cross flow zones(Bundle no.1)

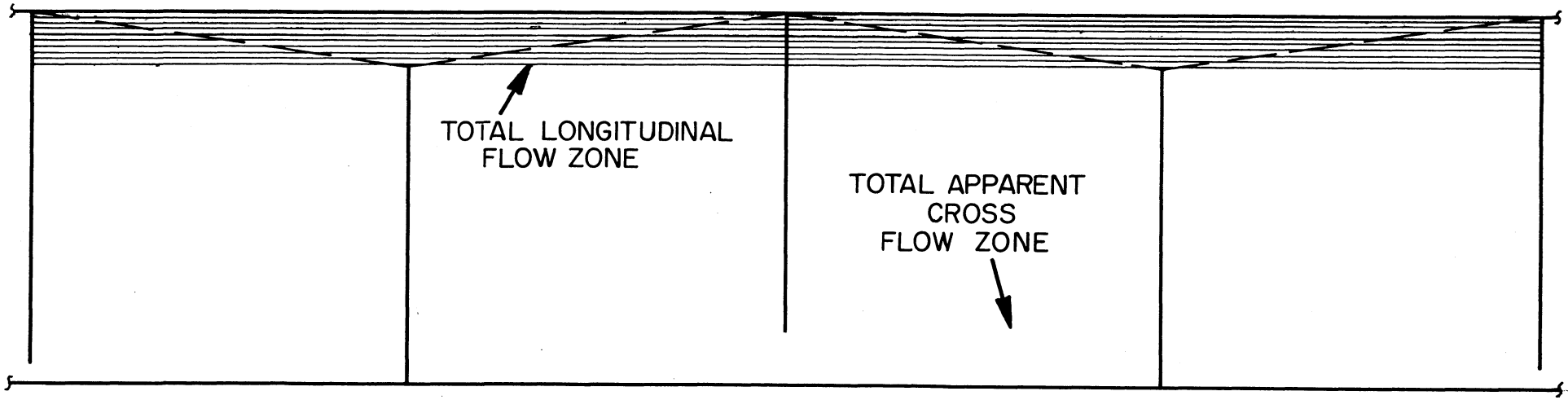

Fig 23 Summation of the longitudinal flow zones(Bundle no.1)

exchanger for a particular bundle are identical, and are represented in the two-dimensional view of this figure as the horizontal-cross-hatched isosceles triangles. The various apparent cross flow zones are likewise identical. An examination of Figure 22 will reveal that the triangles representing the longitudinal flow zones when combined together will give a rectangle with its width equal to the baffle cut and the length equal to the length of the bundle. This is shown in Figure 23 in which the triangles at the bottom have been combined with the triangles at the top to give a rectangular strip representing the total volume of the longitudinal flow regime in the exchanger. In three dimensions, though the section of the cylindrical shell represented by this rectangle will not exactly equal the summation of all the longitudinal flow zones (due to the curvature of the bases of the wedge-shaped longitudinal zones), it would be a close approximation. The exact area can be calculated accurately from the flow patterns by geometrically calculating the length of each tube in longitudinal flow zones. However, the approximation, besides simplifying the calculations, allows a means of generalizing the calculation of this area for any exchanger. Using this approximation the heat transfer area influenced by longitudinal flow will be given by the outside surface area of the tubes in a baffle window over their effective length. Since in this section flow was divided into two sections only, the heat transfer surface area in the exchanger not affected by longitudinal flow lies in the apparent cross flow zones. Therefore the number of tubes in apparent cross flow will be the total number of tubes in the exchanger minus the number of tubes in a baffle window. Table II of Appendix A gives the number of tubes in a baffle window (N_w) for each of the six bundles tested. The

heat transfer area fractions in the two types of flow regions is then given by:

$$\frac{A_{\ell}}{A_o} = \frac{N_w}{N_o} \tag{33}$$

and

$$\frac{A_{(c+e)}}{A_o} = 1 - \frac{N_w}{N_o} \tag{34}$$

The fractions of the heat transfer area in the zones of longitudinal and of apparent cross flow can be easily calculated using equations (33) and (34) if the number of tubes in a baffle window is known for a particular bundle. They are given in Table II (Appendix A) and also in Figures 16 to 21.

Film Coefficient for the Longitudinal Flow Zones. The flow in the longitudinal flow zones is essentially a case of heat transfer to fluids flowing outside tube bundles and parallel to the tubes. After a critical study of the literature, equation (3) given by Miller, et al.[34] seems to be the most reliable. This correlation, as also some of the others available, is naturally for a tube bundle larger in length than the longitudinal flow zones in the baffled exchangers. The short length of the longitudinal flow zones and the fact that the flow turns before entry to and after exit from these zones may cause the heat transfer in these zones to be different (probably higher) from that in a regular bundle with flow of the fluid outside and parallel to the tubes. However, since no correlations are available for the special geometry involved in the longitudinal flow zones, equation (3) was used for the purpose with the equivalent diameter and the free area of cross-section

for flow evaluated at the window and all the physical properties (namely C_p, μ, and k) evaluated at the shell-side average film temperature. With these modifications equation (3) reduces to the form:

$$\frac{h_\ell (D_e)_w}{k_f} = 0.032\left[\frac{(D_e)_w G_w}{\mu_f}\right]^{0.8}\left[\frac{C_p \mu}{k}\right]_f^{0.33} \qquad (35)$$

This equation (35) was used for the calculation of the heat transfer film coefficient for the longitudinal flow zones.

Film Coefficient for the Apparent Cross Flow Zones. These zones, as was pointed out in discussing the results of the flow pattern studies, doe not really have the flow across the tubes. But in this section these were assumed to be cross flow zones. The best correlation available for cross-flow with the Reynolds numbers encountered in the present study is equation (4) in the literature review which was first proposed by Colburn.[10] In terms of the apparent cross flow zones it can be written as:

$$\frac{h_{(c+e)} D_o}{k_f} = 0.33\left[\frac{D_o G_{(c+e) \text{ at dia.}}}{\mu_f}\right]^{0.6}\left[\frac{C_p \mu}{k}\right]_f^{0.33} \qquad (36)$$

For Reynolds numbers below 2000 encountered in the present study, the curve of Figure 115 (p. 230) of McAdams' book,[37] which is drawn parallel to the curve for single tubes, is used, as recommended by McAdams. Since the number of rows of tubes in cross flow (taken as the number of rows of tubes below baffle cut, i.e., the total number of rows in exchanger minus the number of rows in the baffle window) is always less than 10, as recommended by McAdams, the heat transfer coefficients obtained from equation (36) were multiplied with a constant, C_N, from

Table VI (p. 228) of McAdams' book.[37] The value of C_N depends upon the number of rows of tubes in cross flow. The use of this constant has the effect of using $C_N\, h_{(c + e)}$ in place of $h_{(c + e)}$ in equation (30) making it:

$$h_o = h_\ell \frac{A_\ell}{A_o} + C_N\, h_{(c + e)} \frac{A_{(c + e)}}{A_o} \qquad (37)$$

Significance of the Eddy Zones. Calculating $\frac{A_\ell}{A_o}$ from equation (33), $\frac{A_{(c + e)}}{A_o}$ from equation (34), h_ℓ from equation (35), $h_{(c + e)}$ from equation (36) and the alternative procedures suggested, and C_N from Grimison's Table reported by McAdams,[37] the value of h_o, the total heat transfer film coefficient can be calculated from equation (37) which is essentially equation (30) with $h_{(c + e)}$ replaced by $C_N\, h_{(c + e)}$. These calculations were made for representative runs for the six bundles tested, calculating the value of h_o for each of the flow rates in a run.

The runs selected as representative for the different bundles and used for the correlation calculations throughout this analysis were:

Run 19 for Bundle No. 1,
Run 26 for Bundle No. 2,
Run 28 for Bundle No. 3,
Run 34 for Bundle No. 4,
Run 35 for Bundle No. 5,
and Run 36 for Bundle No. 6.

For the bundles for which more than one run was carried out, the run which gave the lowest value of the sum of the squares of the deviations, s^2, for the Wilson Plot was selected as the representative run.

Table V in Appendix A lists the values of h_o calculated from equation (37) for each of the flow rates for the representative runs for all the six bundles, along with the major steps in the calculation of these h_o (eq. 37) values. The values of h_o so calculated do not

match with the values of h_o obtained by Wilson plot analysis of the experimental heat transfer data. Table V (Appendix A) gives the differences between the values of h_o calculated from equation (37) and those of h_o obtained from experimental data [namely h_o (eq. 37) - h_o (exp.)]. These deviations are shell-side-flow-rate-dependent. The algebraic values of the deviation for a particular bundle decrease with increasing shell-side flow rate. The variation of the deviation with the Reynolds number for the apparent cross flow zones [$Re_{(c + e)}$] is approximately linear on a semi-log plot (plotting the deviations along the linear scale and the Reynolds numbers along the logarithmic scale). Figure 24 shows the deviations plotted in this fashion against the apparent cross flow zone Reynolds numbers for all the representative runs of the six bundles tested. Though the variation of the deviation with the variation of the Reynolds number for the apparent cross flow zones is essentially linear on this plot for each of the six bundles, the slopes and intercepts for the lines for each of the six bundles are quite different. The lines for individual bundles are not shown in Figure 24. An overall line for the points for all the six bundles is shown in this figure and could be used for predicting the deviation for design purposes. However the use of this line will be limited to the range of the present data.

The usefulness of Figure 24 is not so much for design purposes as for indicating the significance of the eddy zones. Equation (37) and equation (30) (original form of equation 37) are based on the assumption that the mechanism of heat transfer in the true cross flow zones and the eddy zones is essentially the same and that these two types of zones can be treated together as zones of cross flow. The discussion on flow

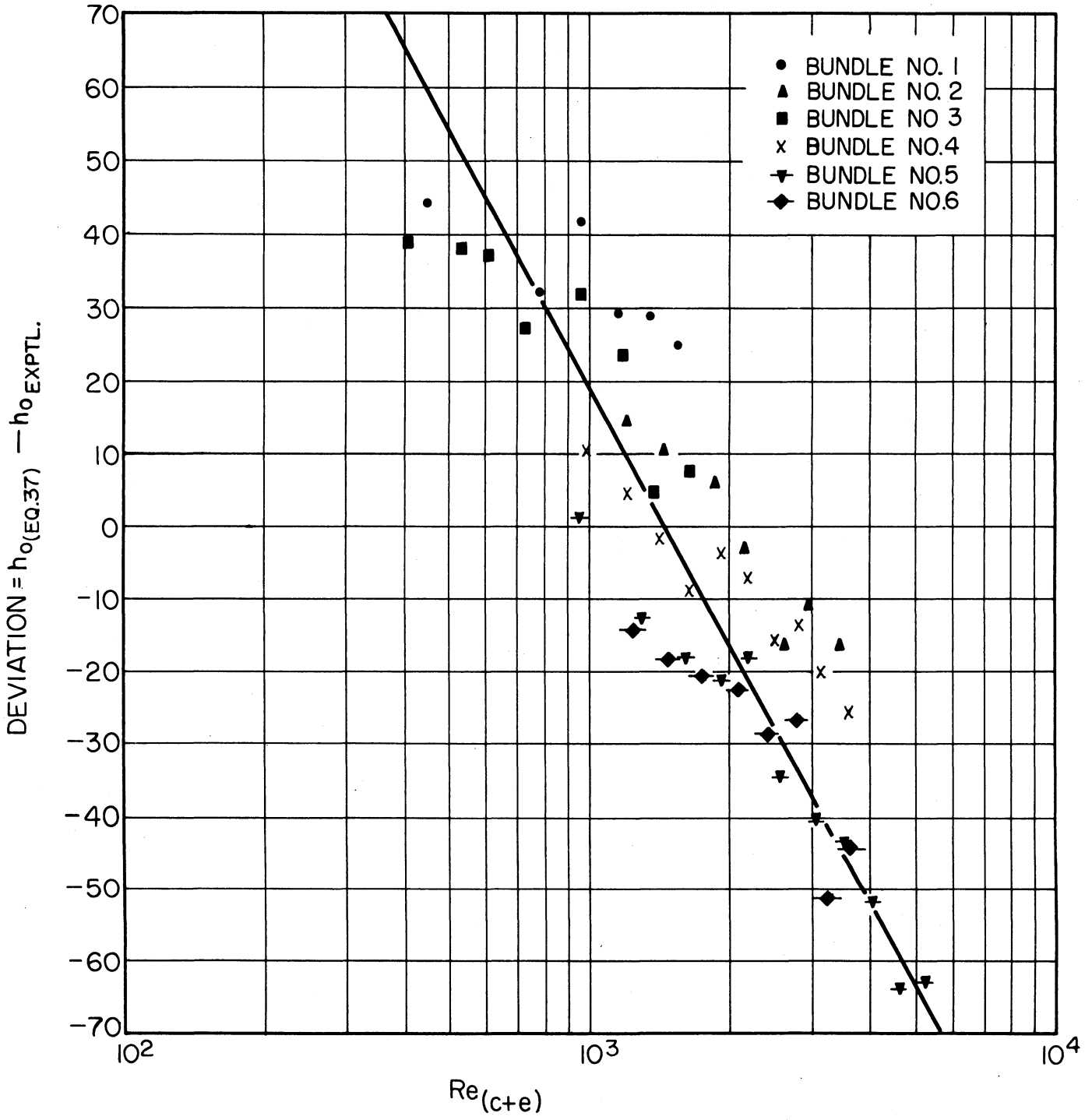

Fig 24 Plot of deviation of equation 37 from experimental results versus apparent cross flow zone Reynolds numbers for the six bundles tested

patterns has already indicated that the mechanism of fluid flow is significantly different in these two types of zones. It would be reasonable to believe that the mechanism of heat transfer would also be different for these two types of zones. The deviation of the calculations by equation (37) from the experimental results indicates the inadequacy of this equation. Further, the flow-rate-dependence of the deviations and the fact that the slopes and intercepts of the semi-log linear plots of Figure 24 are different for the different bundles points to this inadequacy of equation (37) being a result of the assumption about the mechanisms for heat transfer for the true cross flow and the eddy zones being the same. The conclusion, therefore, seems to be that this assumption stated by equation (31) is not valid, and that the eddy zones should be considered separately from the true cross flow zones.

Since, as was pointed out earlier, there are no direct means of computing the heat transfer film coefficient for the eddy zones, the best alternative available is to use the experimental heat transfer data for obtaining a reasonable correlation for the heat transfer in the eddy zones. This can be done if the information obtained in the present study on the shell-side flow patterns is used to separate the eddy zones from the true cross flow zones.

Treating the True Cross Flow and the Eddy Zones Separately

If the true cross flow zones and the eddy zones are treated separately, equation (29) is applicable for the summation of the heat transfer film coefficients for the zones of the three different types of flow. Since, no correlations are available to evaluate the eddy zone film coefficient, h_e, knowing the experimental value of h_o, equation

(29) can be utilized for the calculation of the eddy zone heat transfer. For this purpose, transposing terms, equation (29) becomes:

$$h_e = \frac{A_o}{A_e}\left[h_o - \left(h_\ell \frac{A_\ell}{A_o} + h_c \frac{A_c}{A_o}\right)\right] \qquad (38)$$

To evaluate h_e, the eddy zone heat transfer film coefficient, from equation (38), the film coefficient for the longitudinal flow zones and that for the true cross flow zones, as well as the fractions of the heat transfer area in the three types of zones, must be evaluated.

The Longitudinal Flow Zones. The longitudinal flow zone term, $h_\ell \frac{A_\ell}{A_o}$, in equation (38) is the same as in equations (30) and (37) which apply to the case when the eddy zones and the true cross flow zones are treated jointly as apparent cross flow zones, since physically the longitudinal flow zones remain the same irrespective of the fact whether the eddy zones and the true cross flow zones are treated jointly or separately. Therefore, the film coefficient for the longitudinal flow zones, h_ℓ, to be used in equation (38) can be calculated by equation (35), and the fraction of the heat transfer area in the longitudinal flow zones can be calculated by equation (33).

Film Coefficient for True Cross Flow Zones. The film coefficient for the true cross flow zones can be calculated by an equation of the form of equation (36), though the same equation cannot be used because the cross-sectional area for flow is different in the true cross flow zones than in the apparent cross flow zones. The cross-sectional area for flow in the true cross flow zones has to be determined from the flow patterns. Once this cross-sectional area, S_c, is evaluated, the film coefficient for the true cross flow zones can be evaluated by the following modification of equation (36):

$$\frac{h_c D_o}{k_f} = 0.33 \left[\frac{D_o G_c \text{ (at dia.)}}{\mu_f} \right]^{0.6} \left[\frac{C_p \mu}{k} \right]_f^{0.33} \qquad (39)$$

The only difference between equations (39) and (36) is that the mass velocity, G, is evaluated for a true cross flow zone in equation (39) and for an apparent cross flow zone in equation (36). Though the cross-sectional area for flow in both cases changes as the liquid traverses the bundle (due to the varying number of tubes in successive rows), it is evaluated at the diameter (according to conventional practice) for both cases. The recommendations about Reynolds numbers below 2000 and about bundles with less than 10 rows of tubes in cross flow given with equation (36) also apply to equation (39). The latter recommendation (about the multiplication of h_c with a constant factor, C_N, dependent the number of rows of tubes in cross flow) changes equation (38) to:

$$h_\ell = \frac{A_o}{A_e} \left[h_o - \left(h_\ell \frac{A_\ell}{A_o} + C_N h_c \frac{A_c}{A_o} \right) \right] \qquad (40)$$

Cross-Sectional Area for True Cross Flow. As defined earlier the apparent cross flow zones are combinations of true cross flow zones and eddy zones. Figures 16 to 21 give the division of the apparent cross flow zones into the true cross flow and the eddy zones based on the flow pattern studies on the six bundles. The flow patterns of Figures 10 to 15 indicate that the apparent cross flow zones are divided into the true cross flow zones and the eddy zones by planes perpendicular to the shell axis. This means that the cross-sections for the cross flow can be obtained from the true cross-flow regions shown in Figures 16 to 21. Figure 25 shows an apparent cross flow zone for a typical flow pattern (Bundle No. 1) divided into the true cross flow zone and

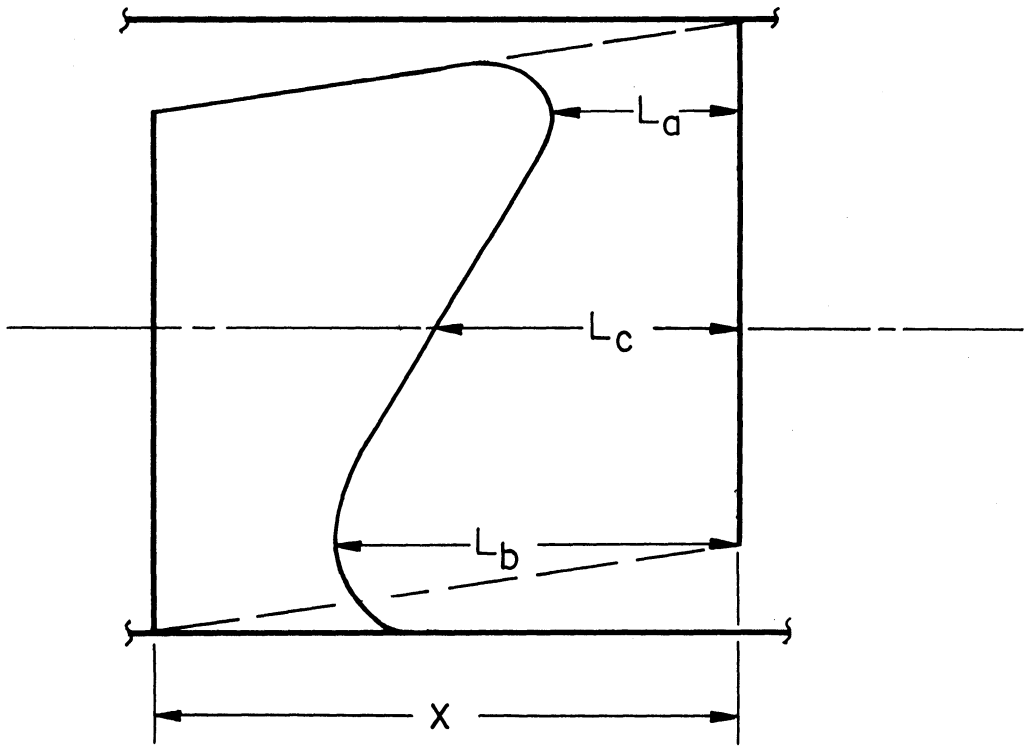

Fig 25 Division of apparent cross flow zone (Bundle no 1)

the eddy zone showing the width of the true cross flow zone as L_a and L_b at the top and bottom (near entrance window and exit window) respectively, and as L_c at the shell diameter. Though in the flow patterns for Bundles 4, 5, and 6, L_a is greater than L_b in contrast to the case for Bundles 1, 2, and 3, for which L_a is less than L_b, the value of L_c, the width of the true cross flow zone at the diameter in all the bundles is approximately equal to the mean of L_a and L_b. The cross-sectional areas for flow for both the apparent as well as the true cross flow zones are taken at the diameter. Since the number of tubes at the diameter is constant for both the types of zones, the ratio of the free cross-sectional area for true cross flow to that for apparent cross flow is given by the ratio of the width of the true cross flow zone to the width of the apparent cross flow zone both at the shell diameter. It may be noted that the width of the apparent cross flow zones, by definition, is equal to the spacing between successive baffles. Therefore:

$$\frac{S_c}{S_{(c+e)}} = \frac{L_c}{X} \qquad (41)$$

Since $S_{(c+e)}$, the free cross-sectional area for apparent cross flow can be easily calculated from the bundle geometry, using equation (41), with the value of L_c obtained from the flow patterns, the value of S_c, the free cross-sectional area for true cross flow can be calculated. The values of $S_c/S_{(c+e)}$ thus obtained for the six bundles tested are listed in Table IV (Appendix A). Figure 26 gives a plot of these values as a function of the area-fraction baffle cut with the baffle spacing as a parameter. As a baffle cut of zero is approached the true cross flow zone will be expected to vanish, thus giving a value of zero for $S_c/S_{(c+e)}$. Therefore, zero was used as a common

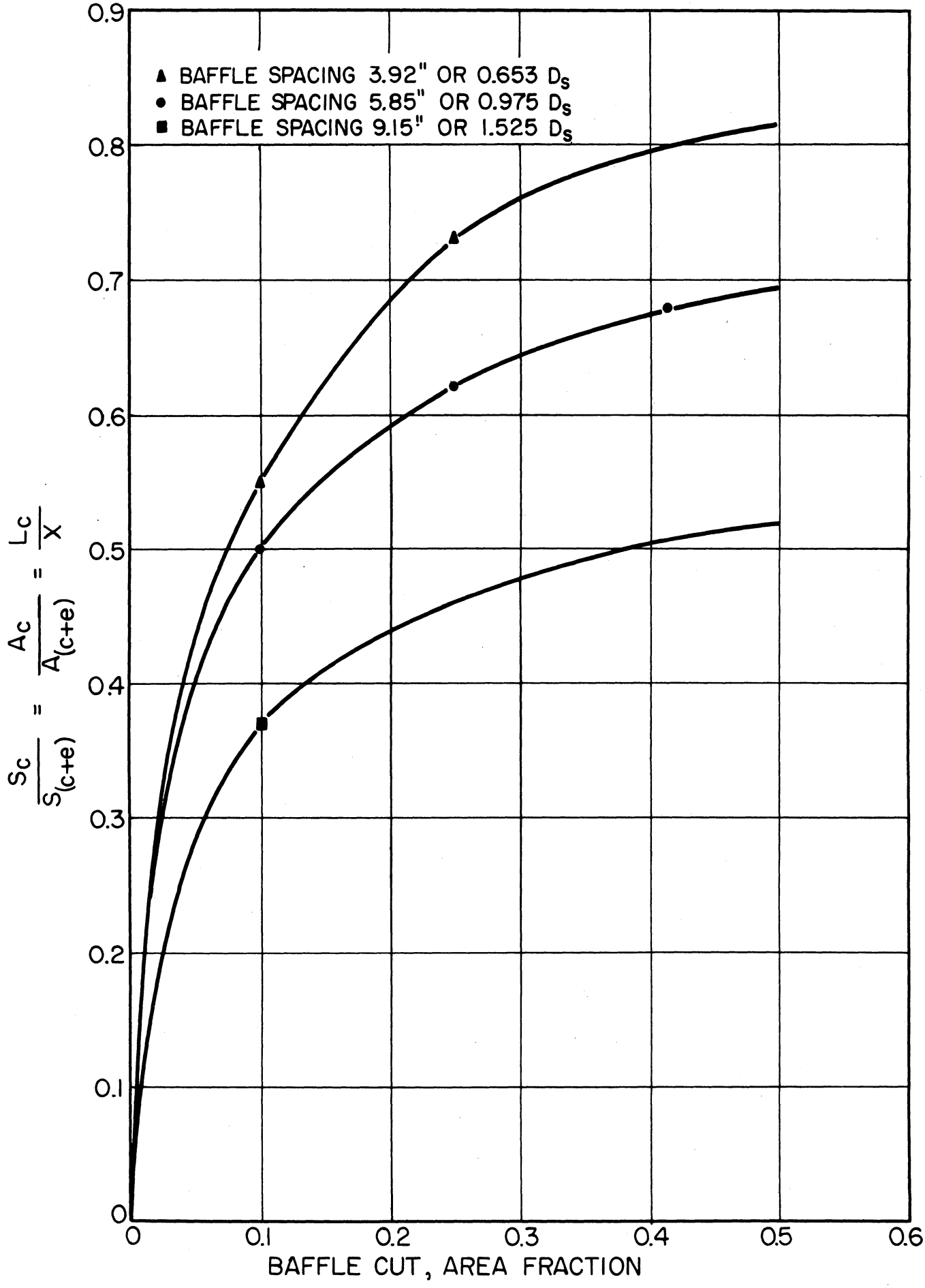

Fig 26. Ratios of free cross-sectional areas for flow and of heat transfer aeras between true and apparent cross flow zones

point for all the three curves. It must be pointed out that the reliability of these curves may not be very good for the baffle cuts beyond the ones tested in the present study. All the three curves (for the three baffle spacings tested) have been extended to a baffle cut of 0.5 area fraction. Naturally the reliability of the curve for the baffle spacing of 9.15 in. (only one baffle cut tested for this spacing) beyond the baffle cut tested (0.0997 area fraction) will be questionable. These curves of Figure 26 were drawn to show the trend of the variation rather than to be used as master curves for design purposes. However, their use for design purposes within the range of baffle cuts and spacings used in this study should be quite reliable. For obtaining master curves for design purposes considerable amount of data on a wide range of baffle spacings and baffle cuts, as well as on different shell diameters, tube diameters, and tube arrangements must be obtained. Since the purpose of the present study was mainly to show the significance of the flow patterns in determining the shell-side heat transfer, the extensive work mentioned above was not considered within its scope.

Fractions of Heat Transfer Area in the True Cross Flow and the Eddy Zones. An examination of Figure 25 will reveal that the length L_c represents not only the width of the true cross flow zone at the diameter but also the average (approximately) length of the tubes in the true cross flow zone. Since the heat transfer area of a tube is given by πDL, the number of tubes in the true cross flow and the apparent cross flow zones being the same, the ratio of the heat transfer area in the true cross flow zones to that in the apparent cross flow zones is given by:

$$\frac{A_c}{A_{(c+e)}} = \frac{L_c}{X} \tag{42}$$

It will be noticed that equation (42) is identical to equation (41) which was developed for obtaining $S_c/S_{(c+e)}$. Comparing these two equations it is apparent that:

$$\frac{S_c}{S_{(c+e)}} = \frac{A_c}{A_{(c+e)}} = \frac{L_c}{X} \tag{43}$$

The values of $A_c/A_{(c+e)}$ are given in Table IV (Appendix A) and are plotted in Figure 26 as a function of the area-fraction baffle cut with the baffle spacing as parameter. They are also shown in Figures 16-21. Once the value of $A_c/A_{(c+e)}$ has been obtained, the value of $A_e/A_{(c+e)}$ can also be calculated easily by using equation (32), which can be written as:

$$\frac{A_e}{A_{(c+e)}} = 1 - \frac{A_c}{A_{(c+e)}} \tag{44}$$

Since $A_{(c+e)}/A_o$ is the same irrespective of whether the true cross flow and the eddy zones are treated jointly or separately, it can be calculated from equation (34). Knowing $A_c/A_{(c+e)}$, $A_e/A_{(c+e)}$, and $A_{(c+e)}/A_o$ from the above calculations, A_c/A_o and A_e/A_o, required in equations (38) and (40), can be easily calculated.

Calculation and Correlation of Eddy Zone Film Coefficients. The heat transfer film coefficients for the eddy zones for each of the flow rates in the representative runs for the six bundles tested were calculated according to equation (40). These values along with the major steps in their calculation are listed in Table V (Appendix A).

For correlating these coefficients Nusselt's numbers, $h_e D_o/k_f$, for the eddy zones were calculated. The general form of the correlation for these eddy zones can be assumed to be similar to that of the correlations for the other zones. It can be written as:

$$\frac{h_e D_o}{k_f} = C\,(Re)^m\,(Pr)_f^n \qquad (45)$$

The exponent n on the Prandtl number is usually 0.33 on most of the correlations for the other zones. Since the present data does not permit a rigorous evaluation of this exponent, the conventional value of 0.33 was chosen for n. There is a question as to which Reynolds number should be used in equation (45). A Reynolds number for the eddy zones cannot be used because it would have no physical significance. As pointed out earlier, the eddy zones are zones of partial recirculation. The whole fluid stream does not seem to pass through the eddy zones. The movement of the fluid in and out of the eddy zones is through movement of the eddies, and, thus, no definite cross-sectional area for flow can be established. However, the flow pattern studies indicated that the movement in the eddy zones is flow-rate-dependent. The variation of the deviation of equation (37) from the experimental h_o values also indicated that the mechanism of heat transfer in the eddy zones was flow-rate-dependent. So the only problem is to get the correct cross-sectional area to give the Reynolds number to be used in equation (45). The Reynolds number for the apparent cross flow zones seems to give the best results. It may be recalled that this Reynolds number is based on the free cross-sectional area for

vertical flow between baffles at the shell diameter. Thus equation (45) can be written as:

$$\frac{h_e D_o}{k_f} = C \left[\frac{D_o G_{(c + e) \text{ at dia.}}}{\mu_f} \right]^m \left[\frac{C_p \mu}{k} \right]_f^{0.33} \qquad (46)$$

According to equation (46) a plot of:

$$\frac{h_e D_o}{k_f} \Bigg/ \left(\frac{C_p \mu}{k} \right)_f^{0.33} \quad \text{vs.} \quad \frac{D_o G_{(c + e)}}{\mu_f}$$

should be a straight line on a log-log paper. The values of the variable

$$\frac{h_e D_o}{k_f} \Bigg/ \left(\frac{C_p \mu}{k} \right)^{0.33}$$

are listed in Table V (Appendix A) [under the heading $Nu_{e\ (eq.\ 40)}/Pr^{0.33}$] for all the flow rates in the representative runs of the six bundles tested. Figure 27 gives a plot of $Nu_{e\ (eq.\ 40)}/Pr^{0.33}$ versus $Re_{(c + e)}$ for the six bundles tested. Though the points for each bundle lie on a straight line, different lines, almost parallel to each other, are obtained for the six bundles. The lines are not drawn in Figure 27.

If the correlation for the eddy zones is to characterize the heat transfer mechanism in these zones a single line should be obtained for all the bundles. The fact that in Figure 27 the data for the different bundles form parallel lines indicates that the constant C in equation (46) varies with the bundles. Considering the degree of difference between the various bundles, the reason for the discrepancy

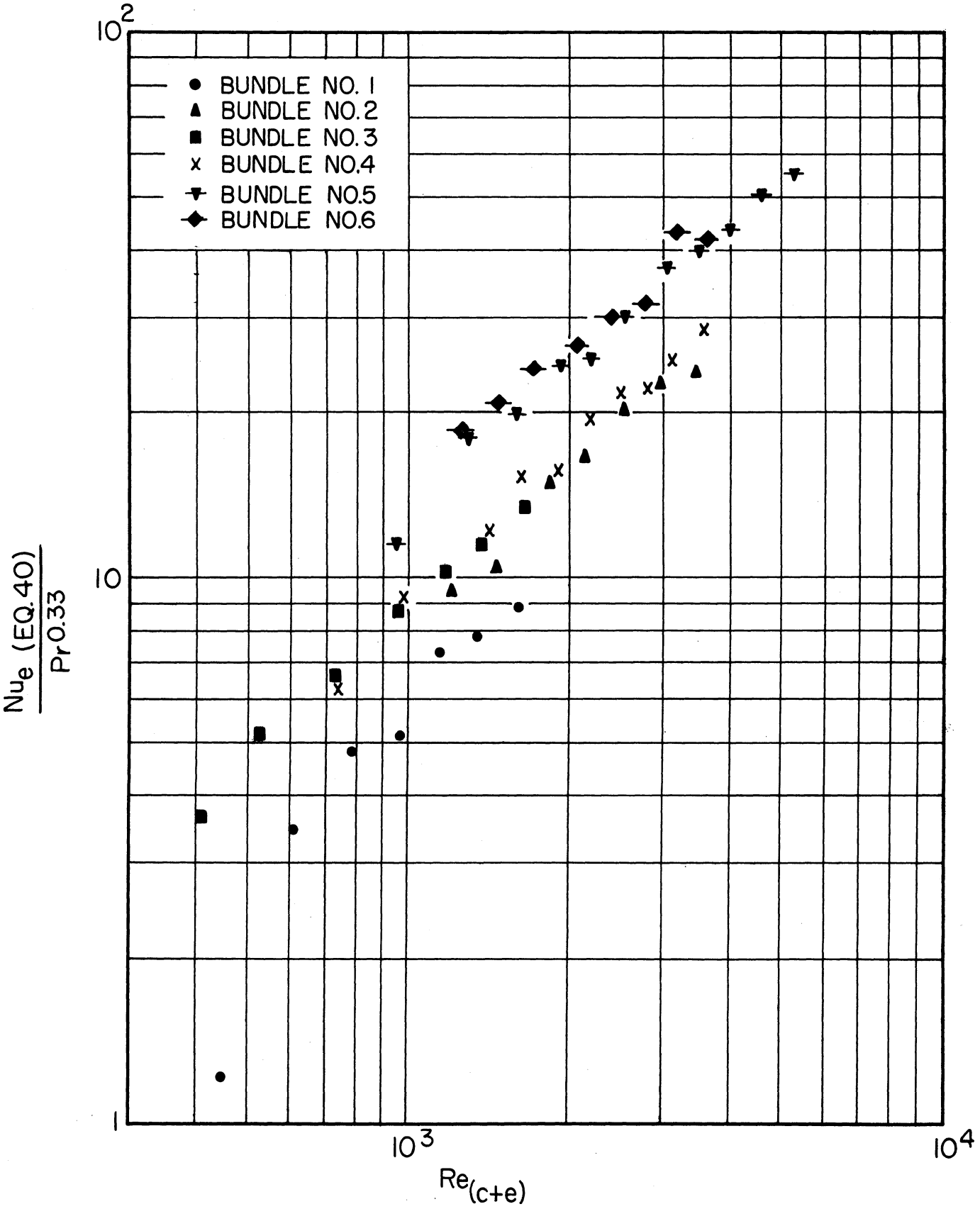

Fig 27 Correlation of eddy zone film coefficients calculated by equation 40

seems to be due to the use of the multiplying factor C_N, used to correct the true cross flow heat transfer film coefficient for the number of rows of tubes in cross flow. The use of C_N for geometries involving only cross flow and containing less than 10 number of rows of tubes in cross flow is necessary to compensate for the different degrees of turbulence introduced by the first few rows. In the true cross-flow zones in the exchanger shell, however, the fluid enters the cross flow zone from a longitudinal flow zone. Thus the first few rows of tubes in cross flow are not really the first in the flow as they would be if no longitudinal flow zones were involved, and, therefore, the turbulence introduced by them may not be different from that introduced by the later rows of tubes in cross flow. This is further supported by the work of Bergelin, et al.,[5] who obtained a similar effect in their work and reasoned that in the baffled exchanger "each window turnaround may have caused enough turbulence to maintain a high rate of heat transfer throughout the exchanger." If this is true, the heat transfer coefficient in the true cross flow zones will be the same whether there are ten or less number of rows of tubes in cross flow. This would have the effect of neglecting C_N in equation (40), which changes this equation to equation (38).

The values of h_e were, therefore, calculated by equation (38) and used for correlation. The values of h_e from equation (38) and those of $Nu_{e\ (eq.\ 38)}/Pr^{0.33}$ based on these values of h_e are listed in Table V (Appendix A). Figure 28 gives a plot of $Nu_{e\ (eq.\ 38)}/Pr^{0.33}$ versus $Re_{(c + e)}$ for the six bundles tested. The data for the various bundles are considerably closer in this plot than in the plot of Figure 27, except for a scatter of the data at low Reynolds numbers. Further attempts at bringing the data closer than in Figure 28 were not

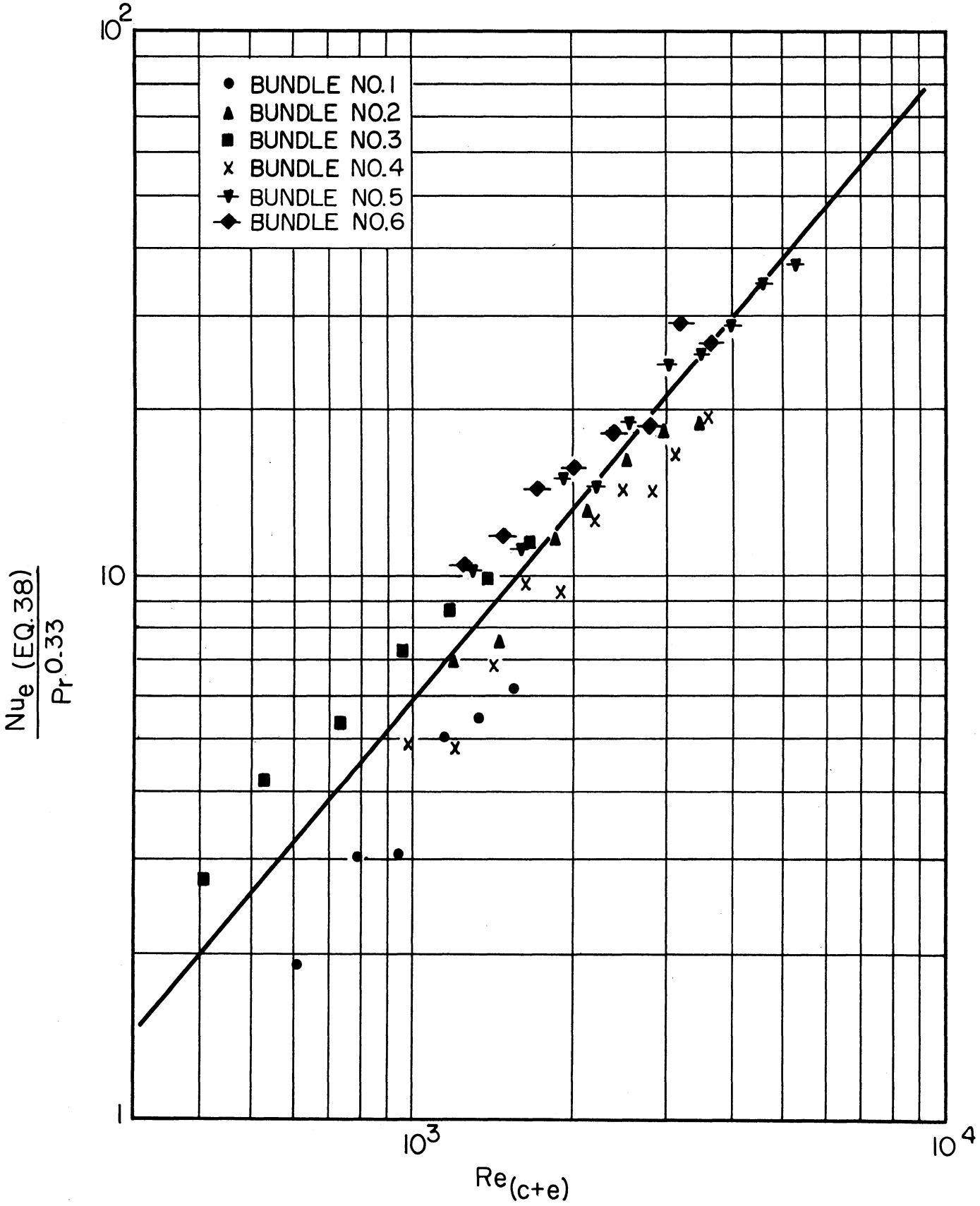

Fig 28 Correlation of eddy zone film coefficients calculated by equation 38

successful. Some of the possible reasons for the scatter of the data are discussed in Appendix B. A line is drawn through the data in Figure 28 representing the data for all the six bundles. This line gives a value of 0.00187 for C and 1.168 for m in equation (46), thus giving the following correlation for the heat transfer in the eddy zones:

$$\frac{h_e D_o}{k_f} = 0.00187 \left[\frac{D_o G_{(c + e) \text{ at dia.}}}{\mu_f} \right]^{1.168} \left[\frac{C_p \mu}{k} \right]_f^{0.33} \qquad (47)$$

Discussion of Correlation. Though the scatter of the data in Figure 28 is considerable (especially for Reynolds numbers below 1,500), considering that the correlation represented by this figure is only for a small part of the shell side heat transfer film coefficient, the coefficients predicted by this procedure using equation (47) for the calculation of the eddy zone heat transfer film coefficients, should be quite reliable. For example, at the low Reynolds number end of Figure 28 the worst deviation from the line is about ± 75 percent. At these Reynolds numbers the term $h_e \frac{A_e}{A_o}$ representing the share of the film coefficient for the eddy zones, is at most 10 to 15 percent of h_o, the total shell-side film coefficient. Thus, even in these worst regions of the correlation, the values of h_o calculated from the above procedure (based on flow patterns) will not differ from the experimental values of h_o by more than ± 10 to 12 percent. This reliability in predicting the shell-side heat transfer film coefficient by the present method is much better than that usually obtained by any of the available empirical correlations for the prediction of shell-side film coefficients.

An attempt was made to predict the shell-side coefficients for the water runs of the three plain tube bundles, for which data have been reported by Williams and Katz[62], using the present method. These bundles have different shell sizes, tube sizes, and tube pitches. The reason for choosing these data was because in some of the other data reported in the literature, some bundle characteristics necessary for the present method of calculation were not available. For Bundle No. 5 of that reference (6 in. shell and 5/8 in. tubes) the present method predicted the shell-side film coefficient (for all the runs attempted) within about ± 10 percent of the experimental values reported. For Bundle Nos. 1 (8 in. shell and 3/4 in. tubes) and 3 (8 in. shell and 1/2 in. tubes), however, the predicted values were higher from the experimental values by as much as 35 percent in the first case and as much as 70 percent in the second case. The Reynolds numbers used by Williams and Katz were considerably (about 10 times) higher than those used in the present study. The large deviations obtained by the present method in predicting Bundles 1 and 3 of Williams and Katz points out that the flow patterns are probably affected by the shell size, tube size, and the tube arrangements. This calls for further work directed towards establishing the effect of these design variables on the present method. Since the present work was aimed mainly at establishing the significance of the flow patterns in determining the shell-side heat transfer film coefficients, a more extensive study, which is necessary to extend the range of application of the present method, was considered out of its scope.

Correlation of Pressure Drop Data

Though the total pressure drop on the shell-side of a baffled shell and tube heat exchanger would be a summation of the pressure drops in the various zones of different flow characteristics, the analysis used to compute the shell-side heat transfer film coefficients from the flow patterns cannot be extended to calculate the shell-side pressure drop because in the case of pressure drop there is no simple extensive property (like A, the heat transfer area, in the case of heat transfer calculations) which can be used to combine the pressure drop characteristics of the component zones. Undoubtedly for the total pressure drop, we have the equation:

$$\Delta P = (\Delta P)_{\ell} + (\Delta P)_{c} + (\Delta P)_{e} \qquad (48)$$

corresponding to equation (27) for heat transfer. But there are no simple means available to calculate the three component pressure drops of the right hand side of equation (48).

The nearest approach to the use of equation (48) is the method of correlation of shell-side pressure drop proposed by Donohue.[14] Donohue's method divides the pressure drop into two components, namely, a) the pressure drop during flow through baffle windows, and b) the pressure drop during flow across tubes. The pressure drop during flow through the windows, $(\Delta P)_{w}$, is calculated by Donohue from the equation:

$$(\Delta P)_{w} = \frac{2.9\ G_{w}^{2}\ N_{B}}{10^{13}\ (\text{sp. gr.})} \qquad (49)$$

and the pressure drop during flow across tubes (obtained by difference) correlated as a friction factor with the cross flow Reynolds number. The cross flow friction factor, f, is defined as:

$$f = 9.35 \times 10^{8} \frac{g_c' \text{ (sp. gr.) } (\Delta P)_{cross}}{N_c \, G^2_{(c + e) \text{ at dia.}}} \left(\frac{\mu}{\mu_{wall}} \right)^{0.14} \qquad (50)$$

and is considered a function of the apparent cross flow Reynolds number. Donahue in his paper gives different curves for the relationship between f and $Re_{(c + e)}$ for different values of p/D_o of the bundle. His Figure 28 gives the curve for p/D_o of 1.2 which is closest to that value for the bundles used in the present work.

The values of $(\Delta P)_w$ and f from the equations (49) and (50) for the pressure drop data in the present study [reported in Table IV (Appendix A)] were calculated and are listed in Table V (Appendix A) for the representative runs of the six bundles tested. In the calculation of f the factor $(\frac{\mu}{\mu_{wall}})^{0.14}$ was neglected because the change in viscosities in the present study is not appreciable to make a difference in this factor. Even if it were taken into consideration its value will be quite close to one. Figure 29 shows a plot of f versus $Re_{(c + e)}$ for the representative runs of the six bundles tested along with the curve from Figure 28 of Donohue's paper which is suggested for a p/D_o of 1.2. As can be seen from Figure 29, there is very little agreement between the data and Donohue's curve. Most of the data lie below the curve. Even in Donohue's original work (his Figure 28) all the data that he used for the correlation lay below this curve. In this sense the present data is similar to the data used by Donohue[14] as against the data of Williams and Katz[62] which lie above Donohue's curve.

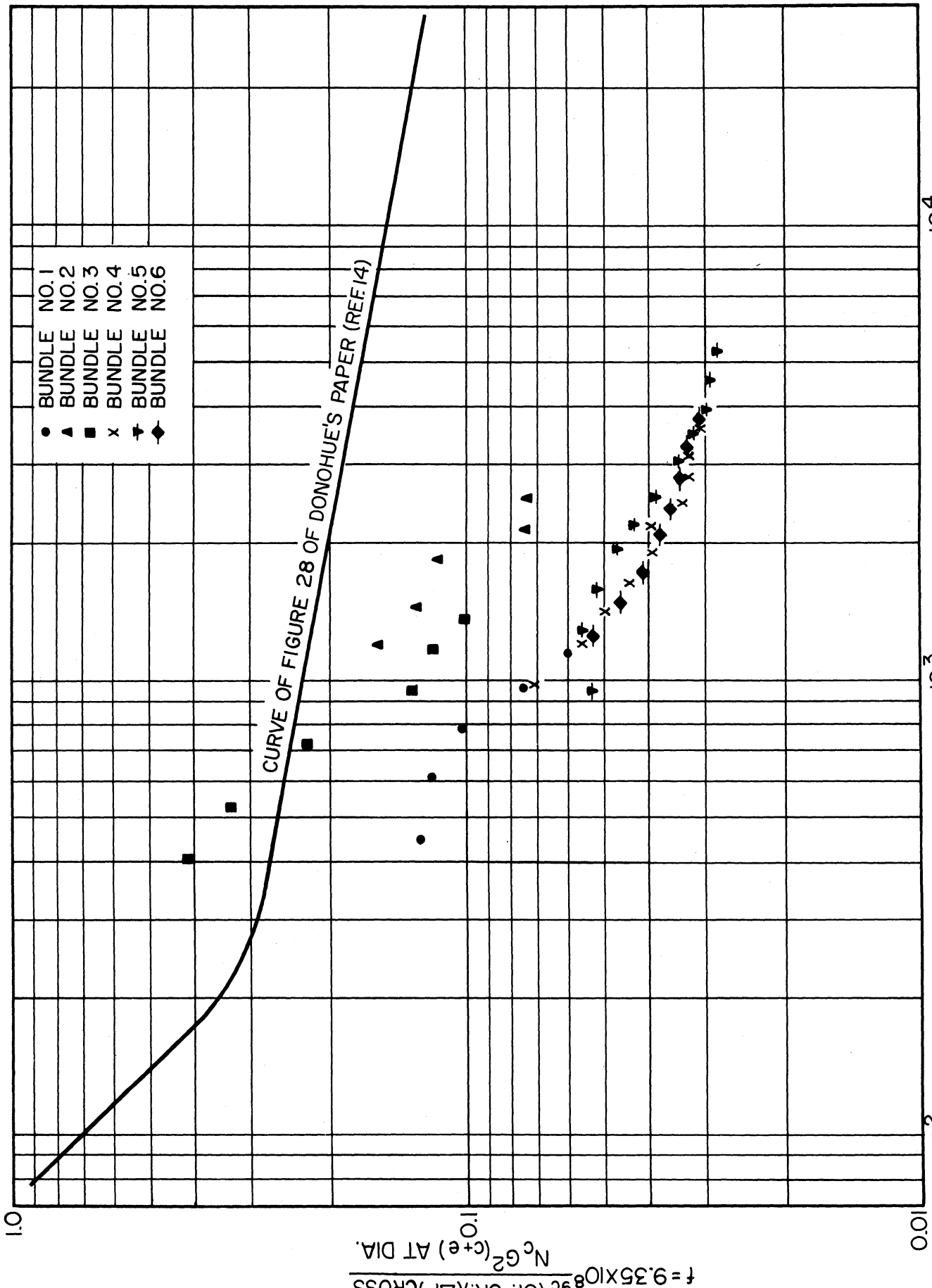

Fig 29 Friction factor for flow across tube bundles in the six bundles tested (by the method of ref. 14)

Figure 29 shows the inadequacy of the method of correlation proposed by Donohue. One thing that may be said in favor of this method is that the correlation represented by Figure 29 is only for a small part of the pressure drop since in most designs the pressure drop for flow through the baffle windows forms the major part of the total pressure drop. Moreover, Donohue's correlation almost always predicts pressure drops higher than the experimental values, thus giving a conservative estimate of the pressure drop.

In view of the inadequacy of Donohue's correlation, an attempt was made to correlate the data obtained in the present study by some direct empirical method. It was felt that since the pressure drop for flow through the windows forms a major portion of the total pressure drop the attempted correlation should be based on the window velocity rather than on the cross flow velocity. It was found that if $\Delta P \frac{X}{L}$ is plotted against G_w on a log-log plot the entire data (all the runs reported) for the six bundles tested lie on a straight line. The values of $\Delta P \frac{X}{L}$ are listed in Table IV (Appendix A). Figure 30 gives a plot of $\Delta P \frac{X}{L}$ in inches of mercury versus the window mass velocity, G_w, in pounds per hour per square foot. The dimensionless ratio $\frac{X}{L}$ is the ratio of the spacing between successive baffles to the total effective length (not just the baffled length) of the tube bundle. In Figure 30, the scatter of the experimental data from the straight line relationship is very small. The line of correlation in Figure 30 can be represented by the equation:

$$\Delta P \frac{X}{L} = 1.041 \times 10^{-11} (G_w)^{1.8} \qquad (51)$$

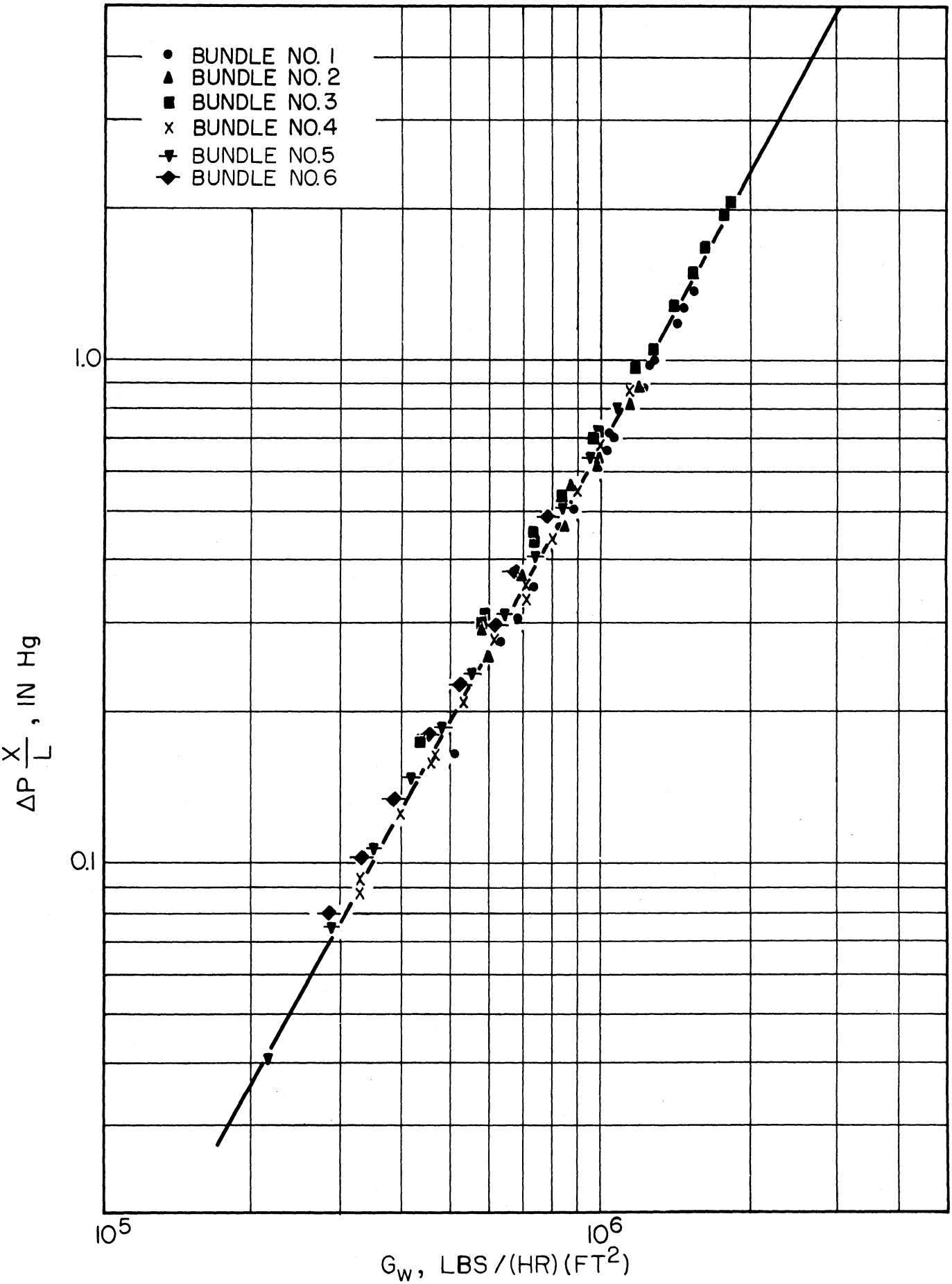

Fig. 30 Correlation of pressure drop data

if ΔP is expressed in inches of mercury, and:

$$\Delta P \frac{X}{L} = 5.12 \times 10^{-12} (G_w)^{1.8} \qquad (52)$$

if ΔP is expressed in pounds per square inch.

To compare the proposed correlation with pressure drop data from the literature, a plot similar to that of Figure 30 was made for some of the pressure drop data reported by Williams and Katz[62] and by Short.[52] Some water runs for the three plain tube bundles (Nos. 1, 3, and 5) were used from the data of Williams and Katz, and most of the data for the 3/8 in. tube diameter and 1/2 in. tube pitch bundles with 19, 15, and 11 baffles (marked as Bundles 1, 2, and 3 respectively) for Short's pressure drop data were used. Figure 31 shows a plot of $\Delta P \frac{X}{L}$ versus G_w for all these data along with the correlating line of Figure 30. Though the deviation of the data from the correlating line is considerably more than that in Figure 30, it is still tolerable. Since the data plotted in Figure 31 were obtained on bundles radically different from those used in obtaining the correlation of Figure 30, the deviation is not unexpected. It is hoped that multiplication of $\Delta P \frac{X}{L}$ with some factor representing the different bundle characteristics would generalize the correlation and thus give much less deviation than in Figure 31. This would require collecting all the pressure drop data available and probably obtaining further data by experimentation, and then to study the effect of various correlating factors. An extensive study of this nature was not considered within the scope of the present work. However, the present work indicates that the proposed correlation holds promise for a good method of predicting shell-side pressure drops for baffled shell-and-tube heat exchangers.

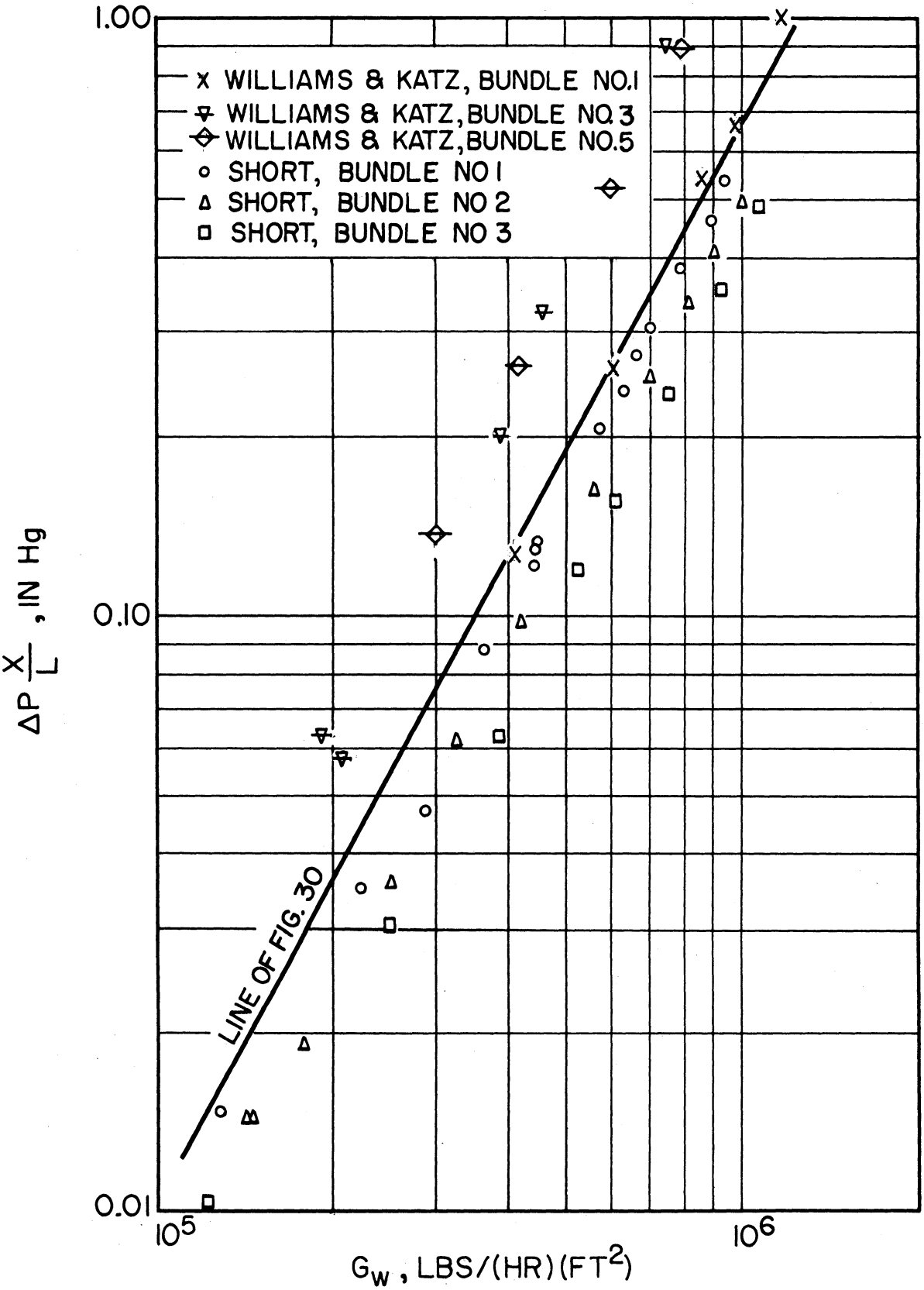

Fig 31 Comparison of proposed pressure drop correlation with data from refs. 52 and 62.

In plotting the data in Figure 30, the effects of viscosities and of equivalent diameters were neglected since these effects are negligible for the present study. To generalize the correlation of Figure 30, it can be expressed in terms of a friction factor. If the friction factor for the overall flow in the shell, f_o, is defined as:

$$f_o = \frac{\Delta P \, g_c \, \rho \, X}{2 \, L \, G_w^2} \tag{53}$$

The correlation of Figure 30 (represented by equations 51 and 52) will give:

$$f_o = 0.02462 \left[\frac{(D_e)_w \, G_w}{\mu_b} \right]^{-0.2} \tag{54}$$

In obtaining the constant 0.02462 for equation (54) an average value (0.0433) for

$$\frac{\mu^{0.2}}{(D_e)_w^{0.2} \, \rho_b}$$

for all the six bundles was used in the calculations. The variation of this value was from 0.0422 to 0.0464 for all the data plotted in Figure 30. This indicates that neglecting the effect of the physical properties and of the equivalent diameters in plotting the data in Figure 30 was justified.

To generalize equation (54) for use with bundles of different shell sizes, tube sizes, and tube arrangements, a correlating factor incorporating these design variables should be included in equation (54). This, however, is considered out of the scope of the present work.

CHAPTER VII

CONCLUSIONS AND RECOMMENDATIONS

Conclusions

The following conclusions can be drawn from the present study.

1) Fluid flow patterns play an important role in determining the shell-side heat transfer film coefficients.

2) The shell-side fluid flow can be divided into regions of three different flow characteristics, namely a) longitudinal flow zones, b) true cross flow zones, and c) eddy zones.

3) The mechanism of fluid flow and heat transfer in the eddy zones is significantly different from that in the other two types of zones.

4) The shell-side heat transfer film coefficient can be calculated by a weighted (on heat transfer area) summation of the heat transfer film coefficients for the various characteristic flow zones.

5) Using the correlations available in the literature for predicting the film coefficients for flow of fluids outside and parallel to tube bundles and those for flow of fluids across tube bundles, a correlation for the eddy zone heat transfer coefficients can be obtained from a knowledge of experimental total shell-side film coefficients and of the flow patterns. Based on the flow pattern and heat transfer studies on six tube bundles with constant tube size and tube spacing but with different combinations of baffle cut and baffle spacing, the following correlation is proposed for the heat transfer in the eddy zones:

$$\frac{h_e D_o}{k_f} = 0.00187 \left[\frac{D_o G_{(c + e) \text{ at dia.}}}{\mu_f}\right]^{1.168} \left[\frac{C_p \mu}{k}\right]_f^{0.33} \qquad (47)$$

6) The use of the proposed method of calculating shell-side film coefficients incorporating the use of the correlation of equation (47) predicts the coefficients within about ±10 to 12 percent within the range of the bundle designs studied.

7) Further work is needed to widen the range of application of the proposed method to bundles with different shell sizes, tube sizes, tube arrangements, baffle spacings and baffle cuts, than those used in the present study.

8) Further work is needed to obtain correlations for longitudinal and cross flow zones which are applicable to the shapes of these zones and the entrance and exit conditions pertaining to these zones in a baffled shell-and-tube heat exchanger.

9) The pressure drop data obtained in the present study are correlated by relating the overall shell-side friction factor, defined as

$$f_o = \frac{\Delta P \, g_c \, \rho \, X}{2 \, L \, G_w^2} \quad ,$$

with the window Reynolds number by the following equation:

$$f_o = 0.02462 \left[\frac{(D_e)_w \, G_w}{\mu_b}\right]^{-0.2} \qquad (54)$$

10) All the pressure drop data reported for the six bundles tested fit the correlation of equation (54) with deviations less than

± 10 percent. However, further work is needed to extend the range of application of the correlation represented by equation (54) to bundles with different shell sizes, tube sizes, and tube arrangements.

Recommendations for Future Research

In light of the knowledge gained in the present study about the flow patterns and the mechanism of heat transfer on the shell-side of baffled shell-and-tube heat exchangers, the following recommendations are made for future research.

1) Simultaneous flow pattern and heat transfer studies should be conducted on baffled shell-and-tube heat exchangers with a wider range of the shell-side design variables than was possible in the present study. The results of the present study hold promise that such an extensive study could lead to an accurate design method applicable to a wide range of design variables for the shell-side of baffled shell-and-tube heat exchangers. Specifically, bundles with different shell sizes, tube sizes, and tube arrangements and with a wider range of combinations of baffle cuts and baffle spacings should be tested in a manner similar to that used in the present study. This, it is hoped, would lead to a universal correlation for the eddy zone heat transfer.

2) Along with attempts at finding an empirical correlation for the eddy zone heat transfer, an effort should be made to study the exact nature of the flow in the eddy zones. The flow patterns and the heat transfer calculations in the present study showed that the eddy zones were zones of partial recirculation. Attempts should be made to determine the degree of recirculation in these zones by means of local studies using velocity and temperature probes. The variation of the

degree of recirculation with the shell-side design variables should also be studied. A study of the local velocities and temperatures in the eddy zones, in addition to yielding useful information about the degree of recirculation in these zones, would also lead to a better understanding of the mechanism of heat transfer in these zones.

3) The correlations available for flow of fluids outside and parallel to tube bundles are scarce and are mostly for fairly long bundles with a large number of tubes. The longitudinal flow zones in a baffled shell-and-tube heat exchanger, though involving flow of the fluid outside and parallel to the tubes, are somewhat different in geometry than the bundles used in developing the longitudinal flow correlations reported in the literature. The longitudinal flow zones in baffled exchangers are usually relatively short and are wedge shaped. The length of the tubes in these zones varies from zero near the baffle cut edge to a length approximately equal to twice the spacing between successive baffles. Further, the fluid makes sharp turns before entering and after leaving the longitudinal flow zones. In the case of heat transfer to fluids flowing inside tubes the heat transfer coefficients obtained are higher than usual if the tube L/D ratio is less than a certain critical value.[38] Not only is the heat transfer dependent on the length of the tube but is also affected by the entrance conditions. No such data are available for flow of fluids outside and parallel to tube banks. It is recommended that future research on heat transfer to fluids flowing outside and parallel to banks of tubes be conducted on bundle shapes and entrance and exit conditions similar to those of the longitudinal flow zones in baffled shell-and-tube heat exchangers.

4) For the calculation of the heat transfer coefficient for the cross flow zones in baffled shell-and-tube heat exchangers, all the correlations available are based on data for square bundles with equal number of tubes and equal tube length in each row. For most of the work reported the fluid entered perpendicular to the bundle. The geometry as well as the entrance and exit conditions for the true cross flow zones in baffled shell-and-tube heat exchangers are usually quite different from those used in developing the correlations. The true cross flow zones are of the shape of truncated wedges rather than being square bundles. Both the number and the length of the tubes in successive rows is different. The fluid makes sharp turns before entering and after leaving the true cross flow zones. Future work on heat transfer to fluids flowing across tube bundles, for being applicable to the true cross flow zones in baffled shell-and-tube exchangers, should be conducted on bundle shapes and entrance and exit conditions similar to those encountered in the true cross flow zones of baffled exchangers. The importance of the effect of entrance conditions on the cross flow coefficients is indicated by the present work. It seems that the window turnarounds in a baffled exchanger probably cause enough turbulence to maintain a high degree of heat transfer throughout the true cross flow zones, thus making the heat transfer in these zones almost independent of the number of rows of tubes in cross flow.

APPENDIX A

DATA AND CALCULATIONS

Bundle Characteristics	(Table II)
Sample Data Sheet	(Table III)
Summary of Experimental and Processed Data	(Table IV)
Summary of Correlation Calculations	(Table V)

TABLE II

BUNDLE CHARACTERISTICS

Characteristic	Bundle 1	Bundle 2	Bundle 3	Bundle 4	Bundle 5	Bundle 6
Shell diameter, inside, inches	6	6	6	6	6	6
Number of tubes	26	26	26	26	26	26
Tube outside diameter, inches	0.75	0.75	0.75	0.75	0.75	0.75
Tube inside diameter, inches	0.69	0.69	0.69	0.69	0.69	0.69
Tube pitch, center to center, on equilateral triangles, inches	15/16	15/16	15/16	15/16	15/16	15/16
Effective length of tubes, inches	119.5	119.5	119.5	119.5	119.5	119.5
Effective heat transfer surface, sq. ft.:						
External	50.8	50.8	50.8	50.8	50.8	50.8
Internal	46.8	46.8	46.8	46.8	46.8	46.8
Baffle cut: Percent of shell diameter	15.62	15.62	15.62	29.70	29.70	43.25
Percent of shell cross-sectional area	9.97	9.97	9.97	24.90	24.90	41.45
Length of baffled section of exchanger, inches	102.875	102.875	102.875	102.875	102.875	102.875
Baffle thickness, inches	3/16	3/16	3/16	3/16	3/16	3/16
Number of baffles	18	26	12	18	26	18
Baffle spacing (face to face), inches	5.85	3.92	9.15	5.85	3.92	5.85
Number of tubes in Window	1	1	1	5	5	10
Window equivalent diameter, ft.	0.06845	0.06845	0.06845	0.06655	0.06655	0.06390
Window free area, sq. ft.	0.01652	0.01652	0.01652	0.03352	0.03352	0.05070
Free area for cross flow, at diameter, sq. ft.	0.06100	0.04085	0.09535	0.06100	0.04085	0.06100
Total number of rows of tubes in bundle	7	7	7	7	7	7
Number of rows of tubes below baffle cut	6	6	6	5	5	4
$A\ell/A_o$	0.03845	0.03845	0.03845	0.1922	0.1922	0.3845
$A_{(c+e)}/A_o$	0.96155	0.96155	0.96155	0.8078	0.8078	0.6155
Baffle spacing/Effective bundle length = $\frac{X}{L}$	0.0490	0.0328	0.0766	0.0490	0.0328	0.0490

TABLE III

SAMPLE DATA SHEET

HEAT TRANSFER AND PRESSURE DROP DATA

Date: 6/29/56

Bundle No. 6

Run No. 36

Shell-side liquid - Propylene glycol + water

Tube-side liquid - Water

Baffle cut - 41.45 area percent

Baffle spacing - 5.85 in.

End baffle spacing - 8 in.

Avg. shell-side temp. - 45°C

Avg. tube-side temp. - 20.9°C

Shell-side liquid ref. index - 1.4046

Propylene glycol concentration - 67.0

Shell-side fluid density - 1.024 gms/cc

Tube-side fluid density - 0.998 gms/cc

Shell-side fluid C_p - 0.795

Tube-side fluid C_p - 0.999

		Rotameter #1	Rotameter #2	Rotameter #3	Rotameter #4	T_1 (Tube Outlet)		T_2 (Shell Inlet)		T_3 (Shell Outlet)		T_4 (Tube Inlet)	
	ΔP	W_1	W_2	W_3	W_4								
No.	In. Hg	(Shell)	(Shell)	(Tube)	(Tube)	mv	avg mv	mv	avg mv	mv	avg mv	mv	avg mv
1	9.88	162.0	173.0	160.0	162.0	0.933	0.9332	1.944	1.9389	1.743	1.7384	0.774	0.7766
						0.936		1.943		1.745		0.777	
						0.934		1.942		1.741		0.780	
						0.933		1.940		1.740		0.777	
						0.931		1.939		1.740		0.776	
						0.932		1.938		1.739		0.776	
						0.934		1.939		1.738		0.777	
						0.933		1.937		1.734		0.779	
						0.934		1.934		1.734		0.777	
						0.932		1.933		1.730		0.773	
2	7.68	142.0	151.0	160.0	162.0	0.931	0.9309	1.948	1.9478	1.726	1.7265	0.779	0.7802
						0.930		1.954		1.731		0.781	
						0.933		1.950		1.730		0.786	
						0.933		1.948		1.728		0.781	
						0.931		1.947		1.723		0.780	
						0.931		1.949		1.729		0.777	
						0.930		1.947		1.729		0.780	
						0.930		1.946		1.726		0.780	
						0.930		1.946		1.723		0.779	
						0.930		1.943		1.720		0.779	
3	6.02	124.5	133.5	160.0	162.0	0.930	0.9296	1.960	1.9604	1.716	1.7163	0.783	0.7830
						0.933		1.958		1.717		0.783	
						0.929		1.958		1.716		0.782	
						0.930		1.962		1.717		0.786	
						0.930		1.960		1.718		0.783	
						0.930		1.960		1.714		0.783	
						0.930		1.961		1.716		0.782	
						0.927		1.964		1.716		0.781	
						0.930		1.961		1.717		0.783	
						0.927		1.960		1.716		0.784	
4	4.62	108.0	116.0	160.0	162.0	0.925	0.9265	1.983	1.9777	1.708	1.7028	0.784	0.7836
						0.929		1.985		1.708		0.783	
						0.925		1.984		1.708		0.781	
						0.926		1.979		1.703		0.782	
						0.927		1.977		1.701		0.786	
						0.927		1.979		1.702		0.783	
						0.927		1.977		1.701		0.785	
						0.927		1.970		1.699		0.784	
						0.926		1.970		1.699		0.783	
						0.926		1.973		1.699		0.785	
5	3.60	94.5	101.0	160.0	162.0	0.922	0.9239	1.987	1.9850	1.680	1.6832	0.787	0.7876
						0.922		1.988		1.689		0.790	
						0.927		1.991		1.690		0.791	
						0.926		1.986		1.683		0.787	
						0.925		1.981		1.683		0.788	
						0.924		1.983		1.681		0.788	
						0.923		1.982		1.681		0.787	
						0.921		1.985		1.680		0.787	
						0.925		1.981		1.682		0.784	
						0.924		1.986		1.683		0.787	
6	2.67	79.5	85.0	160.0	162.0	0.920	0.9203	2.004	2.0036	1.668	1.6665	0.790	0.7894
						0.920		2.007		1.664		0.791	
						0.920		2.004		1.667		0.790	
						0.921		2.004		1.668		0.787	
						0.920		2.004		1.667		0.788	
						0.919		2.004		1.669		0.790	
						0.921		2.004		1.669		0.790	
						0.921		2.001		1.664		0.790	
						0.921		2.002		1.664		0.789	
						0.920		2.002		1.665		0.789	
7	2.07	68.5	73.0	160.0	162.0	0.917	0.9167	2.022	2.0208	1.649	1.6477	0.794	0.7913
						0.917		2.023		1.650		0.793	
						0.919		2.024		1.649		0.792	
						0.917		2.023		1.647		0.790	
						0.916		2.021		1.646		0.790	
						0.915		2.019		1.645		0.789	
						0.916		2.018		1.647		0.790	
						0.917		2.018		1.648		0.792	
						0.917		2.019		1.647		0.792	
						0.916		2.021		1.649		0.791	
8	1.62	60.5	60.0	160.0	162.0	0.917	0.9145	2.045	2.0429	1.630	1.6290	0.796	0.7942
						0.916		2.042		1.630		0.797	
						0.916		2.047		1.631		0.794	
						0.914		2.047		1.632		0.795	
						0.914		2.044		1.630		0.796	
						0.912		2.043		1.629		0.792	
						0.916		2.043		1.627		0.792	
						0.914		2.038		1.624		0.796	
						0.913		2.038		1.627		0.792	
						0.913		2.042		1.630		0.792	

W = Actual Rotameter Readings

T = Actual Potentiometer Readings

TABLE IV

SUMMARY OF EXPERIMENTAL AND PROCESSED DATA

Bundle No.	Run No.	Shell Side (Propylene Glycol-Water Solution) Flow Rate Lbs Per Hr	Shell Side Temperature, °F In	Shell Side Temperature, °F Out	Shell Side Temperature, °F Drop	Propylene Glycol Conc., %	Shell Side Heat Transfer Q_s Btu Per Hr	Pressure Drop In. Hg	Tube Side (Water) Temperature, °F In	Tube Side (Water) Temperature, °F Out	Tube Side (Water) Temperature, °F Rise	Tube Side (Water) Flow Rate Lbs Per Hr	Heat Transfer Q_t Btu Per Hr	LMTD °F	U_o based on Q_t	$\frac{10^3}{U_o}$	$\frac{10^3}{W_s^{0.65}}$	Shell Side Mean Film Temp., °F	$\frac{10^3 \mu_f^{0.32}}{C^{0.65} P_f^{0.33} k_f^{0.67}}$	Wilson Plot - Least square fit Slope b	Intercept a	Deviation s_c	h_o	$S_c/S_{(c+e)}$ and $A_c/A_{(c+e)}$	$\Delta P_s \frac{X}{L}$
1	19	31,200	120.50	104.30	16.20	80.75	372,000	off scale	41.90	51.40	9.50	37,620	357,500	65.35	107.70	9.300	1.191	99.33	12.020	0.290	5.882	0.0054	286.4	0.50	-
		27,600	121.15	103.45	17.70	"	359,800	off scale	41.70	50.90	9.20	"	346,000	66.20	102.90	9.720	1.291	98.34	13.130				262.4	"	-
		24,180	122.65	102.45	20.20	"	359,200	25.95	42.00	50.85	8.85	"	333,000	66.25	99.10	10.100	1.390	97.83	14.220				242.3	"	1.271
		20,730	123.00	101.65	21.35	"	325,500	19.75	42.40	50.85	8.45	"	318,000	65.45	95.70	10.460	1.562	97.08	16.120				213.8	"	0.968
		17,220	124.30	100.40	23.90	"	302,700	14.45	42.23	50.20	7.97	"	300,000	66.10	89.40	11.190	1.754	95.85	18.220				196.2	"	0.708
		13,700	126.35	98.75	27.60	"	278,200	9.50	42.80	50.15	7.35	"	276,500	65.95	82.60	12.110	2.042	94.79	21.330				161.8	"	0.466
		10,390	129.85	96.35	33.50	"	256,000	5.55	43.22	49.90	6.68	"	251,300	65.90	75.10	13.320	2.440	93.82	25.750				134.0	"	0.272
"	20	30,380	120.05	104.15	15.90	80.75	355,300	off scale	41.20	51.60	10.40	32,870	342,000	65.30	101.60	9.850	1.213	98.26	12.560	0.292	6.054	0.0161	272.8	0.50	-
		25,350	121.20	102.80	18.40	"	342,700	28.05	41.05	51.10	10.05	"	330,500	66.00	98.60	10.150	1.361	97.56	14.140				242.2	"	1.376
		21,200	122.70	102.00	20.70	"	322,700	20.15	41.60	51.20	9.60	"	316,000	66.45	93.60	10.690	1.528	96.98	15.900				215.5	"	0.987
		17,400	124.40	100.90	23.50	"	300,800	14.25	41.85	50.95	9.10	"	299,300	66.45	88.70	11.290	1.740	96.26	18.310				187.1	"	0.698
		14,540	125.25	99.00	26.25	"	281,300	10.25	41.90	50.25	8.35	"	274,500	66.00	82.00	12.200	1.961	94.55	20.930				163.8	"	0.502
		11,290	128.20	97.10	31.10	"	258,300	6.20	42.40	50.10	7.70	"	253,300	65.70	75.90	13.190	2.325	93.82	24.950				137.3	"	0.304
		9,640	129.70	95.25	34.45	"	244,000	4.50	42.75	49.80	7.05	"	231,800	65.40	69.80	14.330	2.565	92.55	27.780				123.3	"	0.221
"	21	31,600	120.25	104.40	15.85	80.75	368,500	off scale	41.90	51.40	9.50	37,620	357,500	66.60	105.70	9.470	1.177	99.16	12.110	0.289	5.968	0.0156	285.8	0.50	-
		26,800	121.30	103.30	18.00	"	355,200	off scale	41.90	51.00	9.10	"	342,500	66.20	101.90	9.820	1.309	98.38	13.540				255.7	"	-
		23,400	122.00	102.20	19.80	"	341,000	24.10	42.20	50.80	8.60	"	323,700	65.80	96.90	10.330	1.430	97.29	14.880				232.6	"	1.181
		19,870	123.40	101.30	22.10	"	323,200	17.90	42.15	50.25	8.10	"	304,800	66.15	90.80	11.020	1.601	96.28	16.860				205.5	"	0.877
		16,930	124.50	100.30	24.30	"	303,000	13.50	42.60	50.45	7.85	"	295,400	66.10	88.00	11.370	1.771	95.89	18.690				185.2	"	0.661
		14,580	125.55	99.00	26.55	"	285,000	10.30	42.45	49.95	7.50	"	282,200	66.00	84.15	11.890	1.961	95.20	20.760				166.8	"	0.505
		12,110	127.75	97.65	30.10	"	268,200	7.10	43.05	50.10	7.05	"	265,300	65.75	79.50	12.590	2.222	94.54	23.680				146.1	"	0.348
		10,080	129.85	95.95	33.90	"	251,600	5.00	43.30	49.80	6.50	"	244,500	65.70	73.30	13.660	2.470	93.50	26.480				130.8	"	0.245
		8,460	132.40	94.90	37.50	"	233,400	3.30	43.70	49.70	6.00	"	225,700	65.90	67.45	14.830	2.802	92.98	30.270				114.3	"	0.162
2	25	25,920	122.00	103.45	18.55	66.10	387,000	off scale	48.40	58.33	9.93	37,620	373,700	59.15	124.20	8.060	1.342	104.63	9.690	0.206	6.070	0.0080	501.0	0.55	-
		22,000	122.88	102.05	20.83	"	369,500	off scale	48.45	58.13	9.68	"	364,200	59.20	121.10	8.260	1.492	103.91	10.830				448.5	"	-
		18,810	123.85	100.25	23.60	"	358,000	24.70	48.70	57.93	9.23	"	347,500	58.60	116.60	8.590	1.653	102.74	12.120				400.5	"	0.810
		16,170	123.95	98.35	25.60	"	333,500	18.70	48.97	57.65	8.68	"	326,500	57.55	111.60	8.970	1.819	101.14	13.480				360.3	"	0.614
		13,880	124.55	96.30	28.25	"	316,000	14.10	49.10	57.55	8.45	"	318,000	56.60	110.60	9.050	2.020	100.41	15.090				321.8	"	0.463
		11,690	126.30	94.55	31.75	"	299,300	10.40	49.40	57.40	8.00	"	301,200	56.35	105.30	9.500	2.260	99.53	16.960				286.2	"	0.341
		9,800	127.65	92.38	35.27	"	278,000	7.70	49.80	57.25	7.45	"	280,300	55.60	99.40	10.070	2.540	98.26	19.180				253.5	"	0.253
"	26	25,650	121.70	103.30	18.40	66.5	380,500	off scale	48.67	58.35	9.68	37,620	364,200	59.10	121.30	8.250	1.361	104.56	9.930	0.212	6.161	0.0024	475.0	0.55	-
		22,150	122.85	102.15	20.70	"	369,500	off scale	48.73	58.15	9.42	"	354,500	58.95	118.50	8.450	1.481	104.07	10.870				434.5	"	-
		19,230	123.55	100.90	22.65	"	351,200	26.70	48.85	57.95	9.10	"	342,500	58.70	114.90	8.710	1.612	103.17	11.880				397.5	"	0.876
		16,290	125.45	99.70	25.75	"	338,000	19.25	48.95	57.80	8.85	"	333,200	58.85	111.50	8.970	1.819	103.31	13.410				351.8	"	0.631
		14,300	126.80	98.63	28.17	"	324,000	16.80	49.15	57.65	8.50	"	320,000	58.80	107.00	9.350	1.981	102.19	14.700				321.0	"	0.551
		11,470	129.30	96.55	32.75	"	302,500	11.20	49.35	57.45	8.10	"	304,800	59.00	101.80	9.840	2.300	101.47	17.130				272.3	"	0.368
		9,650	131.30	94.45	36.85	"	286,800	8.70	49.60	57.30	7.70	"	289,800	58.20	98.10	10.200	2.563	100.72	19.270				244.7	"	0.285
3	28	34,030	119.05	107.30	11.75	70.90	312,000	off scale	59.15	67.15	8.00	37,620	300,800	49.35	120.00	8.340	1.119	102.88	9.040	0.368	5.150	0.0108	300.7	0.37	-
		29,420	119.30	106.38	12.92	"	297,200	25.50	59.30	66.90	7.60	"	285,700	50.10	112.00	8.930	1.235	101.62	10.100				268.8	"	1.953
		25,420	120.25	105.85	14.40	"	286,800	19.50	59.55	66.70	7.15	"	268,800	49.75	106.40	9.410	1.361	101.08	11.170				243.7	"	1.495
		20,990	121.43	104.80	16.63	"	278,500	13.60	59.60	66.45	6.85	"	257,500	49.80	101.80	9.830	1.539	100.56	12.700				214.0	"	1.042
		16,260	122.80	103.50	19.30	"	244,700	9.20	59.98	66.30	6.32	"	237,700	49.75	94.00	10.640	1.819	99.66	15.070				180.6	"	0.705
		12,120	124.65	101.75	22.90	"	216,700	5.80	60.25	65.90	5.65	"	212,400	49.75	84.15	11.890	2.207	98.39	18.480				147.1	"	0.445
		9,640	126.40	99.77	26.63	"	200,200	4.00	60.50	65.55	5.05	"	189,900	49.25	76.00	13.170	2.565	97.34	21.670				125.4	"	0.307
"	31	34,000	118.48	107.20	11.28	70.30	299,300	off scale	60.88	68.62	7.74	37,730	291,700	48.09	119.40	8.380	1.124	102.65	9.110	0.366	4.950	0.0164	300.0	0.37	-
		29,820	118.65	106.70	11.95	"	278,200	26.75	60.95	68.40	7.45	"	280,700	48.10	115.10	8.690	1.220	101.85	9.970				274.2	"	2.050
		26,580	119.75	106.25	13.50	"	284,200	21.60	61.02	68.30	7.28	"	274,200	48.10	112.20	8.910	1.317	101.75	10.740				254.3	"	1.656
		23,250	120.45	105.50	14.95	"	271,500	16.80	61.13	68.13	7.00	"	263,800	48.05	108.10	9.250	1.440	101.26	11.800				231.8	"	1.288
		19,530	121.28	104.55	16.73	"	255,000	12.55	61.30	67.90	6.60	"	248,700	48.20	101.70	9.840	1.613	100.45	13.310				205.4	"	0.961
		16,200	122.25	103.65	18.60	"	235,300	9.10	61.38	67.75	6.37	"	240,000	48.10	98.25	10.190	1.827	100.08	15.120				180.8	"	0.697
		13,870	123.23	102.75	20.48	"	221,800	6.95	61.67	67.53	5.86	"	220,800	48.40	89.85	11.130	2.020	99.13	16.710				163.5	"	0.533
		12,160	124.35	102.10	22.25	"	211,200	5.65	61.78	67.40	5.62	"	211,800	48.15	86.50	11.570	2.200	98.94	18.290				149.7	"	0.433
		9,660	126.00	100.55	25.45	"	192,400	3.80	62.15	67.20	5.05	"	190,300	47.90	78.25	12.790	2.565	98.04	21.470				129.0	"	0.291
		7,270	128.85	97.97	30.88	"	175,300	2.25	62.50	66.90	4.40	"	165,800	47.60	68.50	14.610	3.098	97.00	26.050				104.9	"	0.172
4	33	38,000	117.70	108.68	9.02	67.10	272,700	17.20	68.10	75.00	6.90	37,620	259,000	41.64	122.80	8.150	1.042	107.85	7.370	0.295	6.120	0.0084	460.5	0.62	0.843
		33,470	118.00	107.95	10.05	"	267,300	13.50	68.23	74.85	6.62	"	249,000	41.44	118.30	8.460	1.131	107.07	8.025				422.5	"	0.661
		30,150	118.65	107.67	10.98	"	263,200	11.00	68.30	74.70	6.40	"	240,600	41.40	114.50	8.740	1.212	106.76	8.640				392.5	"	0.539
		27,000	119.18	107.22	11.96	"	256,700	8.90	68.35	74.70	6.35	"	238,700	41.75	112.70	8.880	1.300	106.58	9.260				366.2	"	0.436
		23,750	119.80	106.70	13.10	"	247,500	6.90	68.50	74.60	6.10	"	229,300	41.70	108.30	9.240	1.409	106.05	10.060				337.5	"	0.338
		20,780	120.45	106.18	14.27	"	235,800	5.50	68.52	74.53	6.01	"	226,000	41.70	106.70	9.380	1.576	105.91	11.280				300.7	"	0.270
		17,730	121.43	105.35	16.08	"	227,500	4.20	68.65	74.40	5.75	"	216,200	41.75	102.10	9.800	1.710	105.38	12.230				277.3	"	0.206
		15,340	122.15	104.50	17.65	"	215,600	3.20	68.75	74.30	5.58	"	209,800	41.45	99.60	10.040	1.888	105.02	13.440				250.3	"	0.157
		13,290	123.07	103.70	19.37	"	204,500	2.50	68.85	74.22	5.37	"	201,800	41.55	95.70	10.460	2.030	104.58	14.650				231.7	"	0.123
		11,030	124.63	102.57	22.06	"	192,600	1.80	68.94	74.00	5.06	"	190.200	41.50	90.20	11.090	2.343	104.04	16.960				200.0	"	0.088
"	34	38,150	117.70	108.70	9.00	66.50	274,800	17.30	68.04	75.13	7.09	37,620	266,300	41.67	125.90	7.950	1.037	107.41	7.490	0.292	5.900	0.0061	457.5	0.62	0.848
		33,420	118.35	108.25	10.10	"	270,000	13.50	68.12	74.97	6.85	"	257,400	41.76	121.30	8.250	1.131	106.93	8.180				419.0	"	0.661
		30,250	118.68	107.75	10.93	"	264,500	11.10	68.28	74.87	6.59	"	247,600	41.90	116.30	8.610	1.212	106.38	8.810				388.7	"	0.544
		27,000	119.20	107.27	11.93	"	257,800	8.90	68.27	74.78	6.51	"	244,500	41.90	114.90	8.710	1.300	106.11	9.440				363.0	"	0.436
		23,900	119.55	106.52	13.03	"	249,300	7.10	68.43	74.70	6.31	"	236,700	41.30	112.90	8.860	1.409	105.73	10.260				334.0	"	0.348
		20,850	120.53	106.18	14.35	"	239,600	5.50	68.50	74.60	6.10	"	229,300	41.80	108.00	9.260	1.551	105.38	11.300				303.3	"	0.270
		17,910	121.37	105.32	16.05	"	230,200	4.20	68.65	74.55	5.90	"	221,700	41.65	104.80	9.550	1.704	105.01	12.420				275.7	"	0.206
		15,580	122.12	104.57	17.55	"	218,600	3.30	68.72	74.40	5.68	"	213,300	41.50	101.20	9.890	1.878	104.57	13.70				250.0	"	0.162
		13,290	123.22	103.70	19.52	"	207,600	2.50	68.90	74.37	5.47	"	205,500	41.50	97.40	10.280	2.063	104.23	15.10				226.5	"	0.123
		11,030	124.75	102.40	22.35	"	197,300	1.90	69.05	74.17	5.12	"	192,300	41.30	91.40	10.910	2.343	103.63	17.23				198.8	"	0.093
5	35	36,350	118.50	108.40	10.10	67.10	292,000	24.90	68.17	75.50	7.33	37,620	275,500	41.67	130.10	7.690	1.079	108.71	7.585	0.229	6.017	0.0047	576.0	0.73	0.186
		32,050	118.80	107.75	11.05	"	281,700	19.55	68.27	75.43	7.16	"	269,400	41.43	128.00	7.815	1.163	108.28	8.200				533.0	"	0.641
		28,350	119.30	107.10	12.20	"	275,200	15.45	68.40	75.40	7.00	"	263,300	41.70	124.30	8.045	1.275	107.77	9.010				485.0	"	0.507
		25,050	120.23	106.57	13.66	"	272,200	12.25	68.53	75.33	6.80	"	255,700	41.45	121.30	8.245	1.371	107.59	9.690				450.5	"	0.402
		21,750	120.80	105.75	15.05	"	260,200	9.45	68.72	75.25	6.53	"	245,500	41.15	117.50	8.515	1.493	107.02	10.600				412.0	"	0.310
		18,510	121.87	104.82	17.05	"	251,000	7.15	68.73	75.05	6.32	"	237,700	41.15	113.90	8.790	1.668	106.61	11.890				367.7	"	0.235
		16,110	122.80	104.00	18.80	"	241,000	5.65	68.75	75.00	6.07	"	228,200	41.20	109.20	9.160	1.837	106.10	13.130				332.3	"	0.185
		14,070	123.57	103.15	20.42	"	228,300	4.45	69.05	74.97	5.92	"	222,400	40.85	107.50	9.310	2.000	105.86	14.310				305.3	"	0.146
		11,770	124.95	102.03	22.92	"	214,200	3.25	69.20	74.90	5.70	"	214,300	40.85	103.50	9.665	2.247	105.49	16.100				271.4	"	0.107
		9,635	126.80	100.45	26.35	"	202,000	2.25	69.25	74.67	5.42	"	203,700	40.75	98.40	10.170	2.553	104.97	18.310				238.3	"	0.074
		7,255	129.60	97.25	32.25	"	186,600	1.25	69.53	74.40	4.87	"	183,000	39.93	90.20	11.095	3.080	103.79	22.330				195.8	"	0.041
6	36	39,800	117.68	109.10	8.58	67.00	271,500	9.88	67.43	74.47	7.04	37,620	264,500	42.44	122.90	8.140	1.011	106.97	7.165	0.335	5.804	0.0025	416.5	0.68	0.484
		34,820	118.00	108.60	9.40	"	260,300	7.68	67.63	74.35	6.72	"	252,500	42.31	117.60	8.515	1.106	106.25	7.890				393.7	"	0.376
		30,630	118.57	108.15	10.42	"	253,800	6.02	67.75	74.32	6.57	"	247,000	42.33	115.00	8.700	1.206	106.00	8.625				346.2	"	0.295
		26,600	119.30	107.58	11.72	"	247,800	4.62	67.77	74.15	6.38	"	239,700	42.50	111.00	9.015	1.317	105.59	9.435				316.5	"	0.226
		23,250	119.62	106.75	12.87	"	237,800	3.60	67.94	74.05	6.11	"	229,700	41.75	108.30	9.235	1.440	105.08	10.360				288.3	"	0.176
		19,620	120.40	106.00	14.40	"	224,800	2.67	68.00	73.90	5.90	"	221,700	42.25	103.30	9.680	1.613	104.47	11.660				256.2	"	0.131
		16,900	121.15	105.20	15.95	"	214,300	2.07	68.10	73.70	5.60	"	210,500	41.95	98.75	10.130	1.771	103.88	12.810				233.2	"	0.101
		14,430	122.10	104.45	17.65	"	202,500	1.62	68.25	73.62	5.37	"	201,800	42.05	94.60	10.580	1.962	103.48	14.270				209.5	"	0.079

TABLE V

SUMMARY OF CORRELATION CALCULATIONS

Bundle No.	Run No.	Shell-Side Flow Rate W_s lbs/hr	$h_{o_{exp}}$	μ_f lbs/hr·ft	C_{p_f} Btu/lb·°F	k_f Btu/hr·ft·(°F/ft)	Pr_f	$(Pr_f)^{0.33}$	$G_w \cdot 10^{-3}$ lbs/hr·ft²	$G_{(c+e)}$ at dia $\cdot 10^{-3}$ lbs/hr·ft²	Re_w	$Re_{(c+e)}$	h_ℓ	$C_N h_{(c+e)}$	h_o eq.37	$-h_{o_{exp}}$	Re_c	$C_N h_c$	h_e eq.40	$\frac{Nu_e \text{ eq.40}}{Pr_f^{0.33}}$	h_c	h_e eq.38	$\frac{Nu_e \text{ eq.38}}{Pr_f^{0.33}}$	ΔP_{exp} psi	ΔP_w psi	f
1	19	31,200	286.4	20.58	0.730	0.157	95.80	4.510	1,889.0	511.5	6,285	1,553	364.0	308.6	311.0	+ 8.47	3,108	465.0	100.7	8.81	495.0	71.5	6.20	---	---	---
		27,600	262.4	21.07	0.730	0.157	98.00	4.540	1,671.0	452.5	5,435	1,341	326.5	289.7	291.1	+ 10.92	2,683	429.0	89.6	7.81	456.0	63.2	5.46	---	---	---
		24,180	242.3	21.55	0.730	0.157	100.10	4.580	1,463.0	396.0	4,650	1,150	292.3	270.4	271.6	+ 12.09	2,302	395.0	84.2	7.28	420.0	59.3	5.08	12.750	10.930	0.0598
		20,730	213.8	22.03	0.730	0.157	102.50	4.600	1,256.0	340.0	3,897	964	253.0	255.3	255.3	+ 19.40	1,928	364.0	59.5	5.13	387.5	36.0	3.07	9.710	8.030	0.0744
		17,220	189.2	22.52	0.725	0.158	103.30	4.620	1,043.0	282.2	3,175	784	216.8	231.0	221.1	+ 16.86	1,568	319.0	56.0	4.80	339.7	35.8	3.03	7.110	5.540	0.1017
		13,700	161.8	23.00	0.725	0.158	105.60	4.650	829.0	224.5	2,465	610	178.9	199.2	198.7	+ 22.82	1,221	282.0	40.6	3.46	300.0	22.7	1.91	4.670	3.503	0.1190
		10,390	134.0	23.73	0.725	0.158	108.90	4.710	628.5	170.2	1,815	448.5	141.8	179.3	178.3	+ 32.83	897	252.2	14.6	1.21	268.3	0	0	2.728	2.015	0.1268
2	26	25,650	475.0	11.31	0.800	0.1816	49.90	3.640	1,553.4	627.9	9,400	3,467	471.5	457.5	458.2	-16.8	6,305	656.0	252.3	23.85	698.5	200.5	18.94	---	---	---
		22,150	434.5	11.45	0.800	0.1816	50.45	3.655	1,341.2	542.2	8,020	2,960	416.0	424.0	423.5	-11.0	5,385	593.5	241.6	22.70	631.0	194.7	18.30	---	---	---
		19,230	397.5	11.68	0.800	0.1816	51.45	3.675	1,164.4	470.7	6,830	2,522	366.5	381.5	380.8	-16.7	4,590	546.5	216.4	20.27	581.5	173.7	16.27	13.120	9.970	0.0729
		16,290	351.8	11.62	0.800	0.1816	51.25	3.665	986.4	398.8	5,805	2,142	324.0	350.0	348.3	- 3.5	3,895	495.0	178.2	16.74	526.5	138.9	13.07	9.460	7.170	0.0739
		14,300	321.0	11.87	0.800	0.1816	52.30	3.695	865.9	350.1	4,995	1,846	287.2	328.0	326.6	+ 5.6	3,356	454.5	160.7	14.96	484.0	124.9	11.62	8.260	5.520	0.1149
		11,470	272.3	12.06	0.800	0.1816	53.10	3.710	694.5	280.8	3,942	1,457	239.5	284.0	282.5	+10.5	2,647	405.0	112.3	10.42	431.0	80.4	7.45	5.505	3.545	0.1279
		9,650	244.7	12.30	0.800	0.1816	54.20	3.740	584.3	236.2	3,255	1,202	206.3	260.6	258.6	+13.9	2,185	363.3	103.1	9.49	386.3	74.6	6.87	4.280	2.510	0.1536
3	28	34,030	300.7	13.55	0.755	0.173	60.65	3.890	2,060.6	356.9	10,400	1,648	519.5	298.8	307.7	+ 7.0	4,455	542.0	144.9	13.47	630.5	124.1	11.54	---	---	---
		29,420	268.8	14.04	0.755	0.173	62.95	3.930	1,781.4	308.5	8,685	1,375	455.0	276.0	273.0	+ 4.2	3,720	491.0	125.9	11.56	571.0	107.5	9.86	12.530	10.670	0.1007
		25,420	243.7	14.16	0.755	0.173	63.45	3.940	1,539.2	266.6	7,440	1,179	405.0	261.5	267.1	+23.4	3,186	451.0	111.0	10.17	525.0	94.1	8.61	9.590	7.940	0.1192
		20,990	214.0	14.40	0.755	0.173	64.50	3.955	1,271.0	220.1	6,045	955	342.3	241.8	245.6	+31.6	2,583	402.0	95.1	8.69	468.0	79.9	7.29	6.685	5.435	0.1323
		16,260	180.6	14.64	0.755	0.173	65.55	3.985	984.6	170.5	4,600	725.5	277.5	205.6	207.6	+27.0	1,968	353.2	72.7	6.59	411.0	59.3	5.37	4.525	3.263	0.2233
		12,120	147.1	15.00	0.755	0.173	67.20	4.005	733.9	127.1	3,345	529.5	215.4	182.7	184.0	+37.9	1,432	292.0	57.5	5.18	340.0	46.4	4.19	2.852	1.811	0.3310
		9,640	125.4	15.49	0.755	0.173	69.40	4.050	583.7	101.1	2,577	409.0	176.1	163.6	164.0	+38.6	1,106	263.8	40.6	3.62	307.0	30.6	2.73	1.967	1.143	0.4150
4	34	38,150	457.5	10.90	0.800	0.1816	48.05	3.590	1,138.1	625.4	6,945	3,585.	369.3	446.0	431.5	-26.0	5,790	589.0	299.0	28.68	647.0	203.0	19.48	8.500	6.590	0.0302
		33,420	419.0	10.99	0.800	0.1816	48.45	3.600	997.0	547.9	6,045	3,117	331.7	414.5	398.6	-20.4	5,030	548.0	263.5	25.22	602.0	174.0	16.63	6.635	5.060	0.0324
		30,250	388.7	11.09	0.800	0.1816	48.90	3.610	902.4	495.9	5,420	2,800	304.2	391.5	374.8	-13.9	4,520	515.5	234.2	22.33	567.5	150.3	14.33	5.455	4.155	0.0326
		27,000	363.0	11.11	0.800	0.1816	49.00	3.615	805.5	442.6	4,825	2,490	278.3	362.7	346.8	-16.2	4,020	477.5	228.7	21.80	525.0	151.6	14.44	4.380	3.315	0.0336
		23,900	334.0	11.17	0.800	0.1816	49.15	3.620	713.0	391.8	4,250	2,193	250.7	344.5	326.6	- 7.4	3,540	445.0	205.3	19.55	489.5	132.0	12.57	3.490	2.515	0.0392
		20,850	303.3	11.21	0.800	0.1816	49.45	3.627	622.0	341.8	3,695	1,903	224.6	316.6	299.1	- 4.2	3,074	417.0	166.7	15.81	459.0	98.6	9.37	2.705	1.970	0.0389
		17,910	275.7	11.27	0.800	0.1816	49.60	3.630	534.3	293.6	3,160	1,628	198.2	283.3	266.8	- 8.9	2,605	374.3	162.4	15.40	412.0	102.0	9.66	2.065	1.454	0.0439
		15,580	250.0	11.31	0.800	0.1816	49.90	3.640	464.8	255.4	2,735	1,410	176.9	265.0	248.0	- 2.0	2,276	351.8	129.7	12.28	387.0	72.4	6.79	1.622	1.101	0.0494
		13,290	226.5	11.38	0.800	0.1816	50.10	3.645	396.5	217.9	2,320	1,199	156.0	246.0	228.8	+ 2.3	1,934	328.2	104.2	9.84	361.3	50.8	4.80	1.230	0.803	0.0555
		11,030	198.8	11.50	0.800	0.1816	50.70	3.655	329.1	180.8	1,906	983	133.6	227.0	209.0	+10.2	1,587	285.0	98.4	9.28	313.5	52.1	4.92	0.935	0.551	0.0707
5	35	36,350	576.0	10.65	0.790	0.179	47.00	3.565	1,084.4	889.8	6,785	5,230	359.5	603.5	513.1	- 62.9	7,160	651.0	561.0	55.00	716.0	384.2	37.62	12.240	8.640	0.0280
		32,050	533.0	10.77	0.790	0.179	47.50	3.580	956.1	784.6	5,910	4,560	321.0	554.5	469.3	- 63.7	6,255	608.0	520.0	50.70	669.0	354.3	34.58	9.610	6.710	0.0290
		28,350	485.0	10.89	0.790	0.179	48.00	3.593	845.8	694.0	5,170	3,980	290.7	514.5	433.2	- 51.8	5,460	561.0	449.5	43.70	618.0	298.7	29.10	7.600	5.275	0.0298
		25,050	450.5	10.91	0.790	0.179	48.20	3.595	747.3	613.2	4,555	3,505	264.8	484.5	407.1	- 43.4	4,805	526.0	410.0	39.85	579.0	266.2	25.88	6.025	4.105	0.0316
		21,750	412.0	11.01	0.790	0.179	48.60	3.603	648.9	532.4	3,920	3,018	232.7	444.5	371.7	- 40.3	4,140	480.5	385.0	37.27	529.0	255.4	24.74	4.650	3.087	0.0340
		18,510	367.7	11.16	0.790	0.179	49.20	3.620	552.2	453.1	3,297	2,538	205.8	399.8	333.3	- 34.4	3,480	439.5	316.7	30.53	483.5	198.0	19.08	3.517	2.242	0.0384
		16,110	332.3	11.21	0.790	0.179	49.45	3.630	480.6	394.4	2,855	2,200	182.9	379.5	313.9	- 18.4	3,017	407.0	262.8	25.25	448.0	153.0	14.71	2.780	1.699	0.0429
		14,070	305.3	11.25	0.790	0.179	49.60	3.633	419.8	344.4	2,485	1,913	163.3	343.5	283.7	- 21.6	2,623	369.4	258.0	24.77	406.0	158.0	15.18	2.187	1.296	0.0464
		11,770	271.4	11.30	0.790	0.179	49.90	3.640	351.1	288.1	2,066	1,593	141.9	307.5	253.1	- 18.3	2,183	336.7	208.4	20.02	370.5	117.9	11.30	1.599	0.906	0.0515
		9,635	238.3	11.42	0.790	0.179	50.45	3.655	287.4	235.9	1,672	1,291	120.2	272.2	223.2	- 15.1	1,770	295.6	188.6	18.00	325.0	108.1	10.33	1.107	0.607	0.0554
		7,255	195.8	11.74	0.790	0.179	51.85	3.685	216.4	177.6	1,228	944	95.3	243.3	197.1	+ 1.3	1,293	255.3	123.8	11.72	280.5	55.0	5.21	0.615	0.345	0.0529
6	36	39,800	416.5	11.06	0.790	0.179	48.80	3.610	785.0	652.5	4,540	3,626	275.5	433.0	372.4	- 44.1	5,340	537.5	434.5	42.00	611.0	278.0	26.87	4.855	3.153	0.0308
		34,820	393.7	11.18	0.790	0.179	49.35	3.627	686.8	570.8	3,930	3,193	246.0	403.0	342.6	- 51.1	4,700	504.0	449.0	43.00	573.0	302.2	29.05	3.777	2.415	0.0322
		30,630	346.2	11.25	0.790	0.179	49.60	3.630	604.1	502.1	3,425	2,790	221.7	380.0	319.2	- 27.0	4,105	467.0	331.5	31.90	531.0	196.0	18.88	2.962	1.862	0.0336
		26,600	316.5	11.37	0.790	0.179	50.15	3.645	524.7	436.1	2,950	2,398	196.3	344.8	287.8	- 28.7	3,530	428.0	314.3	30.13	486.0	189.3	18.18	2.273	1.402	0.0353
		23,250	288.3	11.45	0.790	0.179	50.50	3.650	458.6	381.1	2,557	2,080	175.2	322.0	265.6	- 22.7	3,060	395.6	280.5	26.83	450.0	166.0	15.91	1.770	1.070	0.0371
		19,620	256.2	11.57	0.790	0.179	51.03	3.665	387.0	321.6	2,137	1,722	153.0	286.5	235.3	- 20.9	2,535	351.4	255.2	24.25	399.7	153.0	14.56	1.312	0.764	0.0408
		16,900	233.2	11.69	0.790	0.179	51.55	3.675	333.3	277.0	1,821	1,482	134.6	264.2	214.4	- 18.8	2,180	329.4	221.0	21.02	374.5	125.4	11.93	1.019	0.566	0.0455
		14,430	209.5	11.86	0.790	0.179	52.35	3.700	284.6	236.6	1,533	1,248	118.0	242.7	194.8	- 14.7	1,835	298.7	198.2	18.70	340.0	111.1	10.50	0.796	0.414	0.0526

APPENDIX B

POSSIBLE REASONS FOR SCATTER IN EDDY ZONE CORRELATION

The data points in Figure 28, which represents the final correlation obtained for the heat transfer coefficients in the eddy zones, exhibit considerable scatter. The scatter is especially large at low Reynolds number values, the deviations of the data from the line being as high as ± 75 percent for Reynolds numbers below 1000. The following could be the possible reasons for this deviation:

1) In the calculation of the experimental shell-side heat transfer film coefficient the Wilson plots were corrected for the physical property changes. In developing the equation on which to base the Wilson plots (equation 19), the exponent of the shell-side velocity term was established as 0.65 by least square fit of the data. But the exponent for the Prandtl number was arbitrarily chosen as 0.33 from the value most commonly used in the literature. The variation of physical properties for any particular bundle was not sufficient to allow an empirical evaluation of this exponent. It is possible that this exponent should have a value different from 0.33. If the value of 0.33 is slightly off for the Prandtl number exponent, this could introduce some discrepancy between the experimental shell-side film coefficients calculated by this equation for runs with appreciable difference in physical properties. The runs for Bundle No. 1 were all carried out with a propylene glycol concentration of 80.75 in the shell-side solution. The propylene glycol concentration for the runs for all the other bundles was between 66.5 to 70.9 percent. An examination of Figure 28 reveals that all the data for the first bundle lie below the correlation line and are responsible for a major part of the scatter.

If the effect of using the correct exponent (different from 0.33) in equation (19) were to raise the data points for Bundle No. 1 in Figure 28, a considerable amount of the scatter will be eliminated, though this will have the effect of reducing the slope of the correlating line in Figure 28.

2) The lengths of the tubes in the longitudinal zones are quite short as compared to the bundle lengths for which the longitudinal flow correlations used for these zones were reported. Also the flow turns before entrance into and after exit from the longitudinal flow zones. Both these factors probably cause a higher rate of heat transfer than that evaluated by equation (35). However, the exact nature of this effect is uncertain. An attempt was made to estimate this effect from the data available for the case of flow of fluids inside tubes. If this data were to hold good for the geometry in the longitudinal flow zones, the above mentioned effect will be quite small. Moreover, as far as the effect of the tube length is concerned, the correction would lead to a larger scatter in Figure 28 than at present. For example, comparing Bundle Nos. 1 and 3, the tube length correction will increase the longitudinal flow coefficients for Bundle No. 1 more than it would those for Bundle No. 3, because the tube lengths in the longitudinal flow zones are shorter in Bundle No. 1 than in Bundle No. 3. This means that the correction would cause the data points in Figure 28 for Bundle No. 1 to be lowered more than those for Bundle No. 3, thus causing a larger scatter than shown in Figure 28. The solution to this problem lies in further research for obtaining correlations for the longitudinal flow zones on bundles similar in geometry to these zones.

3) The reduction of scatter in going from Figure 27 to Figure 28 by taking into effect the turbulence introduced into the true cross flow zones by the window turnabouts points to the necessity of further research for obtaining correlations for the true cross flow zones on bundles similar in geometry to these zones.

4) The Reynolds number used for the correlation in Figures 27 and 28 was chosen to be that for the apparent cross flow zones. Out of the various Reynolds numbers that could be used this seemed to give the best fit of the data. It also seemed the most reasonable since the eddy zones are included in the cross-sectional area in the calculation of the apparent cross flow Reynolds number. Surely the longitudinal flow and the true cross flow Reynolds numbers will be less reasonable since they do not even include the region under consideration. It could be that some kind of a Reynolds number for the eddy zones should be used. A study of the local velocities and temperatures in the eddy zones will throw some light on the mechanism of heat transfer in these zones and may lead to the exact Reynolds number that should be used in the correlation.

APPENDIX C

PROPERTY CHARTS

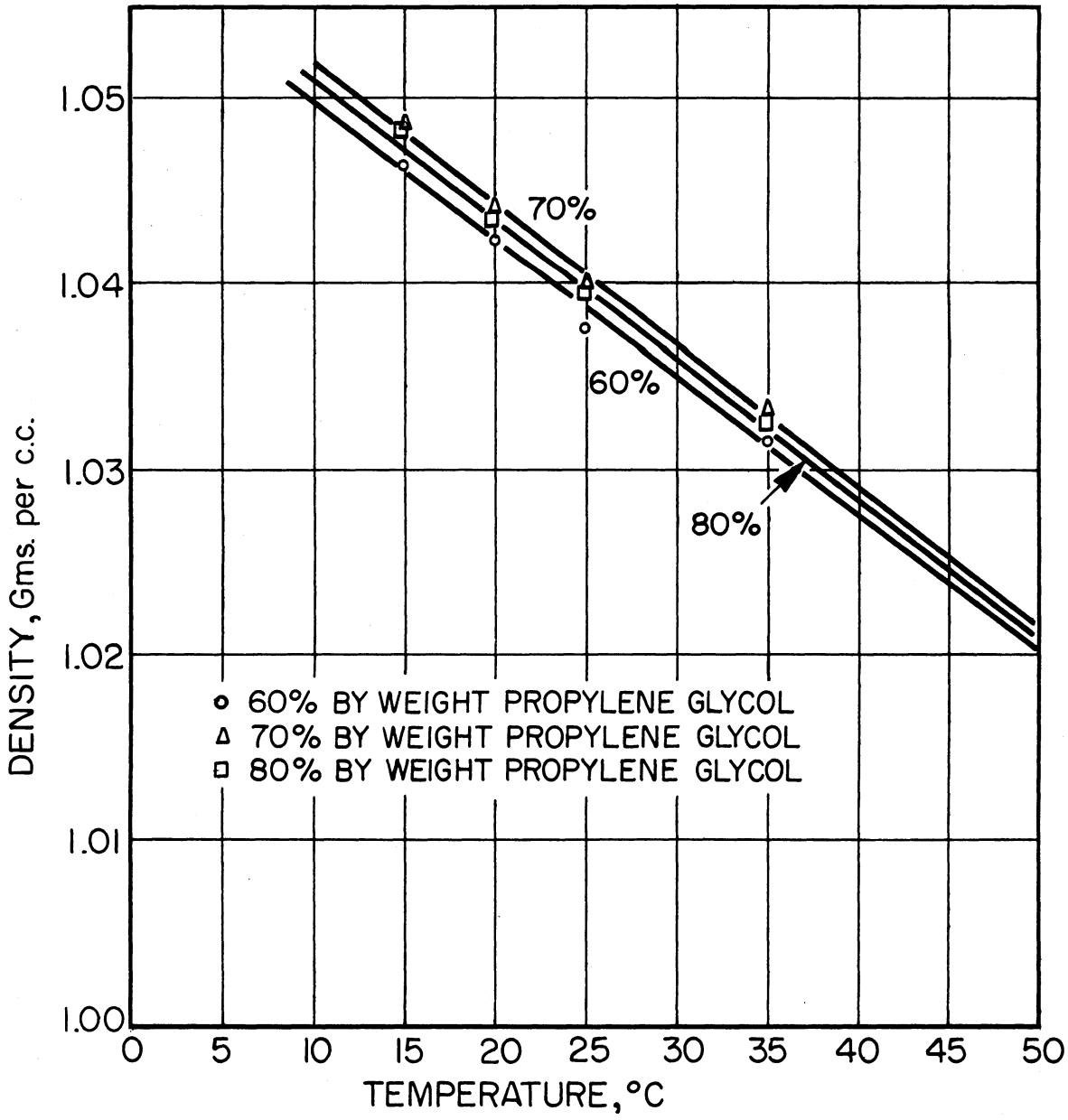

Fig 32 Extrapolation of density - temperature data for 60%, 70% and 80% propylene glycol - water solutions

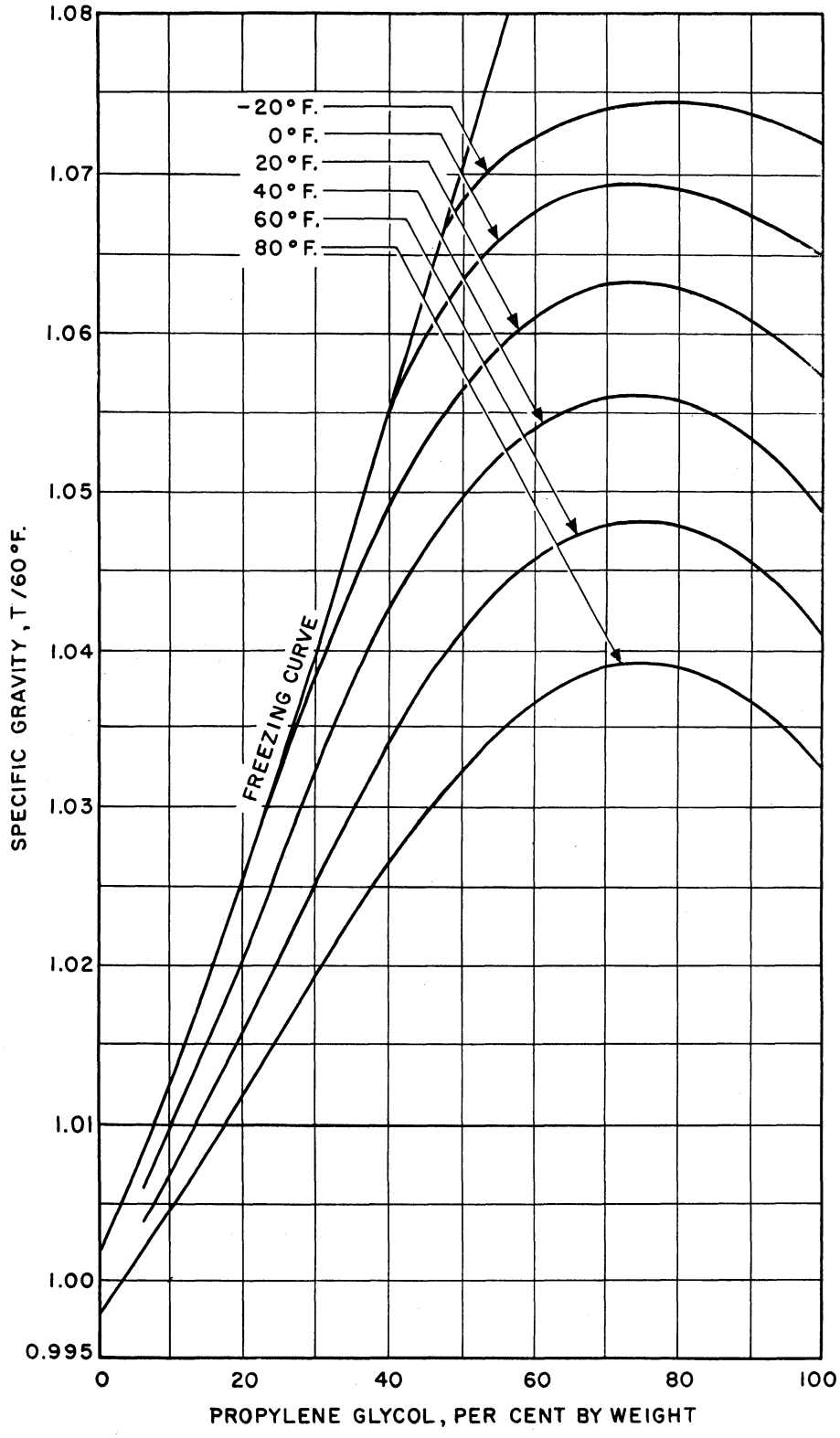

Fig 33 Specific gravity of aqueous propylene glycol solutions

(Courtesy Carbide & Carbon Chem. Co.)

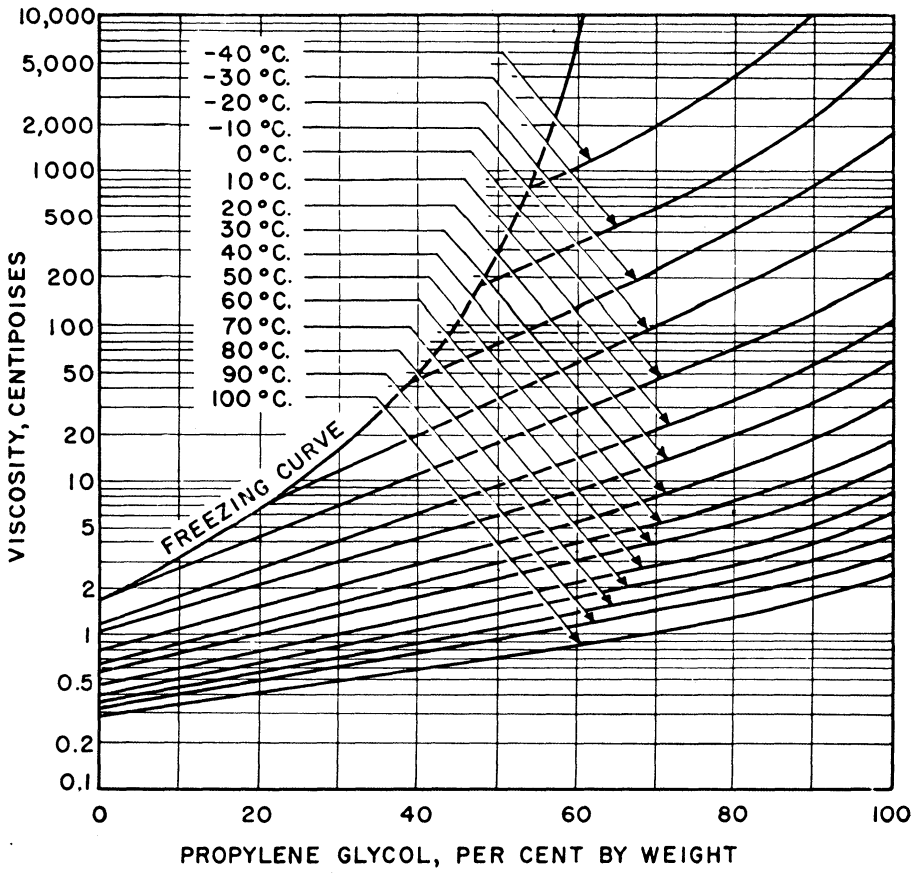

Fig 34 Viscosity of aqueous propylene glycol solutions

(Courtesy Carbide & Carbon Chem. Co.)

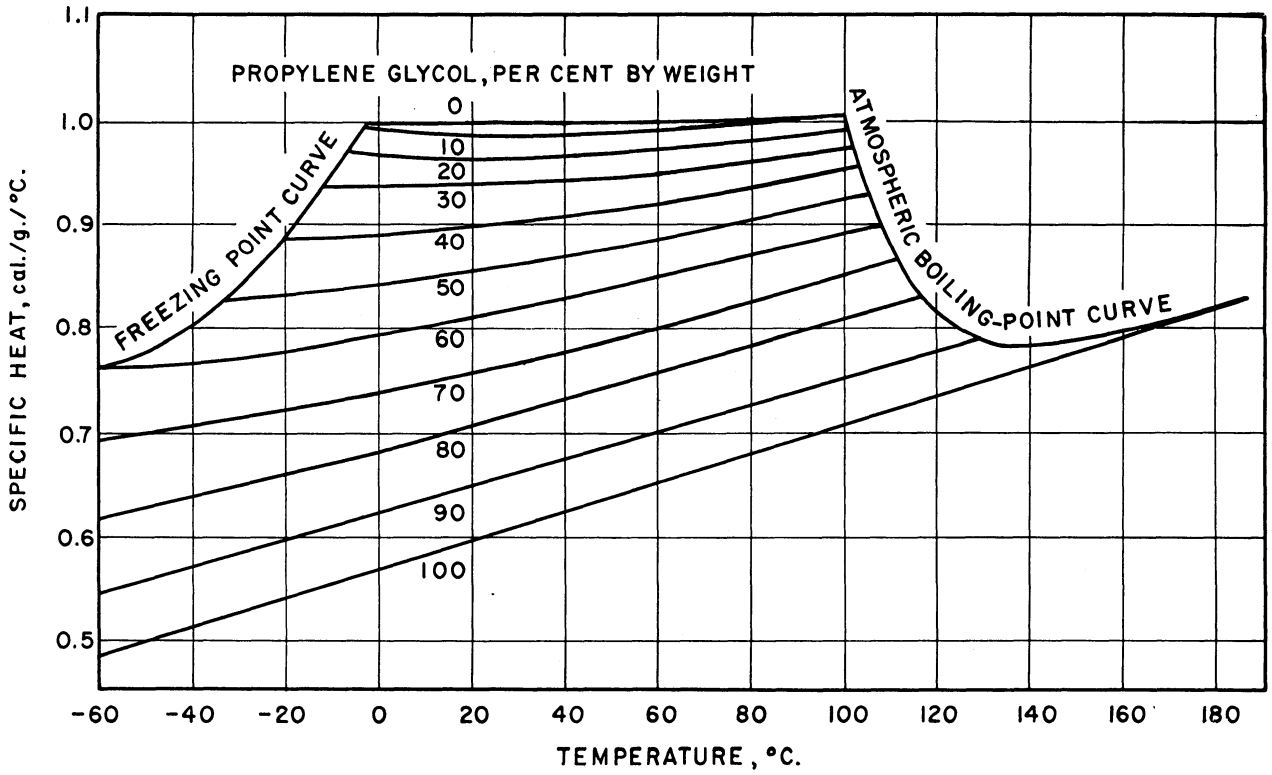

Fig 35 Specific heat of aqueous propylene glycol solutions

(Courtesy Carbide & Carbon Chem. Co.)

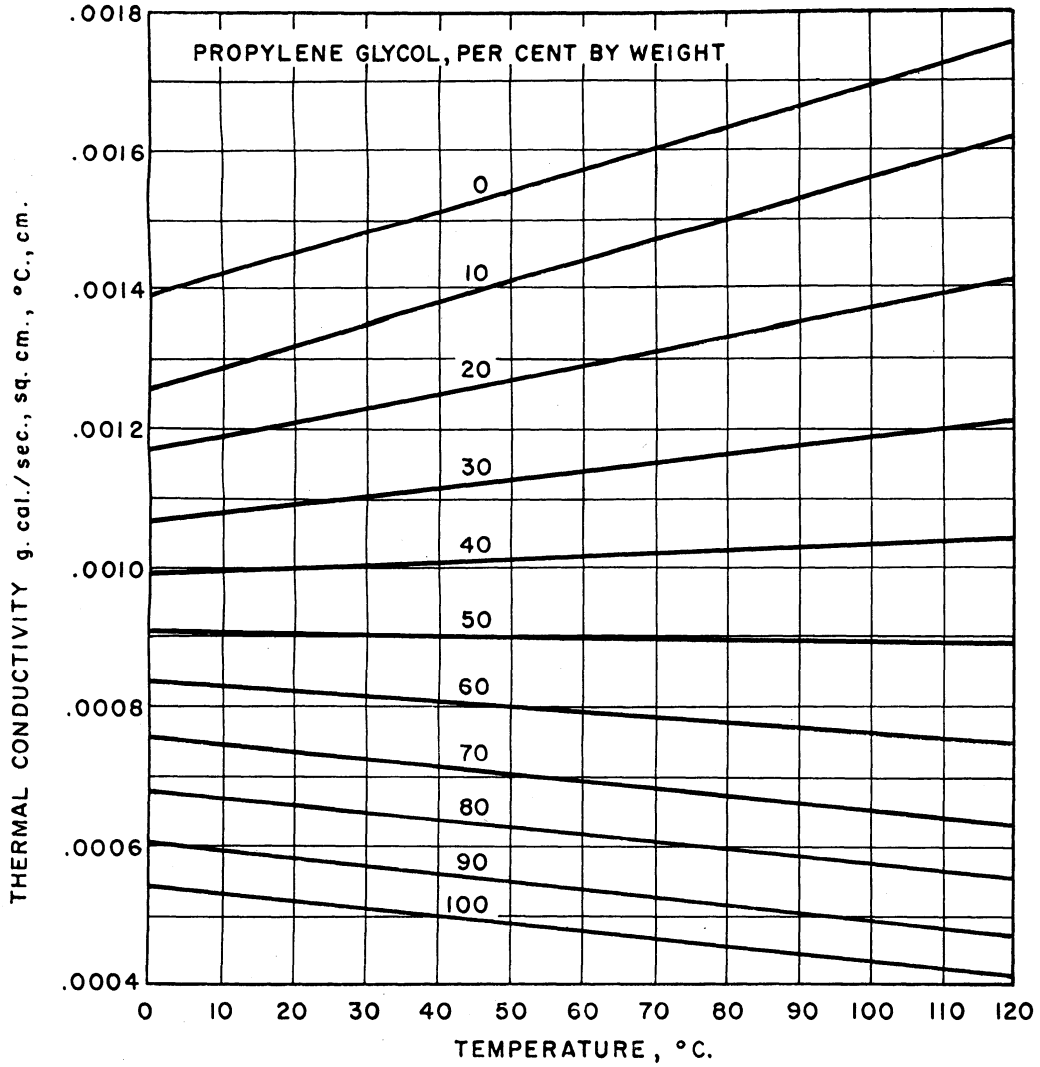

Fig 36 Thermal conductivity of aqueous propylene glycol solutions
(Courtesy Carbide & Carbon Chem. Co.)

BIBLIOGRAPHY

1. Badger, W. L., and Banchero, J. T., Introduction to Chemical Engineering, New York: McGraw-Hill Book Company, Inc., 1955.

2. Bergelin, O. P., Davis, E. S., and Hull, H. L., "A Study of Three Tube Arrangements in Unbaffled Tubular Heat Exchangers," Trans. ASME, 71: 369-373, discussion 373-374; 1949.

3. Bergelin, O. P., Brown, G. A., Hull, H. L., and Sullivan, F. W., "Heat Transfer and Fluid Friction During Viscous Flow Across Banks of Tubes. III - A study of Tube Spacing and Tube Size," Trans. ASME, 72: 881-888; 1950.

4. Bergelin, O. P., Brown, G. A., and Doberstein, S. C., "Heat Transfer and Fluid Friction During Flow Across Banks of Tubes. IV - A Study of the Transition Zone Between Viscous and Turbulent Flow," Trans. ASME, 74: 953-959; 1952.

5. Bergelin, O. P., Brown, G. A., and Colburn, A. P., "Heat Transfer and Fluid Friction Across Banks of Tubes. V - A Study of a Cylindrical Baffled Exchanger without Internal Leakage," Trans. ASME, 76: 841-850; 1954.

6. Bowman, R. A., "Investigation of Heat Transfer Rates on the External Surface of Baffled Tube Banks," Heat Transfer, ASME Unpublished Papers, No. 28: 75-81; 1936.

7. Braun and Company, Private Communication.

8. Brown, G. G., et al., Unit Operations, New York: John Wiley and Sons, Inc.; 1950

9. Carbide and Carbon Chemicals Company, Glycols: Pp. 61; 1955.

10. Colburn, A. P., "A Method of Correlating Forced Convection Heat Transfer Data and a Comparison with Fluid Friction," Trans. AIChE, 29: 174-210; 1933.

11. Corning Glass Works, Pyrex Brand Shell and Tube Heat Exchanger, Bulletin PE-24, Technical Products Division, Corning Glass Works, Corning, New York: Pp. 12; 1954.

12. Curme, G. O., Jr., and Johnston, F., Glycols, ACS Monograph Series No. 114, New York: Reinhold Publishing Corporation; 1952.

13. Dittus, F. W., and Boelter, L. M. K., "Heat Transfer in Automobile Radiators of the Tubular Type," University of California Pub. in Eng., 2: 443-461; 1930.

14. Donohue, D. A., "Heat Transfer and Pressure Drop in Heat Exchangers," Ind. and Eng. Chem., 41: 2499-2511; 1949.

15. Dwyer, O. E., et al., "Heat Transfer Rates for Cross Flow of Water Through a Tube Bank at High Reynolds Numbers," U. S. AEC, Brookhaven National Laboratory, Upton, New York, BNL-203 (Subject Category: Physics): Pp. 78; November 20, 1952.

16. Eckert, E. R. G., Introduction to the Transfer of Heat and Mass, New York: McGraw-Hill Book Company, Inc., 1st ed.; 1950.

17. Eckert, E. R. G., and Irvine, T. F., Jr., "Flow in Corners of Passages with Non-Circular Cross-Sections," Trans. ASME, 78, No. 4: 709-718; May, 1956.

18. Fabregas, J., "Design Heat Exchangers More Exactly," Chem Eng., 63, No. 4: 181-184; April, 1956.

19. Fischer and Porter Company, Hatboro, Penn., Correction Factor Curves for Flowrator Meters, Pub. No. 10602: Pp. 6; 1952.

20. Fritzsche, A. F., Gestaltung und Berechnung von Oelkuhlern, Zurich, Switzerland: Verlag Leemann; 1953.

21. Gardner, H. S., and Siller, I., "Shell-side Coefficients of Heat Transfer in a Baffled Heat Exchanger," Trans. ASME, 69: 687-692, discussion 692-694; 1947.

22. Goldstein, S., Modern Developments in Fluid Mechanics, Vol. I, Oxford: At the Clarendon Press; 1938.

23. Griffiths, E., and Awbery, J. H., "Heat Transfer Between Metal Pipes and a Stream of Air," Proc. Inst. Mech. Engrs., 125: 319-362, discussion 363-379; 1953.

24. Grimison, E. D., "Correlation and Utilization of New Data on Flow Resistance and Heat Transfer for Flow of Gases over Tube Banks," Trans. ASME, 59: 583-594; 1937.

25. Gunter, A. Y., Sennstrom, H. R., and Kopp, S., "A Study of Flow Patterns in Baffled Heat Exchangers," ASME Preprint No. 47-A-103; 1947.

26. Hagerty, W. W., "Use of an Optical Property of Glycerine-Water Solutions to Study Viscous Fluid-Flow Problems," J. Applied Mechanics, ASME, 72: 54-58; 1950.

27. Hauser, E. A., and Dewey, D. R. II, "Visual Studies of Flow Patterns," J. Phys. Chem., 46: 212-213; 1942.

28. Heinrich, E., and Stückle, R., "Warmeübergang von Öl an Wasser," Forschungsarbeiten Auf Dem Gebiete Des Ingenieur Wesens, Heft 271: 60; 1925.

29. Huge, E. C., "Experimental Investigation of Effects of Equipment Size on Convection Heat Transfer and Flow Resistance in Cross Flow of Gases over Tube Banks," Trans. ASME, 59: 573-581; 1937.

30. Jacob, M., Heat Transfer Vol I, New York: John Wiley and Sons, Inc., ; 1949.

31. Kays, W. M., London, A. L., and Lo, R. K., "Heat Transfer and Friction Characteristics for Gas Flow Normal to Tube Banks--Use of a Transient-Test Technique," Trans. ASME, 76: 387-396; 1954.

32. Kern, D. Q., Process Heat Transfer, New York: McGraw-Hill Book Company, Inc., 1st ed., 1950.

33. Knudsen, J. G., and Katz, D. L., Fluid Dynamics and Heat Transfer, Ann Arbor: University of Michigan, Engineering Research Bulletin No. 37: Pp. 243; September, 1953.

34. Leeds and Northrup Company, Philadelphia, Penn., Standard Conversion Tables for L and N Thermocouples, Standard 31031.

35. Loudenslager, O. W., Ross, R. S., and Stimler, F. J., "A Simple Accurate Photographic Method of Three-Dimensional Flight-Path Analysis," Photographic Eng., 4, No. 2: 77-86; 1953.

36. MacBeth, G., and Thompson, A. R., "Densities and Refractive Indexes for Propylene Glycol-Water Solutions," Analytical Chem., 23: 618-619; 1951

37. McAdams, W. H., Heat Transmission, New York: McGraw-Hill Book Company, Inc., 2nd ed., 1942.

38. McAdams, W. H., Heat Transmission, New York: McGraw-Hill Book Company, Inc., 3rd ed., 1954.

39. Miller, P., Byrnes, J. J., and Benforado, D. M., "Heat Transfer to Water Flowing Parallel to a Rod Bundle," AIChE Journal, 2, No. 2: 226-234; June, 1956.

40. Nelson, W. L., "Velocity in Shell of Exchanger," Oil and Gas J., 44: 62 +; February 2, 1946. Also p. 165 +; April 20, 1946.

41. Nelson, W. L., Petroleum Refinery Engineering, New York: McGraw-Hill Book Company, Inc., 3rd ed., 1949.

42. Ohlgren, H. A., Udani, L. H., and Landrum, L. H., Heat Exchanger Design Manual (Shell and Tube Types with Plain Tubes), Ann Arbor: University of Michigan, College of Engineering, Industry Program Report No. IP-139; October, 1955.

43. Omohundro, G. A., Bergelin, O. P., and Colburn, A. P., "Heat Transfer and Fluid Friction During Viscous Flow Across Banks of Tubes," Trans. ASME, 71: 27-34; 1949.

44. Peebles, F. N., Garber, H. J., and Jury, S. H., "Preliminary Studies of Flow Phenomena Utilizing a Doubly Refractive Liquid," Proc. Third Midwestern Conference on Fluid Mechanics: 441-454; June, 1953.

45. Perrone, S. A., "Pressure Drop and Heat Transfer in Exchangers," Oil and Gas J., 33: 71-72, 75-76; March 28, 1935.

46. Perry, J. H. (ed.), Chemical Engineers' Handbook, New York: McGraw-Hill Book Company, Inc., 3rd ed., 1950.

47. Pierson, O. L., "Experimental Investigation of the Influence of Tube Arrangement on Convection Heat Transfer and Flow Resistance in Cross Flow of Gases over Tube Banks," Trans. ASME, 59: 563-572; 1937.

48. Prandtl, L., and Tietjens, O. G., Applied Hydro- and Aero-Mechanics, New York: McGraw-Hill Book Company, Inc., 1934.

49. Relf, E. E., "Photographic Investigation of the Flow Round a Model Aerofoil," Rept. Nat. Adv. Comm. Aeronautics, No. 76: 133; 1913.

50. Sachs, J. P., and Rushton, J. H., "Discharge Flow from Turbine-Type Mixing Impellers," Chem. Eng. Prog., 50: 597-603; 1954.

51. Schmidt, T. E., "Heat Transmission and Pressure Drop in Banks of Finned Tubes and in Laminated Coolers," Proc. General Discussion on Heat Transfer, IME and ASME: 186-188; September 11-13, 1951.

52. Short, B. E., "Heat Transfer and Pressure Drop in Heat Exchangers," Texas Univ. Bur. of Eng. Res., Eng. Res. Ser. No. 37, Bulletin No. 4324: Pp. 55; 1943

53. Short, B. E., "The Effect of Baffle Height and Baffle Clearance on Heat Transfer and Pressure Drop in Heat Exchangers," ASME Preprint No. 47-A-105; 1947.

54. Stoever, H. J., Applied Heat Transmission, New York: McGraw-Hill Book Company, Inc., 1941.

55. Sullivan, F. W., and Bergelin, O. P., "Heat Transfer and Fluid Friction in a Shell and Tube Exchanger with a Single Baffle," AIChE, Preprint No. 18, pp. 18, Presented at Heat Transfer Symposium, National Meeting, Louisville, Kentucky; March 20-23, 1955.

56. Tinker, T., "Shell Side Heat Transfer Characteristics of Segmentally Baffled Shell and Tube Heat Exchangers," Heat Transfer Lectures, Vol. II, NEPA 804-IER-10 (Compiled by Don Cowen), p. 293; 1948. Also Preprint for 1947 Annual ASME Meeting, Pp. 55.

57. Tinker, T., "Shell Side Characteristics of Shell and Tube Heat Exchangers," Proc. General Discussion on Heat Transfer, IME and ASME: 89-116, 205, 209-210, 211, 212, 217-220; September 11-13, 1951.

58. Tubular Exchanger Manufacturers Association, Inc., New York, Standards of TEMA, 3rd ed., 1952.

59. Ullyott, P., "Investigation of Flow in Liquids by Use of Birefringent Colloidal Solutions of Vanadium Pentoxide," Trans. ASME, 69: 245-251; 1947.

60. Weisman, J., "Effect of Void Volume and Prandtl Modulus on Heat Transfer in Tube Banks and Packed Beds," AIChE Journal, 1 No. 3: 342-348; September, 1955.

61. Whistler, A. M., "Effect of Leakage Around Cross-Baffles in a Heat Exchanger," Pet. Ref., 26: 114-118; October, 1947.

62. Williams, R. B., and Katz, D. L., "Performance of Finned Tubes in Shell and Tube Heat Exchangers," Ann Arbor: University of Michigan, Eng. Rés. Inst., Proj. M-592 Report, Pp. 154; January 30, 1951.

63. Williams, R. B., and Katz, D. L., "Performance of Finned Tubes in Shell-and-Tube Heat Exchangers," Trans. ASME, 74: 1307-1320; 1952.

64. Wilson, E. E., "A Basis for Rational Design of Heat Transfer Apparatus," Trans. ASME, 37: 47-82; 1915.